Helsinki University of Technology Publications in Materials Science and Engineering
Teknillisen korkeakoulun materiaalitekniikan julkaisuja
Espoo 2006 TKK-MT-180

MECHANISM AND KINETICS OF TRANSFORMATION OF ALUMINA INCLUSIONS IN STEEL BY CALCIUM TREATMENT

Doctoral Thesis

Minna Lind

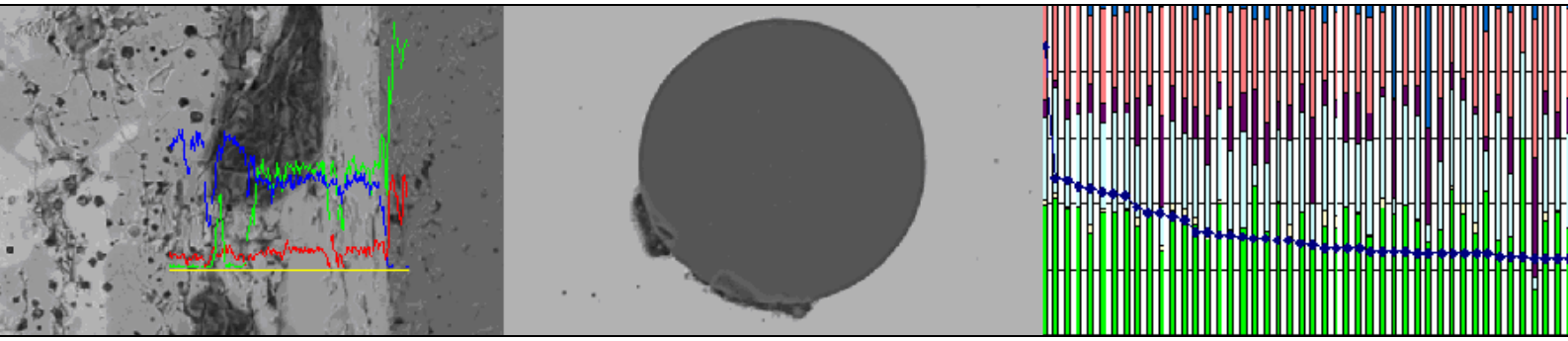

TEKNILLINEN KORKEAKOULU
TEKNISKA HÖGSKOLAN
HELSINKI UNIVERSITY OF TECHNOLOGY
TECHNISCHE UNIVERSITÄT HELSINKI
UNIVERSITE DE TECHNOLOGIE D'HELSINKI

Helsinki University of Technology Publications in Materials Science and Engineering

Teknillisen korkeakoulun materiaalitekniikan julkaisuja

Espoo 2006 TKK-MT-180

MECHANISM AND KINETICS OF TRANSFORMATION OF ALUMINA INCLUSIONS IN STEEL BY CALCIUM TREATMENT

Minna Lind

Dissertation for the degree of Doctor of Science in Technology to be presented with due permission of the Department of Materials Science and Engineering, Helsinki University of Technology for public examination and debate at Helsinki University of Technology (Espoo, Finland) on the 8th of September, 2006, at 12 o'clock noon.

Helsinki University of Technology

Department of Materials Science and Engineering

Laboratory of Metallurgy

Teknillinen korkeakoulu

Materiaalitekniikan osasto

Metallurgian laboratorio

Distribution:
Helsinki University of Technology
Laboratory of Metallurgy
P.O. Box 6200
FIN-02015 TKK, Finland
Tel. +358 9 451 2756
Fax. +358 9 451 2798
email: lea.selin@tkk.fi

Cover: SEM/EDS results concerning alumina inclusion modification by calcium, from left to right: (i) Linescan of the reaction layer between CaO and Al_2O_3, (ii) inclusion in steel after Ca treatment, and (iii) diagram of the inclusions analysis.

ISBN 951-22-8251-8
ISBN 951-22-8252-6 (electronic)
ISSN 1455-2329

Edita Oy
Helsinki 2006

ABSTRACT

In steelmaking, commonly used calcium treatment has the benefit of modifying inclusion composition, and the shape and size of these inclusions are also adjusted. Two of the main advantages of calcium treatment are not only the improvement of the castability but also the improvement of the final properties of the steels' machinability, toughness and surface quality. The effects of calcium are mainly based on its strong ability to form sulphides and oxides. In aluminium deoxidised steels, the inclusion population will generally include alumina inclusions and maybe some silicates and manganese sulphides. After calcium treatment, the inclusions are restricted mainly to calcium aluminates ($CaO\text{-}Al_2O_3$) and the sulphur in the steel is associated with these inclusions as calcium sulphide. The topic of the present study concerns the basic mechanism and kinetics of the transformation process of alumina inclusions in steel when calcium is introduced into the steel e.g., by wire feeding or powder injection.

To clarify the mechanisms, several types of model experiments were performed in laboratory furnaces and on an industrial scale. Reactions between only Al_2O_3 and CaO were studied in a laboratory furnace. The phases formed during the reaction between Al_2O_3 and CaO were examined by SEM-EDS, and a discussion of the proposed reaction sequence of $Al_2O_3 \Rightarrow CA_6 \Rightarrow CA_2 \Rightarrow CA \Rightarrow CA_x$ (liquid) was based on the experimental observations and thermodynamic equilibrium examinations. The kinetics of the reaction of calcium with alumina inclusions were simulated by performing Ca treatments in an induction furnace for 8 kg steel deoxidised with aluminium. Results were compared with observations of inclusion transformation in a real steelmaking process. Based on the results, a kinetic model was proposed.

PREFACE

The research work of this thesis was carried out in the Laboratory of Metallurgy, Helsinki University of Technology, during the years 1999-2006.

Warmest thanks to my supervisor professor Lauri Holappa for his encouragement, comments and interest in my work.

The financial support from Ministry of Education and Academy of Finland in form of the Graduate School on Metallurgy/Graduate School on New Materials and Processes has made this work possible. Also funding from Rautaruukki Oyj, Tekniikan Edistämissäätiö and Finnish Funding Agency for Technology and Innovation (TEKES) projects (Oksidimetallurgia, Sulkeumahallinta and Hot Link) has helped to get this work done.

I am also truly grateful to the staff at Koverhar and Imatra steel plants, at Laboratory of Metallurgy and people who have taken part in the same projects for offering help in this work when needed.

My parents, brother and my husband Sakari deserve lots of thanks for their trust and patience. Many thanks to all of my friends and Simonson's family.

I want to dedicate this work to my daughter Alina and my sons Aarno and Anton.

Espoo, 08.08.2006

Minna Lind

CONTENTS

1. INTRODUCTION

One of the essential tasks in the steelmaking process is to control non-metallic inclusions their amount, composition, size, and other properties. The composition of the inclusions can be controlled through the chemistries of the metal and the slag. Deoxidation is an important start for a kind of inclusion path. The practice of adding calcium to steels for the reduction and control of sulphide and oxide inclusions is now used worldwide.

After rolling, in aluminium deoxidised steels, the inclusion population will generally include elongated Type II manganese sulphides, dispersed alumina inclusions or even clusters and eventually some silicates. However, after calcium treatment, the inclusions are mainly calcium aluminates of the type $CaO–Al_2O_3$. The sulphur in the steel is also associated with these inclusions either as calcium sulphides or as sulphides containing manganese. The calcium aluminate particles are globular in nature and tend to retain their shape on hot rolling.[1, 2]

There are normally three categories to modify the non-metallic inclusions: namely (1) the use of specific elements such as Ca, Ti, Zr, and rare earth metals; (2) the control of solidification conditions; and (3) the control of the composition of molten steel before solidification. By thermodynamic calculations, it is possible to predict the optimal range of content of dissolved aluminium and oxygen and the best possible solidification conditions for particular steels by the generation of ultra-fine dispersed oxide particles as inoculants for fine precipitates and as a simultaneous adjustment of fine grain ferrite structure[3].

The addition of calcium or calcium alloys, usually in wire form, is made for aluminium-killed steels in order to decrease the volume fraction of oxide and sulphide inclusions through deoxidation and desulphurization and to control the composition, morphology, and distribution of those remaining inclusions. A major benefit of this practice is that nozzle clogging in continuous casting can be eliminated: Solid alumina inclusions are transformed to liquid calcium aluminates that do not clog the nozzle. Other benefits are realized in the mechanical properties of various grades of steel. For example, the ductility and toughness of high-strength low-alloy steel and high-quality structural steel are improved as the volume fractions of sulphides and oxides are decreased. In flat-rolled plate and sheet grades, relatively hard manganese sulphide inclusions become “stringers” when deformed, resulting in poor through-thickness ductility and toughness. Calcium complexes the manganese sulphides into inclusions, which do not deform to decrease the incidence of stringers. In free-machining grades, hard alumina inclusions cause excessive tool wear; calcium can transform these inclusions into softer calcium aluminates or calcioaluminosilicates. Any calcium that dissolves in the steel melt will rapidly react and form inclusions. [4]

1.1 Primary products of deoxidation and Ca-treatment

Deoxidation must be made in the tap ladle in order for the liquid steel to be cast and hot worked and for the product to have the desired metallurgical and mechanical properties.[2]

The most common elements used in steel deoxidation are aluminium, silicon, and manganese. Silicon and manganese are often used in conjunction with each others.

An average value for the equilibrium constant, when using aluminium as deoxidizer, is given in Table 1.[5]

Table 1. Deoxidation with aluminium.[5]

(Al_2O_3) (s) → 2[Al] + 3[O]	$K = \frac{[\%Al]^2 [ppmO \times f_o]^3}{a_{Al_2O_3}}$	$\log K = -\frac{62680}{T} + 31.85$

Table 2. Literature survey on equilibrium relation in Fe-Ca-S and Fe-Ca-O systems[6]

System	Author	Solubility product (1873 K)	Impurity concentration	Crucible	Ca addition; method
Ca-S	Ozawa et al.[7]	2.6 x 10^{-5} (1943 K)	50-110 ppm, O	CaO MgO	Ca (g) + Ar
Ca-S	Suzuki et al.[8]	7.9 x 10^{-7}	deoxidized by 0.2 %Al	MgO	Ca wire with iron cover
Ca-S	Haida et al.[9]	2.0 x 10^{-9} (calc.)			Thermochem. calculation
Ca-O	Miyashita et al.[10]	2.5 x 10^{-5}	40 ppm S	MgO, Al_2O_3	Ca granule via quartz pipe
Ca-O	Ozawa et al. [7]	6.0 x 10^{-6}	30-40 ppm S	CaO MgO	Ca (g) + Ar
Ca-O	Kobayashi et al.[11]	3.8 x 10^{-6}	40 ppm S	MgO, Al_2O_3, CaO	Ca granule via steel pipe
Ca-O	Ototani et al.[12]	5.9 x 10^{-9}	40 ppm S	MgO, Al_2O_3, CaO	Ca wire with iron cover
Ca-O	Gustafsson[13]	1.6 x 10^{-6} (1600)	10-20 ppm O	CaO	Ca (g) + Ar
Ca-O	Suzuki et al.[8]	2.5 x 10^{-8} (calc.)			Thermochem. calculation from Ca-S system
Ca-O	Haida et al.[9]	4.0 x 10^{-10} (calc.)			Thermochem. calculation
Ca-O	Suzuki[14]	8.3 x 10^{-10} (calc.)			Thermochem. calculation

The equilibrium content of dissolved oxygen in Al-killed steels (Al content 0.02-0.03 wt%) is as low as 4 ppm [O], depending on the temperature, so that there is lower residual oxygen at lower temperature. Deoxidation with Si-Mn-Al gives residual dissolved oxygen in range 25-40 ppm [O] when dissolved Al content is tens of ppm or less.[5]

The following equilibrium values based on a thermochemical evaluation carried out by Suzuki, were recommended for the reaction CaS (s) = [Ca] + [S]:[6]

$K=a_{Ca}a_S$

Log K (1873K) = -8.91

$\Delta G°$ (1873K) = 319,000 J/mol

e_S^{Ca} == -110

Recommended values for the reaction CaO (s) = [Ca] + [O] are[6]

$K=a_{Ca}a_O$

log K (1873K) = -9.08

$\Delta G°$ (1873K) = 326,000 J/mol

e_O^{Ca} = -515, γ_{Ca}^{o} =2240

where a_{Ca} and a_S are the activities of calcium and sulphur in mass percentage and the reference state is the infinitely dilute solution of liquid iron-calcium and iron-sulphur system.

Calcium is widely used not only as an alloying element for sulphide and oxide shape control but also as a refining agent for liquid steel.

Experimental studies on desulphurization equilibria of calcium in liquid iron are difficult because both solubility of calcium and equilibrium sulphur content are quite low in liquid iron. When studying the equilibria it is essential to exclude participation of oxygen in liquid iron to the reaction; however, the prerequisite mentioned above is not satisfied, as is shown in Table 2.[6]

1.2 Introduction to $CaO-Al_2O_3$ system

With the exception of pure phases, the system $CaO-Al_2O_3$ has four to five nearly stoichiometric compounds, which can be called calcium aluminates. The existence of the phase $C_{12}A_7$ (C=CaO and $A=Al_2O_3$) and also the melting points of different compounds vary from one source to another.

An optimized phase diagram calculated with thermodynamic program FactSage is shown in Figure 1.

The first studies of this system[15,16], indicated the presence of four compounds: $Ca_3Al_2O_6$ (C_3A), $Ca_5Al_6O_{14}$ (C_5A_3), $CaAl_2O_4$ (CA) and $Ca_3A_{l0}O_{18}$ (C_3A_5). Lagerqvist et al.[17], in the year 1937, studied the system by x-ray diffractometer and could identify $Ca_5Al_6O_{14}$ as $Ca_{12}Al_{14}O_{33}$ ($C_{12}A_7$) and $Ca_3Al_{10}O_{18}$ as $CaAl_4O_7$ (CA_2); they also reported a new compound $Ca_3Al_{32}O_{51}$ (C_3A_{16}). By a microscopic study of rapidly chilled samples, this latter compound was later identified as $CaAl_{12}O_{19}$ (CA_6) by Filonenko and Lavrov[18]. Its

composition has been confirmed. The alumina-rich part of the phase diagram has been studied several times with a considerable spread in the results, which is probably related to whether the experiments were performed in air or in moisture-free argon atmospheres.[22]

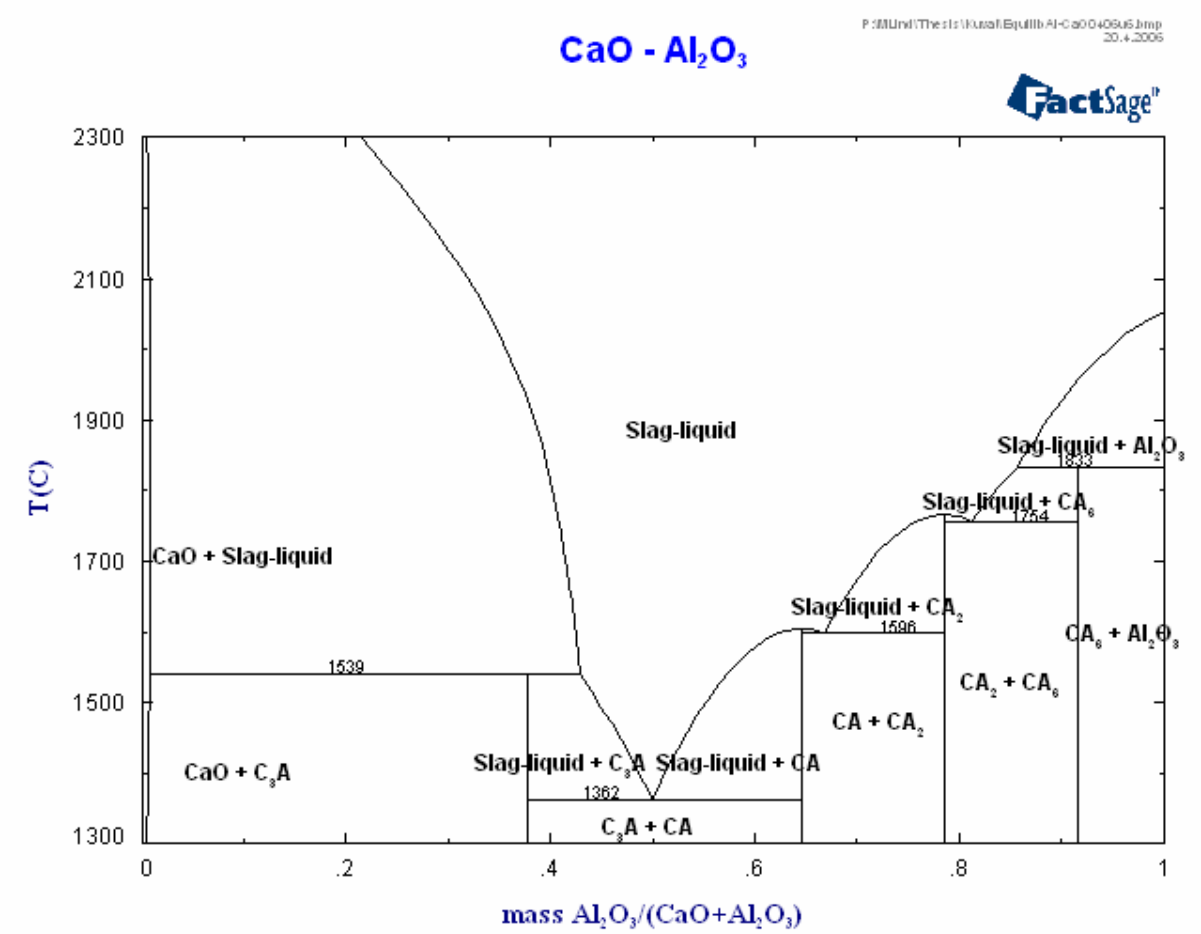

Figure 1. *CaO-Al_2O_3 phase diagram.*[19]

Nurse et al.[20], in 1965, used high-temperature microscopy under controlled atmospheres to conclude that the compound $Ca_{12}Al_{14}O_{33}$ ($C_{12}A_7$) is actually a hydrate, $Ca_{12}Al_{14}O_{32}(OH)_2$, and should not be found in the binary CaO-Al_2O_3 system. Corresponding experimental set-ups were applied for the whole system by Nurse et al.[20] All four compounds were reported to melt incongruently, namely $Ca_3Al_2O_6$ (C_3A) at 1541°C to a liquid of 45.1 mol pct $AlO_{1,5}$; $CaAl_2O_4$(CA) at 1604°C to a liquid of 66 mol pct $AlO_{1,5}$; $CaAl_4O_7$ (CA_2) at 1765°C to a liquid of 80 mol pct $AlO_{1,5}$; and $CaAl_{12}O_{19}$(CA_6) at 1833°C to a liquid of 85 mol pct $AlO_{1,5}$. A deep eutectic at 1362°C and 53.0 mol pct $AlO_{1,5}$ was found. This eutectic temperature and composition have been confirmed by Nityanand and Fine[21].[22]

Table 3 shows the theoretical compositions and physical properties of calcium oxide, aluminium oxide, and possible stoichiometric compounds which can be formed as reaction products.

Table 3. Theoretical compositions and physical properties of calcium oxide, aluminium oxide, and different calcium aluminates (C= CaO and A = Al_2O_3).

Composition of Oxides	**CaO (Wt%)**	**Al_2O_3 (Wt%)**	**Melting point (°C) Ref. 23**	**Melting point (°C) FactSage (Fig. 1) Ref. 19**	**Melting point (°C) Ref. 24 (Part II, p.37)**	**Density at 20 °C (g/cm^3) Ref. 24**	**Crystal structure**
Al_2O_3	0	100	2050	2054	2050	3.96	hexagonal
CaO	100	0	2570	2572	2570	3.34	cubic
C_3A	62	38	1539	1539	1535	3.04	cubic
$C_{12}A_7$	48	52	1395	1362 (deep eutectic)	1455	2.83	cubic
CA	35	65	1590	1596	1605	2.98	monoclinic
CA_2	22	78	1775	1754	~1750	2.91	monoclinic
CA_6	8	92	1833	1833	~1850	3.38	hexagonal

1.3 Inclusion modification and its influence on steels properties

1.3.1 Reactions during inclusion formation and transformation

The thermodynamic constraints of the formation of inclusions in steel must be considered when computing the reaction equilibria relevant to inclusion formation and modification. When simplifying the system to four components (i.e., Al, Ca, O and S), the most essential reactions governing the inclusion formation and transformation are as follows:[28]

$$2[Al]+3[O]=(Al_2O_3)_{inc} \quad (1)$$

$$[Ca]+[O]=(CaO)_{inc} \quad (2)$$

$$[Ca]+[S]=(CaS)_{inc} \quad (3)$$

$$[S]+(CaO)_{inc}=(CaS)_{inc}+[O] \quad (4)$$

$$[Ca]+6\tfrac{1}{3}(Al_2O_3)=(CaO\cdot 6Al_2O_3)_{solid-inc}+\tfrac{2}{3}[Al] \quad (5)$$

$$[Ca]+2\tfrac{1}{3}(Al_2O_3)_{inc}=(CaO\cdot 2Al_2O_3)_{solid-inc}+\tfrac{2}{3}[Al] \quad (6)$$

$$[Ca]+\tfrac{4}{3}(Al_2O_3)=(CaO\cdot Al_2O_3)_{solid-inc}+\tfrac{2}{3}[Al] \quad (7)$$

$$3[Ca]+(Al_2O_3)_{inc}=2[Al]+3(CaO)_{inc} \quad (8)$$

$$3(CaO)_{inc}+2[Al]+3[S]=3(CaS)_{inc}+(Al_2O_3)_{inc} \quad (9)$$

$$(CaS)_{inc}=CaS_{solid-inc} \quad (10)$$

In the above equations, square brackets denote an element dissolved in steel melt, round brackets denote a component dissolved in liquid slag inclusions, and the subscript *solid-inc* denotes a solid (saturation) phase. Reactions (1)-(4) describe deoxidation and desulphurization reactions by calcium and aluminium and reactions (5) and (6) represent modification of alumina inclusions by calcium to form solid calcium aluminates. Reaction (8) is the transformation reaction in a general form. When transformation proceeds via reaction (7), liquid aluminates are formed at steelmaking temperature. Reactions (9) and (10) represent interaction of sulphur between steel and inclusions as well as precipitation/dissolution of sulphides.[28]

1.3.2 Inclusion modification

Today, after Al deoxidation many steel grades are treated with calcium using a Ca-Si alloy, a Ca-Fe(Ni) mixture, or pure Ca, depending on the silicon specification.

During calcium treatment, the alumina and silica inclusions are converted to molten calcium aluminates and eventually silicates, which are globular in shape because of the surface tension effect. Change in inclusion composition and shape is schematically demonstrated in Figure 2. The calcium aluminate inclusions, retained in liquid steel suppress the formation of MnS stringers during solidification of steel. [9]

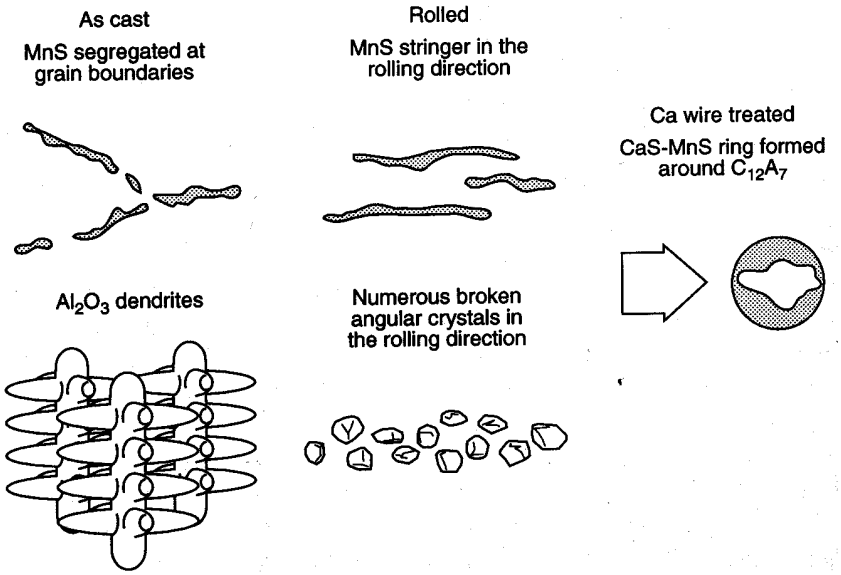

Figure 2. *Schematic illustration of modification of inclusion morphology with calcium treatment of steel* [9].

Figure 3 also shows how manganese sulphides, alumina, and complex oxide inclusions are modified when calcium is added into the steel. Alumina inclusions form calcium aluminates that can be as cores for precipitating "oxysulphide" inclusions (Figure 3). The outer layer contains calcium sulphide (or calcium sulphide with little manganese) when sulphur content is low or calcium-manganese sulphide when sulphur content is higher. The mechanism and stage of formation of the oxysulphides is not fully known, but the favourable influence of these complex inclusions for many products is well known i.e. improving the machinability of hardening and tempering as well as case-hardening steels. The formation of oxide layer on the tool is optimized and results in longer tool life and in possibility to use higher cutting speeds. Better surface quality of the product is also attained. In addition, good castability is an important application of Ca-treatment.

For some products, however, the Ca-treatment and hence modification of inclusions must be avoided. For instance, well deformable silicate type inclusions are desirable for wire materials and undeformable inclusions should be avoided. In general, the properties of final products must be thoroughly considered when choosing the proper ladle treatment. [25]

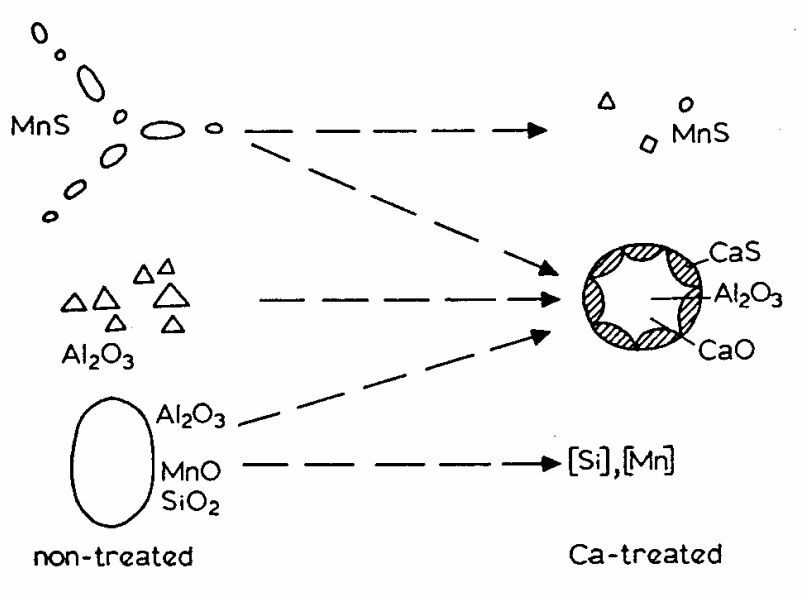

Figure 3. *Schematic presentation illustrating the influence of calcium treatment on inclusions in steel.*[25]

1.3.3 Influence on steel properties

The following goals have been reported for calcium treatment:[5, 26]

1) To improve steel castability in continuous casting (i.e., minimise nozzle blockage during casting with consequential reduction in casting speed and possibly the formation of large aggregated alumina clusters in the solidified product);

2) To get good surface quality and good internal slag cleanliness;

3) To improve mechanical properties especially in transversal and through thickness direction, by modifying manganese sulphides to globular Ca-Mn sulphides, which are nearly non-deformable during rolling;

4) To improve steel machinability at high cutting speeds by forming a protective film on the tool surface that prolongs the life of the carbide tool;

5) To minimise the susceptibility of steel to reheat cracking, as in the heat-affected zones (HAZ) of welds;

6) To prevent lamellar tearing in large restrained welded structures; and

7) To minimise the susceptibility of high-strength low-alloy (HSLA) linepipe steels to hydrogen-induced cracking (HIC) in sour gas or sour oil environment.

1.4 Limits of Ca-addition for continuous casting

As mentioned calcium treatment is used to desulphurize steel and to control sulphide as well as oxide inclusions in order to improve the properties of the steel. The

improvement of the through-thickness properties of plate materials is a well-known application. In these applications, the remaining sulphur content in the steel is essentially low (i.e., far below 0.010%). Calcium treatment at a low sulphur level results in the formation of calcium sulphides or calcium manganese sulphides, whereas pure Mn sulphides, which are typical in conventional steel, are hardly detected. This kind of sulphide control produces the aforementioned beneficial effects. On the other hand in various engineering steel grades, low S-content in not desirable, but the maximum contents allowed by the standards or even higher sulphur contents are nowadays often preferred. These concerns especially affect the steels used for different engineering purposes, such as the automobile industry where excellent machinability must be consistent for high productivity in the automated production line.[27] Sulphur levels in the range of 0.020-0.050% S are attractive as such steels are produced in increasing tonnage worldwide.[28]

So-called free-cutting steels with high sulphur contents of up to 0.3% are produced. In such steels, problems may arise in the steelmaking process with continuous casting as well as with the surface and internal quality and mechanical properties. There is a growing interest in developing free-cutting steel substitutes with respective high mechanical properties but with superior machinability to conventional steel grades with medium sulphur content (below 0.05% S).[29]

The inclusions in aluminium deoxidized, sulphur containing steel melt are essentially alumina inclusions, and the amount of SiO_2 and MnO containing inclusions is dependent on the relative quantities of the deoxidizing elements in steel melt. Sulphur is dissolved and will precipitate as manganese sulphide inclusions during solidification. When such steel is treated with calcium, the situation is more complicated. In any case, the system Al–Ca–O–S, the respective oxide, and the sulphide phases shall be considered. The essential reactions are from a previous chapter (i.e., the reactions (1), (2), (8) and (3)). Pure oxides as well as sulphides (Al_2O_3, CaO, CaS) are formed as solid inclusions, whereas oxide solutions formed by reaction (8) can be either solid or liquid depending on their composition in the interesting temperature range of 1550°-1600°C.[27]

When an Al-deoxidized steel containing mostly alumina inclusions is treated with calcium, except for primary reactions (2) and (3), the transformation of alumina inclusions (8) will take place. Calcium attacks the Al_2O_3 inclusions, aluminium is liberated into the steel melt, and the formed CaO is dissolved into the alumina inclusion. When the steel contains sulphur, the desulphurisation reaction (3) becomes significant and competes with the oxide modifying reaction (8). The equilibrium conditions can be calculated by combining the equations (8) and (3). The thermodynamic values for reactions (1), (2) and (3) were taken from the literature, respectively. Accordingly the following solubility product values were used at 1600°C: [27]

$$a^2_{Al} \cdot a^3_O = 4.3 \times 10^{-14},\ a_{Ca} \cdot a_O = 9 \times 10^{-7},\ a_{Ca} \cdot a_S = 1.7 \times 10^{-5}$$

Gaye et al.[30] have calculated the computed equilibrium diagram for the Fe-Al-Ca-O-S system at temperature 1600°C, as shown in Figure 4. The left side of the diagram shows the conditions for calcium sulphide formation as a function of sulphur content. The right side of the diagram shows that when the Ca content is increased, the alumina inclusions are first transformed into solid aluminates then into liquid aluminates of increasing CaO content until lime saturation is reached. Calcium oxide inclusions, whose formation

would theoretically be possible for Al < 0.02% and very high calcium activities, are very unlikely to be formed in normal industrial conditions.[30]

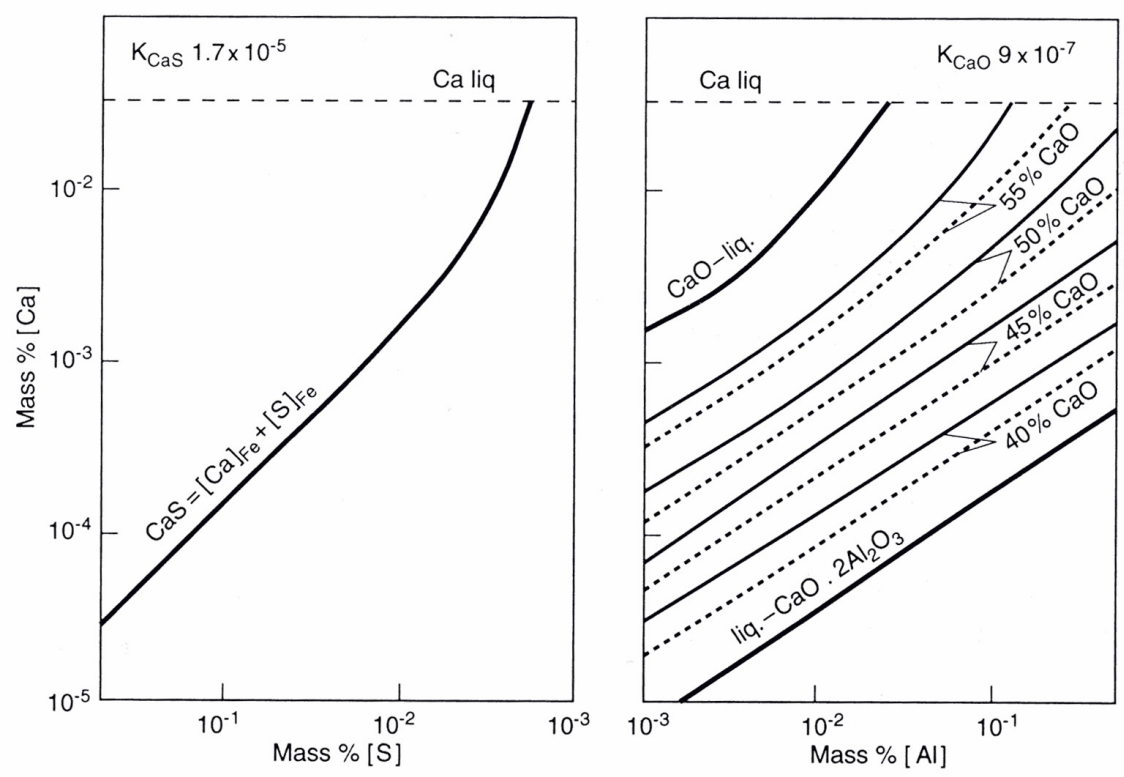

Figure 4. *Equilibrium diagram for Fe-Al-Ca-O-S system at 1600°C.[30] Dotted curves for aluminate inclusions containing 5% SiO_2.[5]*

Calculations to find optimum steel analysis for casting and to understand inclusions behaviour during steel solidification have been done at Helsinki University of Technology (TKK). For basic equilibrium calculations of inclusion formation in liquid steel, the ChemSage program and database with quasi-chemical slag model from GTT Technologies[31] were used. The interdendritic solidification model IDS, developed at TKK by Jyrki Miettinen[32], was coupled with the ChemApp eguilibrium programming library to calculate, interactively and stepwise, steel solidification and inclusion formation/transformation in residual liquid fraction. This interactive program package (ICA) was created for the project by Karri Penttilä at VTT Chemical Technology. It utilizes the CHEMSHEET program by Koukkari et al.[33] to present results.[28]

In Figure 5 and Figure 6, calculations were performed for a steel grade with an analysis:

0.35% C, 0.25% Si, 0.50% Mn.

In Figure 5, oxygen content was chosen as constant (20 ppm), and sulphur content was chosen as a parameter. The limits of the liquid area were determined at temperatures 1600, 1550 and 1520°C by calculating the saturation lines of calcium aluminates ($CaO.Al_2O_3$, $CaO.2Al_2O_3$) and CaS, respectively. The figures clearly show how the growth of sulphur content increases the stability of CaS and contracts the liquid area. Sulphur content had marginal effect on the formation of calcium aluminates and therefore the figures had been drawn with only one calcium aluminate (CaAl =

$CaO{\cdot}Al_2O_3$) saturation line. The results at different temperatures are quite similar: Naturally, the liquid area is larger at the higher temperatures. At 1520°C (the lowest temperature), which is a typical tundish temperature for this steel grade, the window is closed at 400 ppm Al, 250 ppm S. When the temperature is further lowered, the liquid area will rapidly disappear when solidification of the slag inclusions as well as the steel itself occurs.[28]

Oxygen content influences the amount of calcium needed to convert alumina inclusions to calcium aluminates. In Figure 6, the results for total oxygen content of 10, 20 or 40 ppm combined with a sulphur level of 100 and 250 ppm are shown. With low oxygen content, the liquid window is obtained with a small amount of calcium and the window is very narrow. When the oxygen content is increased, the calcium additions increase and the window is widened. The effect of sulphur can be seen in the positions of CaS saturation lines: High sulphur content pushes the line downward and, thus, makes the window narrower. In practical steelmaking, the scatter in the oxygen content before the calcium treatment and the hardly predictable "yield" of calcium to react with Al_2O_3 can make the hitting rate in calcium treatment problematic.

Inclusion formation and behaviour were studied in the temperature range from 1550°C down to the steel solidus temperature. The same basic steel composition as before was used in the calculations but by fixing the following contents: 20 ppm Otot, 20 ppm Ca and 200 ppm Al. The effect of sulphur content was studied at two levels: 50 and 250 ppm. Steel solidification was calculated by using the IDS model with a cooling rate of 1 K/s and a dendrite arm spacing of 0.1 mm.

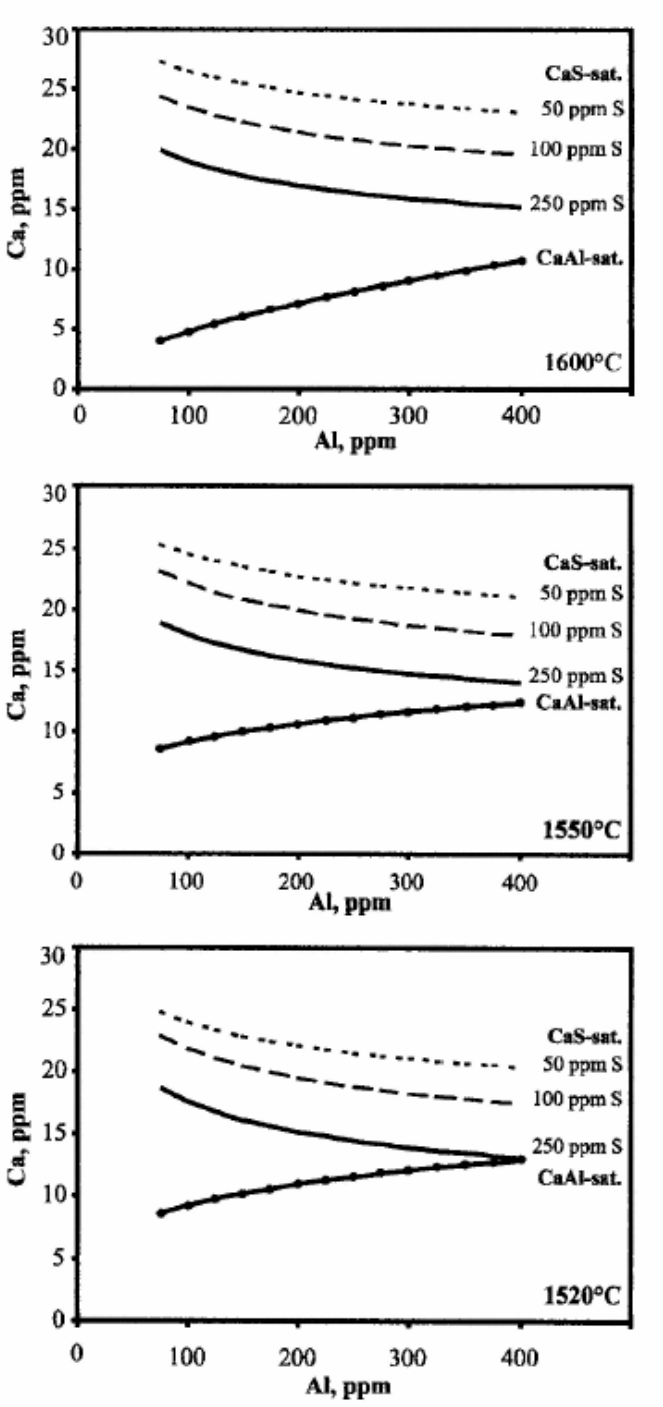

Figure 5. *Saturation lines for Ca aluminates and CaS and Liquid windows at different sulphur levels at 1600, 1550 and 1520°C.*[28]

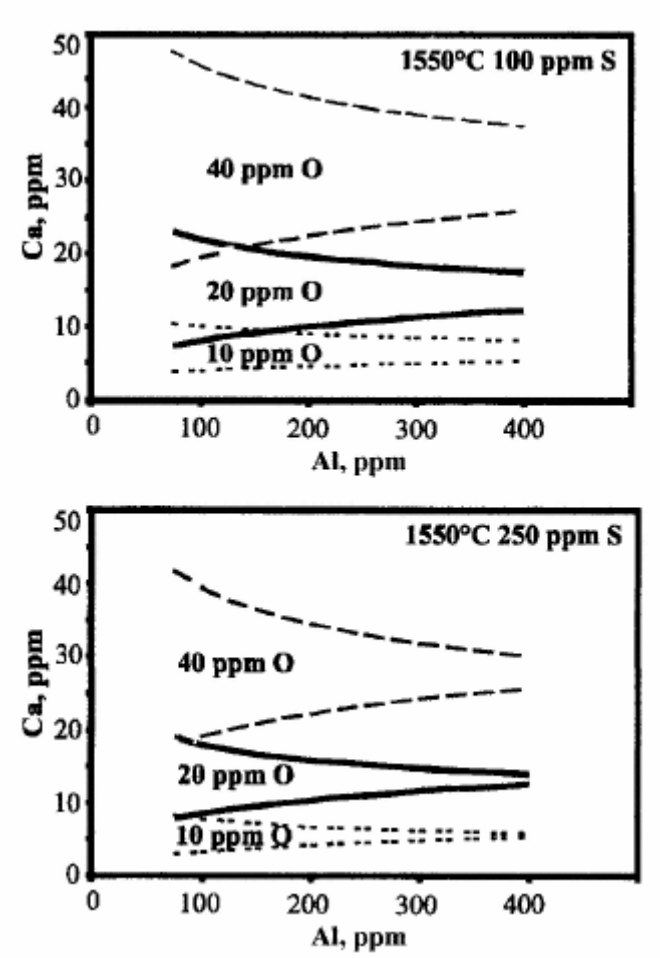

Figure 6. *Effect of total oxygen (10, 20 or 40 ppm) on liquid window with 100 or 250 ppm sulphur.*[28]

Figure 7a (top) shows the results of the low sulphur (50 ppm) steel. From higher temperatures down to 1505°C, liquid steel and liquid slag (inclusions) are the only stable phases. When the steel solidification starts at 1504°C, the formation of solid sulphide gradually starts as a result of sulphur enrichment in the interdendritic melt. At about 1470°C, the liquid slag solidifies as calcium aluminate (CA_2). Sulphide precipitation proceeds further as well. With decreasing temperature, solidification continues and ends at about 1440°C. At the same time, the oxide inclusions that were formed alter from $CaO.2Al_2O_3$ to $CaO.6Al_2O_3$ and finally to Al_2O_3. Sulphides are first formed as almost pure CaS; but at lower temperatures, MnS content is increasing, and the last precipitates are rich in MnS. The results for higher sulphur content (250 ppm) are shown in Figure 7b (bottom) and have only a minor influence on the liquidus temperature (lowering it by 0.7 K), but the solidus temperature drops to 1420°C. Liquid slag disappears at a somewhat higher temperature, solidifying at 1490°C. The formation of solid sulphides is more intense due to high sulphur content. Solid calcium aluminate phases are the same as above, but form at higher temperatures. CaO and Al_2O_3 are the main components in liquid slag inclusions: CaS solubility is up to 5%. Some SiO_2 also forms but was not included in the figures. The curves of slag components are fractions from the total liquid slag. [28]

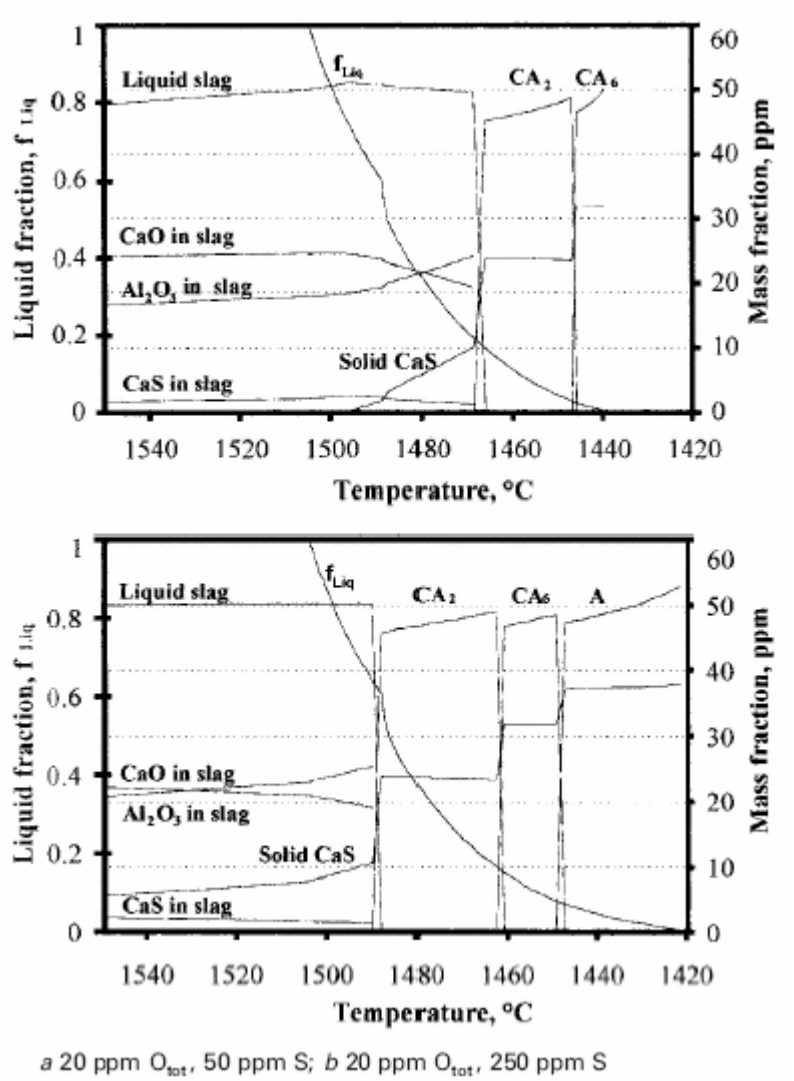

Figure 7. *Equilibrium precipitation of oxide and sulphide inclusions during steel solidification (cooling rate 1 K/s) calculated using IDS model.*[28]

Numerous samples from ladle, tundish, mould and solidified billet, bloom or slab have been analysed by the ladle metallurgy group at TKK (Helsinki University of Technology) in collaboration with the steel industry. In Figure 8 (top), inclusions in a tundish sample were analyzed with SEM-EDS. The main composition corresponded with what is in the calculations above: The inclusion-forming components were 60 ppm Otot, 20 ppm Ca, 250 ppm Al, and 250 ppm S. In the sample taken from the tundish during casting, the typical inclusion type was calcium aluminates the size of which being ≤ 5 μm. A thin CaS ring was detected around globular inclusions. The heat was cast to 140 mm billets and hot rolled to 26 mm diameter wire. Inclusions in a wire sample were investigated (Figure 8, bottom) and showed very similar characteristics: globular calcium aluminate inclusion with a CaS ring on the surface. Inclusions remained almost undeformed during rolling.[28]

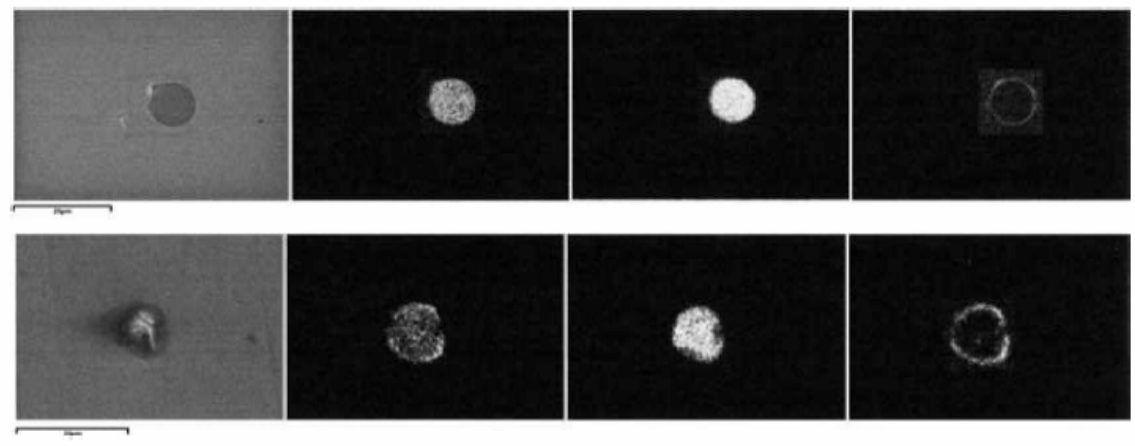

Figure 8. *Left to right: SEM images and Ca, Al, and S element maps of inclusions from tundish (top) and wire samples (bottom). Scale bar 20 μm.* [28]

1.5 Kinetics of reactions related to Ca-treatment

In this chapter reaction kinetics of the formation of CaO, CaS and calcium aluminates as well as dissolution of Al_2O_3 into slag are discussed based on the work by different authors in the literature. Further, determination of rate constant and activation energy for dissolution and reaction of solid Al_2O_3 to form liquid calcium aluminate are presented based on general kinetic treatment.

1.5.1 Kinetics of refining by powder injection

Powder injection technique was first developed for calcium-silicon (CaSi) addition into steel in the 1970s.[26] Later, cored wire technique was developed in which hollow wire was filled with CaSi powder. Such a wire was easy to be fed into the steel in a ladle. Although the technique is, nowadays, well established and widely used there are not many investigations on the basic phenomena occurring in CaSi powder injection.

Lu D.-Z. et al.[34] have applied some of the similar principles to the modelling of calcium treatment of steel as in this work. They fed steel-covered wire, with calcium inside, into 40 kg heats of AISI 1045 steel with various sulphur and aluminium contents under argon atmosphere. Samples were frequently taken during and after calcium injection for chemical and inclusion analysis from twelve experiments. Calcium absorption was found to be enhanced by higher sulphur and oxygen contents in steel. The enhancement was explained by counter current diffusion of calcium against sulphur and oxygen in the boundary layer at the injection point. Calcium diffuses through the boundary layer into the melt where it modifies oxide and sulphide inclusions. The overall interaction between oxides and sulphides with the bulk drives towards the equilibrium between lime, calcium sulphide, and dissolved oxygen and sulphur. The rate of approach to equilibrium was interpreted using a mathematical model for the multiphase kinetics of calcium absorption, deoxidation, desulphurisation, and oxide and sulphide inclusion modification during and after injection. The calcium vaporized when it was injected. Most of it escaped to the argon atmosphere; the remainder dissolved in the liquid through the vapour/melt interface where it was countered with oxygen and sulphur. The primary reaction products (calcium oxide and calcium sulphide) were then mixed into

the melt. The dissolved calcium, which did not react in the boundary layer, diffused into the melt to react with alumina to transform it to calcium aluminate. The calcium aluminate reacted with sulphur and/or manganese to form complex oxysulphide inclusions. Manganese and sulphur diffused to the primary CaO and CaS inclusions to form (Ca,Mn)S inclusions.[34]

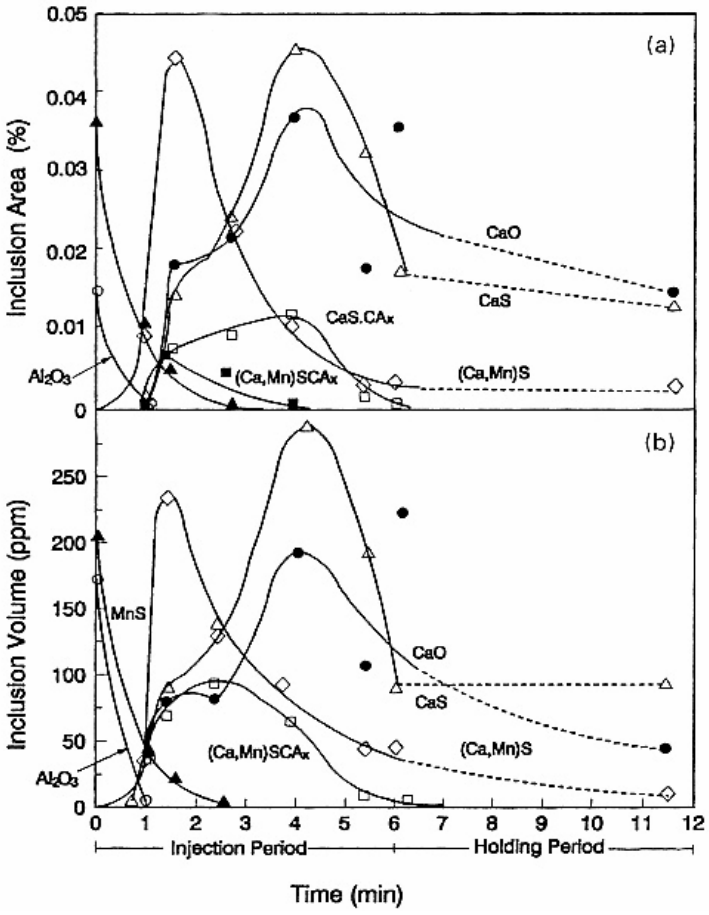

Figure 9. *(a) Area fraction of various inclusion classes throughout injection and (b) corresponding volume fractions.*[34]

All inclusions found in their study were less than 20 μm in diameter and were consistent with many other studies conducted in pilot-scale induction furnaces. Due to the small size of those inclusions, it was not possible to chemically resolve two or more phases that may have been seen in an individual inclusion. The compositions represent an average over one inclusion, and the area fractions of the various inclusion classes varied greatly during an injection. A typical example is shown in Figure 9a. The area fractions were converted to volume fractions. In Figure 9b, an interesting feature is the coexistence of inclusion types that cannot exist in real equilibrium. A dominant feature of all the results is the rapid increase and subsequent decrease of CaO, CaS, and (Ca,Mn)S. The CaO and CaS phases were formed at the calcium vapour interface.[34]

1.5.2 Reactions of CaO with Al_2O_3

Experiments between CaO and Al_2O_3, so that the steel is not present, have been made by different authors. This kind of research concerns also cements properties, because CaO and Al_2O_3 are main substances in cement. In this work reactions between CaO and

Al_2O_3 are carefully observed both with steel and without steel in order to get an idea about inclusions modification and kinetics. Kohatsu I. et al.[35] have made experiments with sintered pellets of CaO and Al_2O_3. For a temperature of 1330°C and heating times of up to twenty days, they found all the known compounds of the system CaO-Al_2O_3: $C_3A/C_{12}A_7/CA/CA_2/CA_6$. Quantitatively, these compounds were present as follows: $C_{12}A_7>>C_3A>CA_2 \sim CA$. The products C_3A, $C_{12}A_7$, and CA have random orientations, but CA_2 and CA_6 are strongly oriented so that important layers of atoms are parallel to the reaction interface. It was suggested that the orientation arises from preferred directions of crystal growth. Pt marker experiments indicated that the reaction is principally carried by Ca-ion diffusion into the Al_2O_3. The importance of grain boundary diffusion was emphasized, and in comparable experiments with single-crystal Al_2O_3, only very thin product layers were obtained. The relative phase development is correlated with properties that can be expected to be related to their diffusivities; low melting point and low packing densities generally appear to favour phase development.[35]

The phase C_3A had a coarse appearance and is obviously different from the $C_{12}A_7$; the boundary between them was very uneven. The phase CA was a thin layer with distinct boundaries. The phases CA_2 and CA_6 were small in amount but were easily seen and exhibited a "columnar" appearance.[35]

If the phase development is controlled principally by diffusion processes, the growth of product thickness ΔX is given by the following equation:

$$d(\Delta X)/dt = k/\Delta X \quad \text{or} \quad (\Delta X)^2 = 2kt \tag{11}$$

Table 4 presents data for ΔX and k values for the reaction in which the product phases were most clearly seen. Values of the melting points and of the oxygen ion densities are also given.

It is seen that k has by far the largest value for the phase $C_{12}A_7$, which has the lowest melting point and the lowest oxygen-ion density. These properties will facilitate diffusion and growth of this particular phase. The phase C_3A has a considerably smaller value of k and clearly comes second in order of phase development. It has a significantly higher melting point and somewhat more closely packed oxygen arrangement. The phases CA and CA_2, with still smaller values of k, have higher melting points, and the oxygen anions are more densely packed. The data for CA_6 seem out of line with those for the other phases; with the highest oxygen packing density equal to that of a close-packed system, it would be expected to have the lowest value of k. However, discussion of k values along these lines, which emphasize bulk rather than surface properties, must not be allowed to obscure the possible and probable importance of grain-boundary diffusion.

Table 4. Data for product phases developed in CaO-Al_2O_3 reaction. Experiments performed in air at 1330°C for 8 days under load of 2 kg/cm^2.[35]

Phases	C_3A	$C_{12}A_7$	CA	CA_2	CA_6
Product thickness, ΔX (microns)	70±5	315±5	14±3	14±3	45±5
$k = (\Delta X)^2/2t$ ($cm^2 \times 10^{-12}$/sec)	15	320	0.6	0.6	6
Melting point, °C	1539	1374	1602	1762	1830
Oxygen density g/cm^3	1.17	1.03	1.21	1.23	1.75

In this complex reaction system, as in previously studied simpler systems a sequence of product phases is formed that corresponds to those of the binary equilibrium diagram. The positions of Pt markers adjacent to the CaO surface after reaction point to the migration of Ca ions as the main cation diffusing species. The phases are formed in very unequal amounts with $C_{12}A_7$ >> C_3A > CA_6 > CA_2 ~ CA and a highly marked preferential orientation of CA_2 and CA_6. The orientation corresponds with an alignment of structural layers that are parallel to the alumina reaction surface and probably arises from preferential growth that is normal to these layers and not from particular orientation in the alumina. Comparisons of reaction-rate constants *k*, which are related to diffusivities, with physical properties (melting point and oxygen ion densities) point to low-melting points and low-packing densities favouring high diffusivity and large product development. The probable importance of grain boundary diffusion as distinct from volume diffusion is considered.[35]

Another experiments, done by Weisweiler, W. et al.[36], followed reactions between aluminium oxide powder (Al_2O_3) and natural calcite crystals ($CaCO_3$). $CaCO_3$ crystal (here calcinated to CaO) was pressed into the Al_2O_3 powder. After forty-eight hours of heat treatment at a temperature of 1400°C, a reaction zone of 200-350 microns thick had formed, as shown in Figure 10, which was analyzed in at least ten places. These so-called line analyses are obtained through the whole thickness of the reaction layers formed. The distribution of elements in such reaction layer was determined by microprobe analysis.[36]

Jerebtsov D.A. et al.[37] studied the CaO-Al_2O_3 system by using different analysis methods in content interval from 0 to 60 mass% CaO. They confirmed the absence of congruently melting compounds in argon atmosphere. They found an absence of $12CaO.7Al_2O_3$ ($C_{12}A_7$) in a dry atmosphere. $C_{12}A_7$ forms in the presence of less than 1% mass of the water absorbed in the solid and does not form after removal of this water. The existence of this compound in the presence of traces of water is confirmed in their work by the appearance of $C_{12}A_7$ that contains eutectic peaks at 1403±5°C on the first melting (synthesis) of the sample. (Trace water was gained by CaO during grinding in air of the oxide mixture but removed after melting).[37]

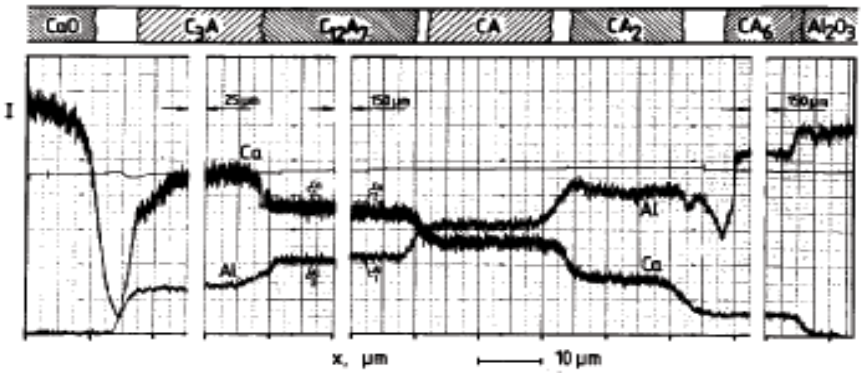

Figure 10. *Microprobe line diagram of the x-ray intensities I that are associated with the concentration, for the CaO/Al_2O_3 system, along the distance x of the reaction layer of a specimen (1400°C for forty-eight hours) containing all possible phases. To shorten the diagram, 25 microns of the C_3A, 150 microns of the $C_{12}A_7$ and 150 microns of CA_6 phases were omitted.*[36]

1.5.3 Dissolution of alumina inclusions in steelmaking slags

Fast dissolution of nonmetallic inclusions such as alumina particles in molten slags has been required in secondary steelmaking, ladle, and tundish to minimize the amount and the size of nonmetallic inclusions in steel products. There are two consecutive processes for removing the inclusions by tundish and ladle fluxes. The first process is transporting the inclusions from bulk steel to the steel/slag interface, which is determined by the fluid-flow pattern. Much work has been carried out on the fluid-flow characteristics in tundish and ladle using mathematical as well as physical water modelling. The second process, which is the dissolution of the inclusion in slag, may take place both at the steel/slag interface and in bulk slag. Cho et al.[38] have investigated the dissolution behaviour of alumina particles in molten $CaO\text{-}Al_2O_3$ and $CaO\text{-}Al_2O_3\text{-}SiO_2$ slags at the temperature between 1450 and 1550°C in terms of kinetics and mechanism. Alumina particles were directly added into the slags, and the variation of the particle size with time was determined using optical and electron microscopes. The conventional types of slag for ladle and tundish were included in the dissolution study. The effects of Al_2O_3, SiO_2, CaF_2, and MgO content on the dissolution rate of alumina particles have been determined. Based on the analysis of kinetic data, the dissolution mechanism has been discussed.

The existence of the diffusion boundary layer, accompanied with the constant dissolution rate, may indicate that the rate-limiting step of the dissolution process is the boundary layer diffusion. However, more studies on the characteristics of the diffusion boundary layer and the dissolution kinetics are necessary to determine the exact mechanism of the dissolution process, because this process involves many factors that may influence it. The relatively high activation energy of the dissolution process should not only be explained by the activation energy of diffusion in slag but also must be explained by considering the effect of temperature on the solubility of alumina in slag, which will in turn change the driving force of the dissolution of alumina. The following results came from Cho et al. and their experiments:[22]

1) The rate of alumina dissolution in $CaO\text{-}Al_2O_3\text{-}SiO_2$ slags decreases with increasing SiO_2 content in the slag;

2) The rate of alumina dissolution in $CaO\text{-}Al_2O_3\text{-}SiO_2$ slags decreases with increasing Al_2O_3 content in the slag;

3) The rate of alumina dissolution in the slags increases significantly as melt temperature increases:

4) The addition of small amounts of MgO and CaF_2 results in significant increase of the rate of alumina dissolution in tundish type slag;

5) The rate of alumina dissolution in the ladle type slags was much faster than that in the tundish type slags;

6) The dissolution process of alumina particles in the molten slags may be controlled by the liquid-phase boundary layer diffusion. However, more work is necessary to conclusively determine the exact mechanism of the dissolution process; and

7) The dissolution rate obtained by the present study is equivalent to the rotating speed of between 100 and 200 rpm by rotating disc method. [38]

Valdez et al.[39] also measured the dissolution kinetics of particles of Al_2O_3, MgO and $MgAl_2O_4$ in different steelmaking slags by direct observation of the dissolution process through the Confocal Scanning Laser Microscope (CSLM). The inclusion dissolution times in the ladle slag were much shorter for 120 micron diameter particles (~75 seconds) than the typical ladle treatment times (~15 minutes) but were significantly longer than the separation times of solid inclusions at the interface (< 5 seconds). Thus, as long as ladle slag chemistries are designed to avoid saturation, large particles should easily be removed. On the other hand, in the tundish slags studies in this work, the corresponding dissolution time of a 120 μm alumina particle was almost 4 minutes. Consequently, the inclusions are expected to remain at the slag/metal interface of the tundish for a significant time, increasing the re-entrainment risk especially during transient operation of the tundish, where operating level can fluctuate significantly. [39]

1.5.4 Determination of rate constant and activation energy

In the experimental part, different model experiments have been carried out in order to clarify kinetics and mechanisms in calcium treatment. Interaction between liquid calcium aluminate phase and alumina inclusion is a feasible step in the process. Consequently, it was taken as an object to derive the reaction-rate constant.

The reaction can be written:

$$(CaO)_{(liquid)} + x\ Al_2O_3\ _{(solid)} = (CaO\text{-}xAl_2O_3)\ _{(liquid)} \tag{12}$$

The flux of CaO in the liquid calcium aluminate transferred through the boundary layer to the surface of alumina by diffusion can be written as[40]

$$r_{CaO,1} = \frac{1}{S}\frac{dN_{CaO}}{dt} = -\frac{D_{eff}}{\Delta x}\left(C^{l}_{CaO} - C^{i}_{CaO}\right) = k_D\left(C^{l}_{CaO} - C^{i}_{CaO}\right) \tag{13}$$

where C^{l}_{CaO} is the concentration of CaO in the liquid calcium aluminate and C^{i}_{CaO} is the concentration of CaO at the interface between liquid calcium aluminate and alumina. Assuming the reaction is of the first order with respect to CaO, the dissolution rate of CaO on unit surface S can be given as the following:

$$r_{CaO,2} = \frac{1}{S}\frac{dN_{CaO}}{dt} = k_R C^{i}_{CaO} \tag{14}$$

At a steady state the flow rate to the surface is equal to the reaction rate at the surface.

As $r_{CaO,1} = r_{CaO,2}$, it follows from Equations (13) and (14): $k_D\left(C^{l}_{CaO} - C^{i}_{CaO}\right) = k_R C^{i}_{CaO}$ which can be written:

$$C^{i}_{CaO} = \frac{k_D}{k_D + k_R} C^{l}_{CaO} \tag{15}$$

Replacing equation (15) into either equation (13) or (14) and then eliminating C^i_{CaO}, which cannot be measured, gives the following:

$$r = r_{CaO,1} = r_{CaO,2} = -\frac{1}{\frac{1}{k_D} + \frac{1}{k_R}} C^l_{CaO} = k_{overall} C^l_{CaO} \qquad \left[\frac{mol}{m^2 \cdot s}\right] \tag{16}$$

Rate, r, in equation (16) means that moles of CaO are reacting per unit volume per unit time.[40]

For the chemical reactions considered in the following paragraphs, we take as the basis of calculation a species A, which is one of the reactants disappearing as a result of the reaction. The limiting reactant is usually chosen as our basis for calculation. The rate of disappearance of A, $-r_A$, depends on the temperature and composition. For many reactions it can be written as the product of a reaction-rate constant *k* and a function of the concentrations (activities) of the various species involved in the reaction. That is to say[41]

$$-r_A = [k(T)][fn(C_A, C_B, ,,,)] \tag{17}$$

This rate law gives the relationship between the reaction rate and the concentration. The reaction-rate constant *k* is not truly a constant but is merely independent of the concentrations of the species involved in the reaction. The quantity *k* is also referred as the specific reaction rate (constant). It is almost always strongly dependent on the temperature. In liquid systems, it can also be a function of total pressure and, in addition, can depend on other variables that normally exhibit much less effect on the specific reaction rate than temperature. So for the purposes of the material presented here, it will be assumed that *k* depends only on the temperature. This assumption is valid in most laboratory and industrial reactions and seems to work quite well.

It was the great Swedish chemist Arrhenius who first suggested that the temperature dependence of the specific reaction rate, *k*, could be correlated by an equation of the type:

$$k(T) = Ae^{-E/RT} \tag{18}$$

where A = pre-exponential factor or frequency factor

E = activation energy, J/mol

R = gas constant =8.314 J/mol·K

T = absolute temperature, K

This equation, known as the Arrhenius equation, has been empirically verified to give the temperature behaviour of most reaction-rate constants within experimental accuracy over fairly large temperature ranges.

The activation energy *E* has been understood as a minimum energy that the reacting molecules should possess before the reaction will occur. From the kinetic theory of

gases, the factor $e^{-E/RT}$ gives the fraction of the collisions between molecules that together have this minimum energy *E*.

The activation energy is experimentally determined by carrying out the reaction at several different temperatures. After taking the natural logarithm of equation (18),

$$\ln k = \ln A - \frac{E}{R}\left(\frac{1}{T}\right) \tag{19}$$

it can be seen that a plot of (ln *k*) versus (1/T) should be a straight line whose slope is proportional to the activation energy. The larger the activation energy, the more temperature-sensitive is the rate of reaction. To determine activation energy it is necessary to measure the rate of the reaction at several temperatures and in a sufficient temperature range. [40]

When the value of the activation energy is known it is possible to make deductions about the rate controlling factor in the reaction. The activation energy value can be different at different temperatures and temperature ranges, this being an evidence of a change in the rate controlling factor or reaction mechanism. The concept is applied in the discussion part.

1.6 Inclusion analysis by automated SEM/EDS program

In this work, a program called INCASteel with INCAFeature and Inclusion Classifier has been used. Similar kind of programs are SULKA program used by Outokumpu Stainless in Tornio, Finland and ASCAT (Automated Steel Cleanliness Analysis Tool) used in Steelworks in the United States of America.

Story S.C. et al.[42] have worked with the ASCAT program and have received results to clarify casting-related issues at U.S. Steel Gary and Fairfield Works. Examinations were made in order to discover the causes of clogging and to predict casting behaviour and erosion.

Until now, usually an analysis is performed on samples using a scanning electron microscope (SEM) or conventional metallography long after the steel has been processed. Also, in any given sample, there are inclusions of varying chemistry present, and an analysis of a single or even several inclusions may not truly reflect the cleanliness or the type of inclusions present. To overcome these problems, the R.J. Lee Group and a number of partners, including several steel companies, with a grant from the U.S. Department of Energy have developed an Automated Steel Cleanliness Analysis Tool (ASCAT). It is designed around a computer-controlled scanning electron microscope (CCSEM) and is capable of rapidly analyzing several hundred inclusions.

The goal of the ASCAT is to take a sample from steel melt, to prepare the sample, perform a complete analysis of the inclusion with respect to size and chemistry, and report the results to the operator in a clear, simple manner in less than one hour. One of the tasks of the overall project is to rapidly analyze the data and to display the results in such a manner that will clearly indicate to the metallurgist or operator whether the steel and/or processes are satisfactory. If the heat is not satisfactory, it could be corrected or

the heat could be downgraded before costly downstream processing, and the problem could be prevented in subsequent heats.

When calcium is added to steel, it can modify alumina (Al_2O_3) inclusions to calcium aluminates or react with sulphur to form CaS. The calcium aluminates can be solid or liquid at steelmaking temperatures. For example, $CaO.6Al_2O_3$ (CA_6) has a high melting point of 1833°C, whereas the eutectic temperature between $3CaO.Al_2O_3$ (C_3A) and $CaO.Al_2O_3$ (CA) is only 1362°C. In general, liquid inclusions are desired to avoid clogging during casting and the occurrence of large alumina clusters in the product. The governing chemical reaction determining what inclusions form can be written as:

$$(Al_2O_3) + 3\ CaS = 3\ (CaO) + 2\ [Al] + 3\ [S] \qquad (20)$$

The parentheses indicate that the species is a part of an inclusion. If the Al and/or S content are high, the reaction shifts to the left, and solid alumina rich oxide inclusions and calcium sulphides are formed. However, if Ca usage is excessive it is possible to get inclusions too rich in CaO, which can cause nozzle or ladle gate erosion.

Fourteen calcium-treated Al-killed heats made at Gary Works representing ladle gate behaviour associated with clogging, erosion, and stable casting (i.e., either clogging or erosion) were analyzed to determine whether the casting performance could be related to the inclusions present. To examine the inclusions in these types of steels, a technique was developed in which the inclusion composition is plotted on a Ca-Al-S ternary diagram. In general, the inclusions were duplex, consisting of a calcium aluminate phase and a calcium sulphide phase. Once an inclusion was identified as an oxide inclusion containing these elements, the composition was normalized to these elements. The boundaries for liquid oxide inclusions are shown in Figure 11. The left boundary is shown at a value of 0.4 mole fraction Al but may be closer to 0.45, according to a published phase diagram. [42]

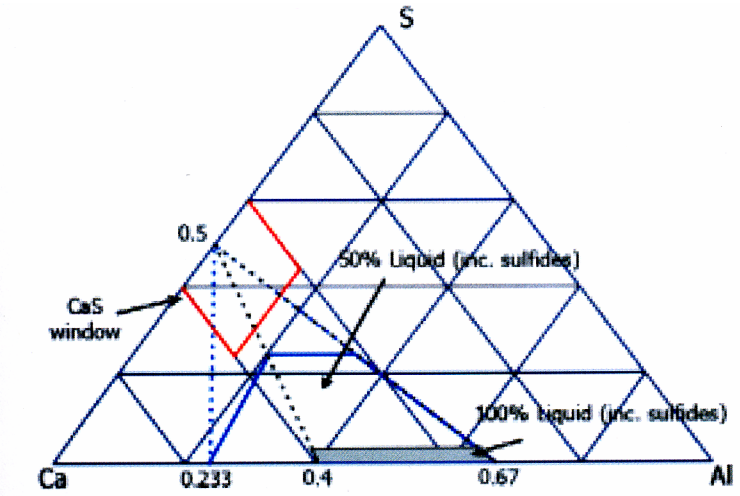

Figure 11. *Liquid oxide inclusion region (grey area) indicated on a "CaO"-"Al_2O_3"- S ternary phase diagram.*[42]

If the inclusion composition is to the right of the right boundary, plugging or clogging may occur; in the liquid region, casting should be stable; and, to the left, erosion may occur.

In the preliminary analysis of the results, it was found that the amount of erosion was proportional to the area of CaS inclusions. Based on these findings, a CaS window in the Ca-Al-S diagram, as indicated in Figure 11, was developed to define inclusions with large amounts of CaS.

A reason why CaS or Ca-rich inclusions cause erosion is the occurrence of Equation 12 on the alumina nozzle, thereby dissolving alumina. Often found that CaS is in the material, clogging a nozzle and occurs when the sulphur content is high (>0.01%) and a mixture of solid $CaO{\cdot}Al_2O_3$ (CA) and CaS clog the nozzle. In the present case, the sulphur is low, typically less than 0.003%. In this case, due to high levels of Ca combined with low sulphur, CaS along with Ca-rich calcium aluminate inclusions form, both of which have the potential to dissolve alumina-based refractories.

The results from the fourteen heats at Gary Works showed a certain pattern. When casting was stable, a significant portion of the inclusions fell within the liquid region. When there was erosion, the inclusion compositions were to the left of the liquid region, and compositions were to the right for clogging. These three heats showed clear evidence of stable casting, erosion or clogging, and the inclusion compositions clearly reflected this.

Considering that some of the Ca is present as CaS, the theoretical parameter that will indicate the type of oxide present is given by

$$"Ca/Al" = \frac{Ca-(S-2)}{Al} \tag{21}$$

where Ca, Al, and S are the Ca, Al, and S content of the inclusions, respectively (atomic%). This parameter has been defined as the “modified Ca/Al ratio” to account for CaS in the duplex inclusions. The deduction of sulphur accounts for Ca and CaS. The number 2 in Equation 21 represents the approximate solubility of S in liquid calcium aluminates. In theory, at 1600°C, this ratio should be between approximately 0.5 and 1.5 for the oxide portion of the inclusions to be liquid. However, in the upper end of this range, erosion may occur. The present case may be affected by the shift to Al-rich inclusions during solidification, but the shift is small for quenched samples.

The results from real heats indicate that stable casting is achieved when the ratio is greater than 0.4, which is in the two-phase region (liquid plus solid $CaO{\cdot}Al_2O_3$). Erosion occurred when the ratio exceeded about 0.8, which is toward the centre of the liquid region for the $CaO{\cdot}Al_2O_3$ system at steelmaking temperatures. When the Ca/Al ratio is below 0.4, plugging of the ladle slide gate occurred at varying points within a heat. Clogging was observed at the middle of a heat when the Ca/Al ratio was in the range of approximately 0.2-0.4. With Ca/Al ratios of less then 0.2, clogging of the ladle gate was evident almost immediately after the ladle was opened.

In one heat, a large fraction of the total inclusion area was from inclusions containing Na, which is indicative of mould slag. This is important in itself, indicating the entrainment of slag from improper pouring or sampling practices. Also, in this case, this

fraction of the inclusions should not be included in computing the Ca/Al ratio, since it skews the results to a generally higher Ca/Al ratio. Based on this, whenever there is evidence of tundish or mould slag, it is reported on the summary sheet.

For the stable heats, the percentage of Al loss during processing was typically 10-20% and was evidently less for those heats where erosion was observed. When there was plugging, more than 30% and often more than 50% of the Al was lost from the steel. In addition, for heats showing a clogging tendency, the Ca content of the steel was also generally lower than normal. Both the low Ca and high Al loss indicate that reoxidation of the steel is the likely cause of the clogging. Unstable oxides, such as FeO, in the ladle slag or exposure of the steel to air due to excessive Ar bubbling, will cause Al to be oxidized and increase the Al_2O_3 content of the calcium aluminate inclusions. Subsequent to these findings, practices have been modified to further reduce FeO levels in the ladle slag in calcium-treated heats. Knowledge of the consequences of reoxidation in Ca-treated heats has also directed attention towards avoidance of excessive stirring, especially after the addition of CaSi wire. In the time since these changes, the occurrence of plugging in CaSi heats has been practically eliminated.

The article by Story S.C. et al.[42] demonstrated that the ASCAT is a valuable tool in identifying casting problems and their causes. The results from trials at Gary Works showed that inclusion compositions from samples of the liquid steel plotted on a Ca-Al-S ternary-phase diagram will predict if there will be stable, eroding or clogging conditions during casting. The modified Ca/Al ratio is also a good predictor of casting behaviour. The results also helped to identify the likely source of clogging caused by solid Al_2O_3-rich calcium aluminate inclusions, which may have been caused by excessive argon stirring or oxidizing ladle slag that caused reoxidation. [42]

2. AIMS OF THE CURRENT WORK

The overall aims of the doctoral thesis were to simulate Al_2O_3 inclusion modification during Ca-treatment in steelmaking. To do this, different methods were used. Alumina inclusion transformation during Ca-treatment could be divided into two steps. In step one, dissolved calcium and oxygen interact and react in molten steel with alumina particle to form a layer of liquid calcium aluminate. The first step is influenced by steel composition. The second step is to study the progress of the modification process through examining the interaction between liquid calcium aluminate and solid alumina. The second step was simulated by studying reaction between CaO and Al_2O_3.

Experimental works were done concerning reactions between Al_2O_3 and Ca or CaO with steel and without steel present. Inclusions in steel samples from real steelmaking practice were studied. The following are the novelty ideas of the work:

- To measure reaction constant k and to calculate activation energies for the reaction between Al_2O_3 and CaO in the temperature range of 1350-1600°C;
- To find a sequence of inclusion transformation during Ca-treatment;
- To propose a kinetic model by using the measured rate constants; and
- To clarify the existence of different calcium aluminates in steels inclusions.

3. EXPERIMENTAL APPARATUS AND PROCEDURE

3.1 Experiments with CaO and Al_2O_3

The reactions between Al_2O_3 and CaO in the temperature range of 1350-1600°C were investigated in a resistance furnace that can attain up to 1700°C. The furnace was heated by platinum-rhodium alloy windings. The temperature was controlled by a B-type thermocouple. The experiments were carried out in air atmosphere.

CaO powder was prepared by calcinating $CaCO_3$ powder at 1050°C for two hours. The $CaCO_3$ powder was delivered by Riedel-de Haen AG Germany. Its composition is listed in Table 5. The CaO powder was pressed with a hydraulic compressor under 100 bars to form a cylinder 6mm in diameter and 2.8 mm in height. Finally, the cylinder was sintered at 1600°C for three hours. After sintering, the CaO cylinder shrunk to 5.2 mm in diameter and 2.4 mm in height, having a density of 2880 kg/m^3 (86% of theoretical density). Alumina plates (density 3790 kg/m^3(95,7% of theoretical density), 3 mm high, and Al_2O_3 content >99.5%) were from a German company, FRIATEC AG. The alumina plates were cut and ground into small cylinders with similar diameter to CaO samples. The picture of the samples and the SEM pictures of the surface of CaO and Al_2O_3 cylinders are shown in Figures 12 and 13.

Table 5. Chemical composition of $CaCO_3$, in weight percentage.

$CaCO_3$	Insoluble in HCl	Ba	Cu	Fe	K	Mg
Min. 99	Max. 0.005	Max. 0.005	Max. 0.0005	Max. 0.001	Max. 0.01	Max. 0.05
Na	Pb	Sr	Cl	N	SO_4	
Max. 0.2	Max. 0.0005	Max. 0.1	Max. 0.005	Max. 0.001	0.01	

When the furnace reached the desired temperature, a CaO cylinder (about 0.142 g) was put above an Al_2O_3 cylinder (about 0.280 g) and pushed into a high-temperature zone within about two minutes. After annealing a certain time, the sample was quenched by pushing it to the cooled end of the furnace. In the lower temperatures less than 1420°C the cylinder of CaO was pushed between two Al_2O_3 cylinders with an alumina tube that was pushed against them. The cylinders were lying on a platinum plate in the furnace. Two identical tests were made; one for SEM-analysis and another to be put in 10 w-% HCl acid to find out the reacted amount of Al_2O_3.

The samples were then coated by carbon and the composition of the reaction products (calcium aluminates) were analyzed by SEM-EDS. Finally, the samples were put into 10w-% HCl solution for about eight hours; the unreacted CaO and the calcium aluminates formed by the reaction were all dissolved into the acid solution; and only the unreacted alumina remained left. The mass of alumina plate did not change after it was

kept in HCl solution for forty-eight hours. It was thus stated that the mass of Al_2O_3, which had reacted and dissolved, could be calculated. Some samples were ground perpendicular to the original interface with the SiC polishing paper. Ethanol was used as grinding liquid. The polished interface was observed by an optical microscope and a SEM to investigate the reaction mechanisms. Combining the compositions measured by EDS, the reaction-rate constant could be measured.

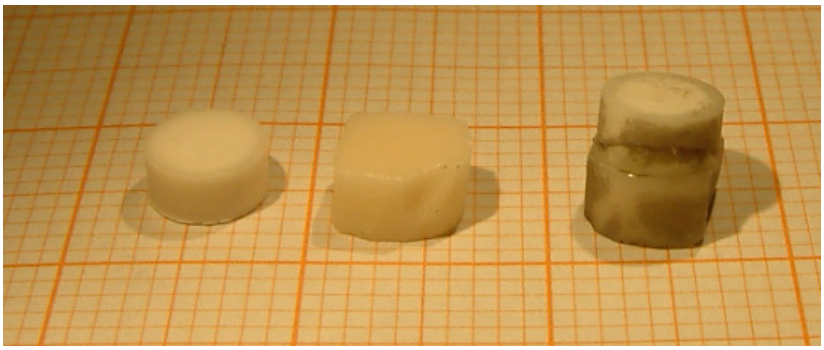

Figure 12. *CaO and Al_2O_3 cylinders before the experiment (left) and a sample package after the annealing (right).*

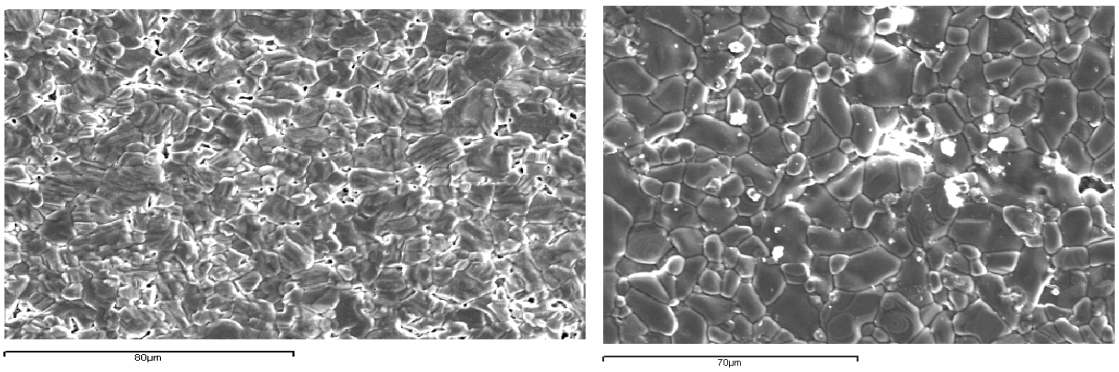

Figure 13. *SEM picture showing the surface of CaO and Al_2O_3 samples. (SEI)*

Scanning electron microscopes (SEM) LEO has been designed to deliver the most informative images in all applications. SEM pictures can be taken as a secondary electron image (SEI) or as backscatter electron image (BEI). From the backscatter electron image it is possible to see different phases better because the contrast of an element or phase depends on its atomic or molecular weight. Some of the SEM images in this work are done with SEI mode and some with BEI mode.

The EDS microanalysis system for SEM has been developed by INCAEnergy Energy Dispersive (EDS) System, Oxford Instruments.

3.2 Ca-treatment on a laboratory scale

Experiments were performed in an 8 kg induction furnace to verify the mechanism of transformation of alumina inclusions during Ca-treatment. A drawing of the vacuum induction furnace is shown in Figure 14, where different parts of the furnace can be

seen. Four different tools (e.g., a thermocouple for temperature check, a dropping tool for additions, and a holder for sample taking), were located in rotating mechanism 20, 23 and 28. All of these tools could only be used one at a time through the pre-vacuum chamber which is located on the top of the big chamber.

Steel deoxidised with aluminium was melted under vacuum and then the atmosphere was turned to 0.6 bar argon (max 2 ppm oxygen). When a proper temperature (1580-1600°C) was achieved, a sample was taken from the melt. Then CaSi powder corresponding to 100 ppm [Ca] was immersed into the melt inside a steel rod. Part of the calcium dissolved into the steel whereas a significant fraction vaporised out from the melt. Samples were first taken at a rate of one per minute and then were taken less often. The samples were analysed for Al and Ca with the AAS (Atomic Absorption Spectroscopy) method. Inclusions were investigated by using the SEM-EDS technique.

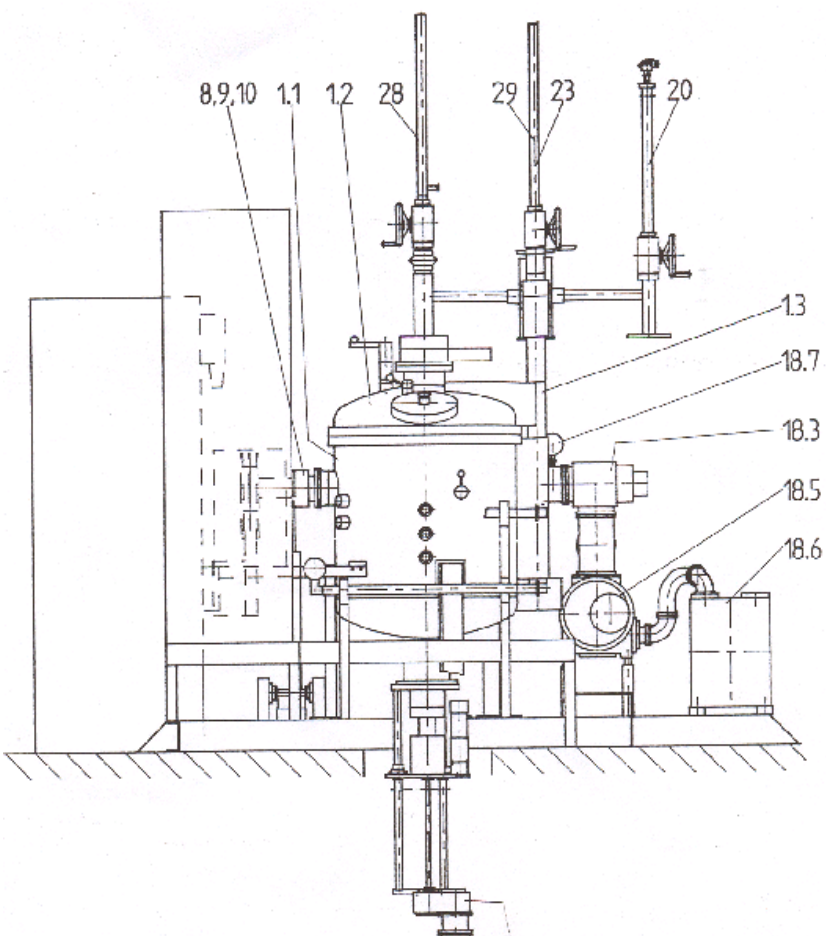

Figure 14. *Vacuum induction furnace and its auxiliary devices.*

3.3 Industrial experiments at steelworks

Industrial samples were taken from selected heats at two Finnish steelworks Koverhar and Imatra. Both steelworks belong to Ovako company; Koverhar belongs to Ovako Wire division and Imatra to Ovako Bar division.

Samples were taken with the standard lollypop shaped sample holder where the steel is sucked through quartz tube into the oval flat steel container. SEM/EDS inclusion analyses were made from the samples flat container section by grinding, polishing and coating with carbon to get a good image without scratches or electrical charging.

Process route for making steel in Koverhar works is shown in Figure 15. Desulphurization is done before BOF and deoxidation is done after it when pouring the steel into a ladle and transferring the ladle to the ladle treatment station. Secondary steelmaking in Koverhar included ladle furnace and calcium-silicon wire feeding system. Imatra steelworks process route is somewhat different from the Koverhar route. It starts with scrap melting in an electric arc furnace (EAF), then the steel is tapped to the ladle and transferred to the secondary metallurgy station which is supplied with facilities for CaSi powder injection via a lance into the steel melt, as well as with the ladle furnace with inductive stirring option and vacuum tank degassing too.

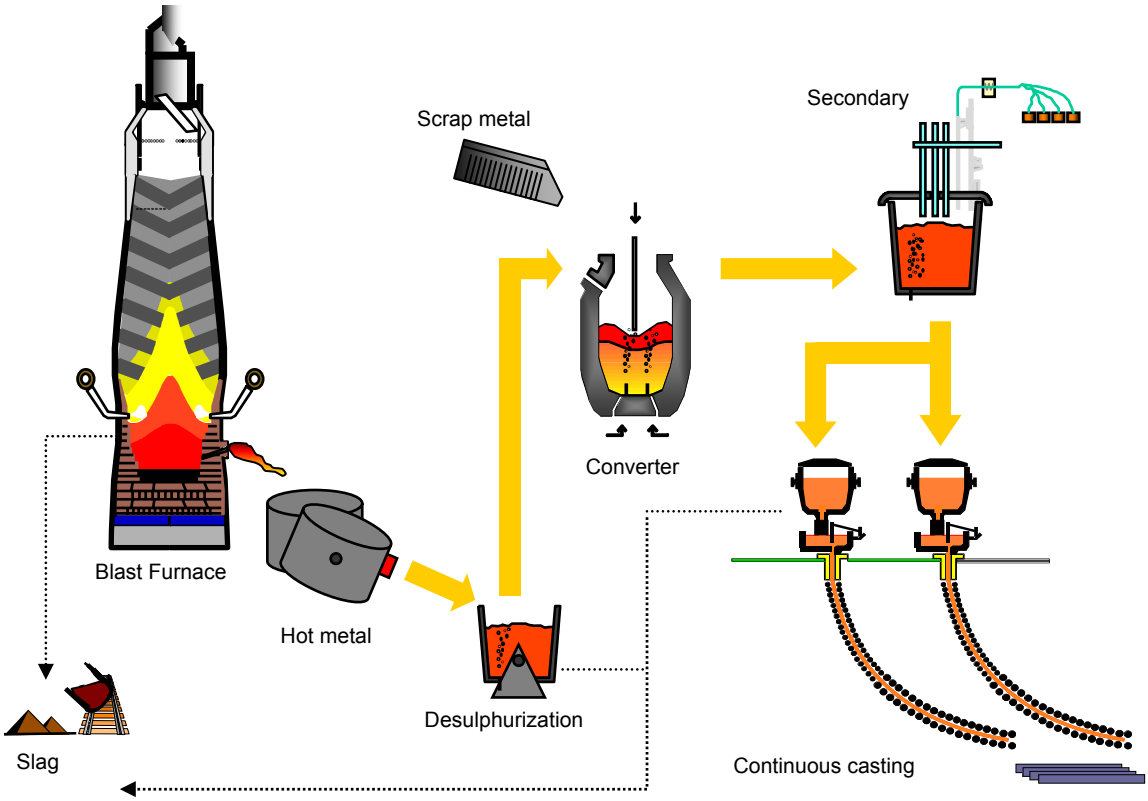

Figure 15. *Process outline of Koverhar steelworks*

4. EXPERIMENTAL RESULTS

Different kinds of experiments have been performed to get more knowledge about the reactions between alumina inclusions and calcium or calcium oxide. The methods and equipment for laboratory experiments have been introduced in the previous section. In this section there are also the results from the series of Ca-treatment test trials in Finnish steel works.

4.1 Reaction kinetics between CaO and Al_2O_3

The experimental results are divided here to a high-temperature range 1420-1600°C where the liquid region in CaO-Al_2O_3 diagram is quite distinct and to a low-temperature range below 1420°C in which the reaction between the two oxides turns more and more to a solid-state reaction. The results of the high-temperature range are first discussed.[43]

4.1.1 High-temperature range 1420−1600°C

The phases formed during the reaction between Al_2O_3 and CaO were examined by a SEM-EDS. The line-scan results of Ca and Al on the cross-section of two typical samples are shown in Figure 16 and Figure 17. In Figure 16 the reaction layer is 1250 µm thick when the sample has been annealed at 1500°C for ten minutes. This layer is almost all liquid, but in both ends of the layer, a thin area with the presence of both aluminium and calcium can be seen: Even the material seems similar with the start materials. In Figure 17 the reaction layer is 580 µm thick when sample has been annealed in 1500°C for five minutes. In Appendix II, values for the calculated, from dissolved amount of Al_2O_3, reaction layer thicknesses are in 1500°C ten minutes 1685 µm and five minutes 706 µm. These values are bigger than the measured value from the SEM image because the reaction layer is not levelled everywhere, which is especially true in the low-temperature range.[43]

When thinking about the reaction between CaO and Al_2O_3, one of the two steps could be the rate-controlling step during the interaction between the liquid calcium aluminate and solid alumina: (1) calcium diffusion in the liquid calcium aluminate layer, or (2) the chemical reaction at the alumina/calcium aluminate interface. If the rate is controlled by the calcium diffusion in the liquid product layer, there should be a significant calcium concentration gradient in the liquid product layer; however, as shown in Figure 16 and Figure 17 the calcium concentration in the liquid layer was quite homogenous. Therefore the chemical or dissolution reaction between alumina and calcium aluminate seems to be the rate-controlling step.[43]

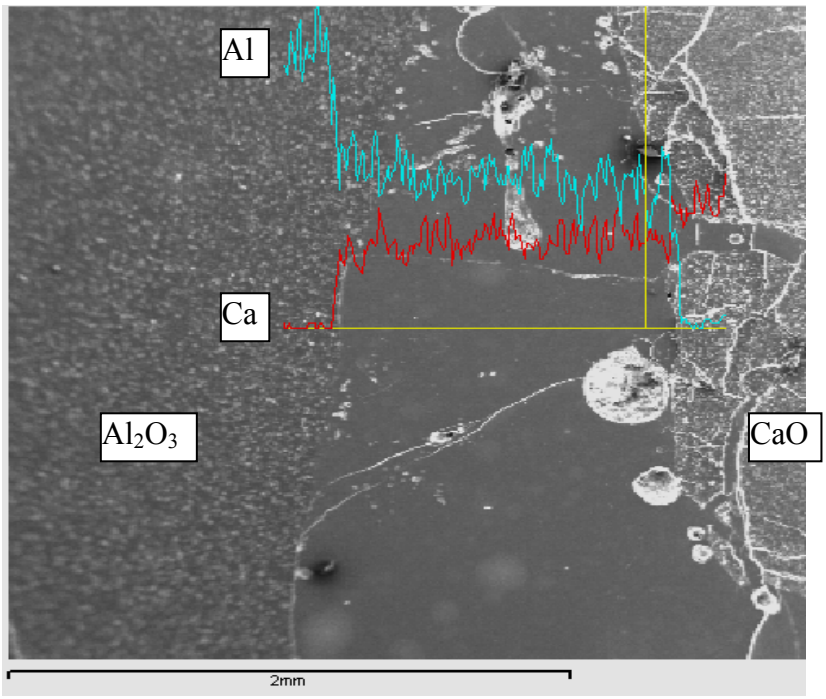

Figure 16. *SEM (SE- image) showing a cross-sectional view of the interfaces and the line scan results of Ca and Al by EDS. Annealed at 1500 ℃ for ten minutes.*[43]

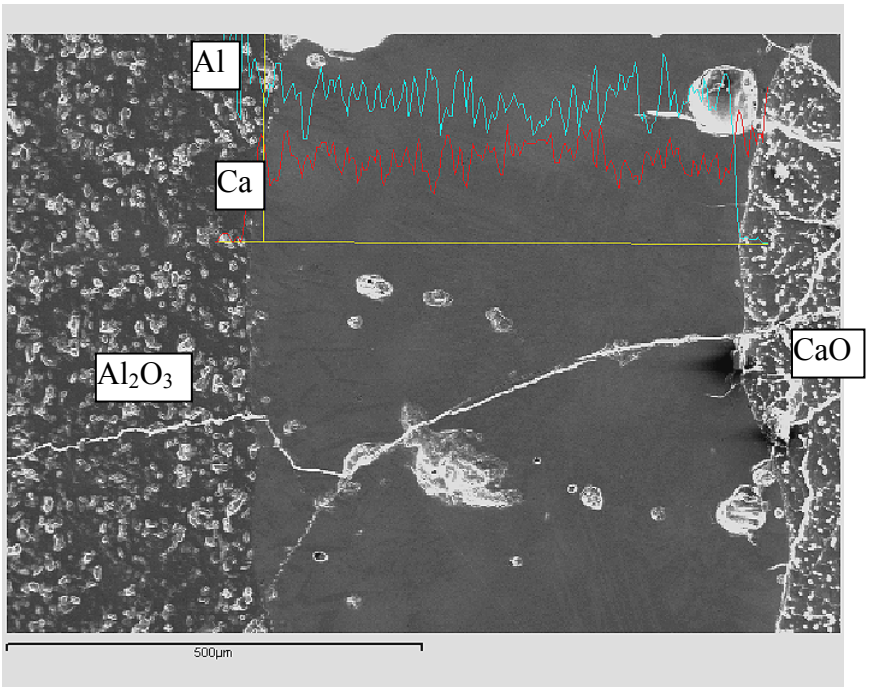

Figure 17. *SEM (SE-image) showing a cross-sectional view of the interfaces and the line scan results of Ca and Al by EDS. Annealed at 1500 ℃ for five minutes.*[43]

On the other hand, by examining the cross section of the reacted couple, any clear layers of CA_6, CA_2, or CA phases could not be found in the reaction product. These phases should be in solid state if they were formed. The modification process, than, should be

controlled by calcium diffusion in the solid phases because the diffusion in the solid state is very slow. In the current experimental work, a 2.4 mm thick CaO cylinder was totally liquidized into calcium aluminate in two or three minutes at 1600°C. The interface between CaO and calcium aluminate as well as between calcium aluminate and Al_2O_3 are shown in Figure 18.[43]

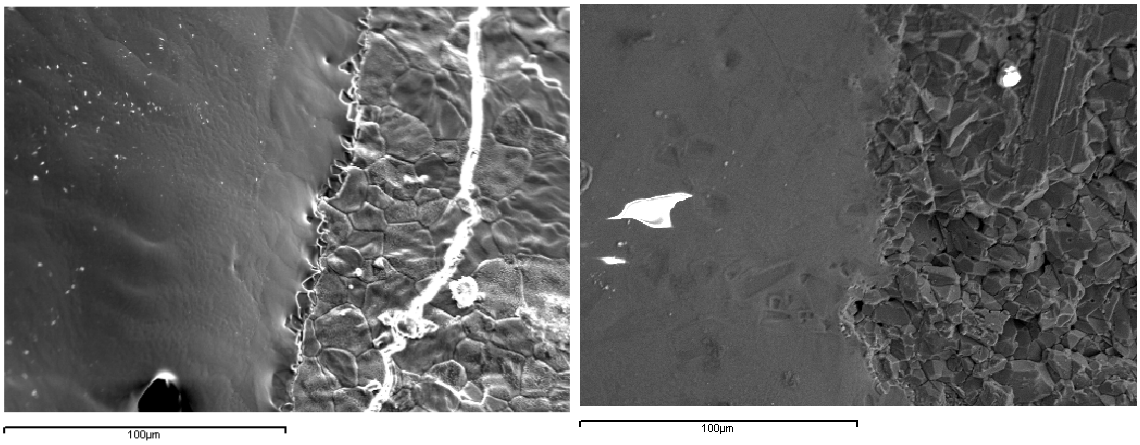

Figure 18. *SEM (SE-image) showing the Calcium aluminate/CaO interface (left) and Calcium aluminate/Al_2O_3 interface (right).*[43]

4.1.2 Low-temperature range below 1420°C

As shown in Figure 1 the liquid region in the CaO-Al_2O_3 phase diagram becomes quite narrow when approaching 1400°C and it totally disappears at 1362°C. Observations of reaction kinetics showed an abrupt slow-down from 1390°C to 1370°C (Figure 19). So the temperature has much larger effect on forming a reaction layer than the holding time in a furnace. At low temperatures (1350°C and 1370°C), the extension of holding time did not greatly affect the amount or thickness of the reaction layer which must be due to disappearance of the liquid calcium aluminate phase when the temperature is decreased. At 1390°C, the liquid region still exists, although quite narrow. At 1370°C, it should almost disappear, and below 1362°C, no liquid phase should be formed.

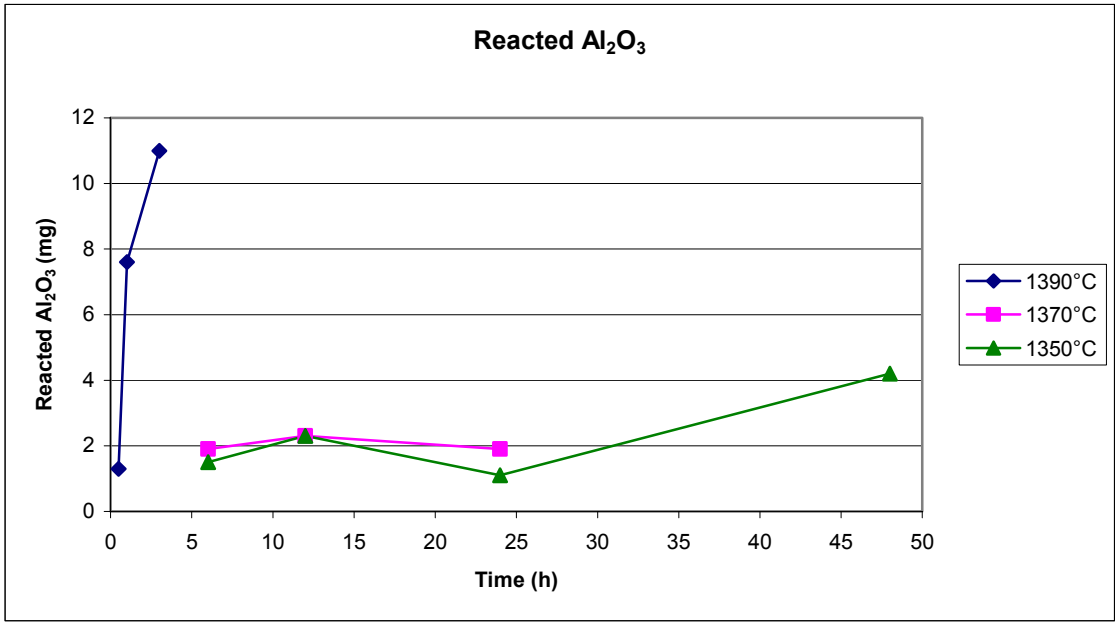

Figure 19. *Reacted Al_2O_3 amount as function of time at three different temperatures.*

Linescan analyses from the experiments at temperatures 1405°C and 1390°C can be seen in Figure 20, Figure 21 and Figure 22. In Appendix I, there are more results from experiments in the low-temperature range (i.e., 1405°C, 1390°C, 1370°C, and 1350°C with different holding times). These figures (a1-a13 in Appendix I) show analyses made with a SEM/EDS, giving the amount of CaO and Al_2O_3 in different points on line in the reaction layer. The point analysis results for Figure 21 are also in Appendix I in Figure a14. In these low temperatures, different calcium aluminates can be found. From the forming phases, $C_{12}A_7$ is the dominant phase in the reaction layer. The next common phase is C_3A. Phases CA_2, CA, and CA_6 could be clearly detected only in some samples as very thin layers.

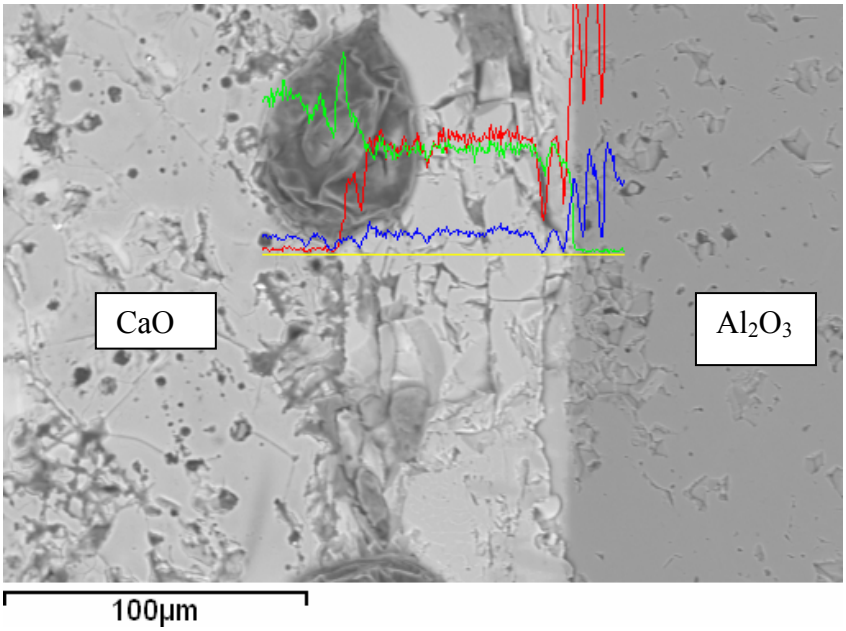

(a)

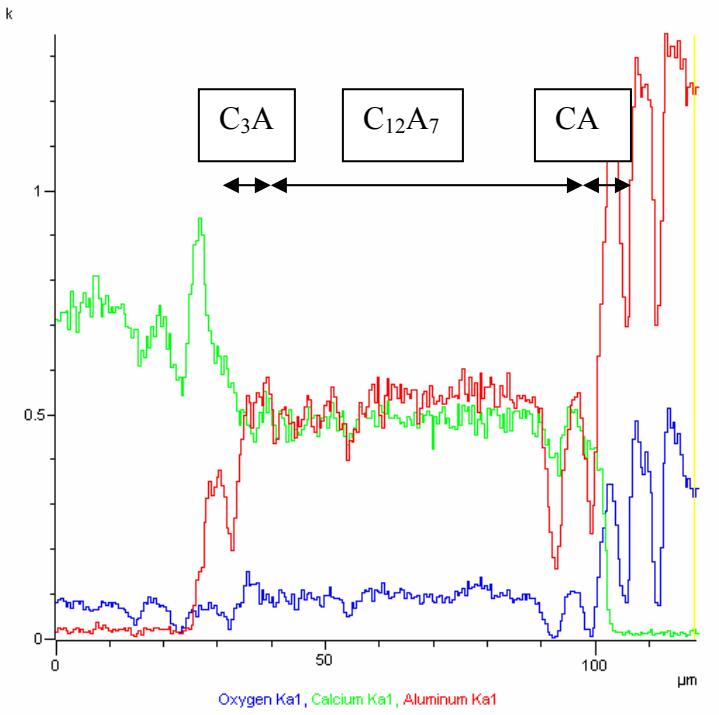

(b)

Figure 20. *Test 18, 1405°C, 12 min. Phases C_3A, $C_{12}A_7$ and CA. (Lines: blue=oxygen, green=calcium and red=aluminium). (a) BE-image from the reaction layer (b) Linescan from the 80 µm thick reaction layer.*

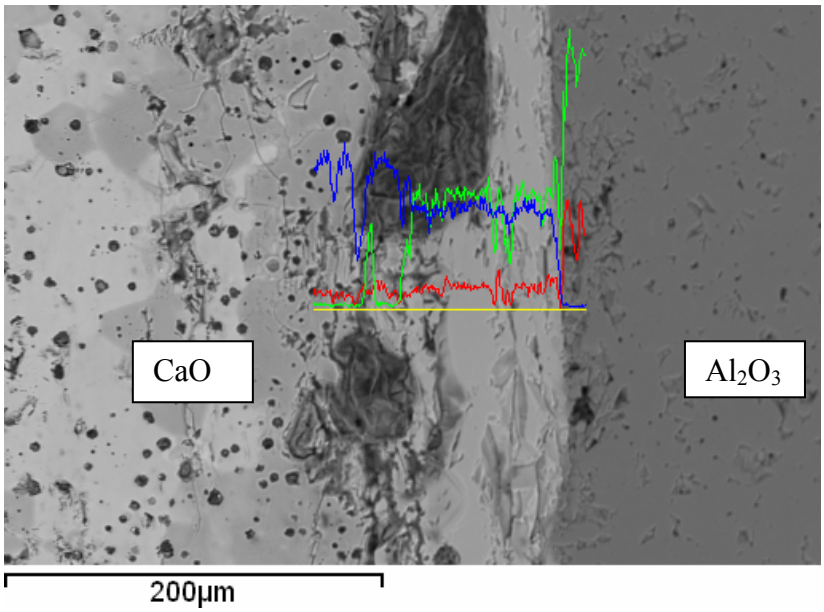

(a)

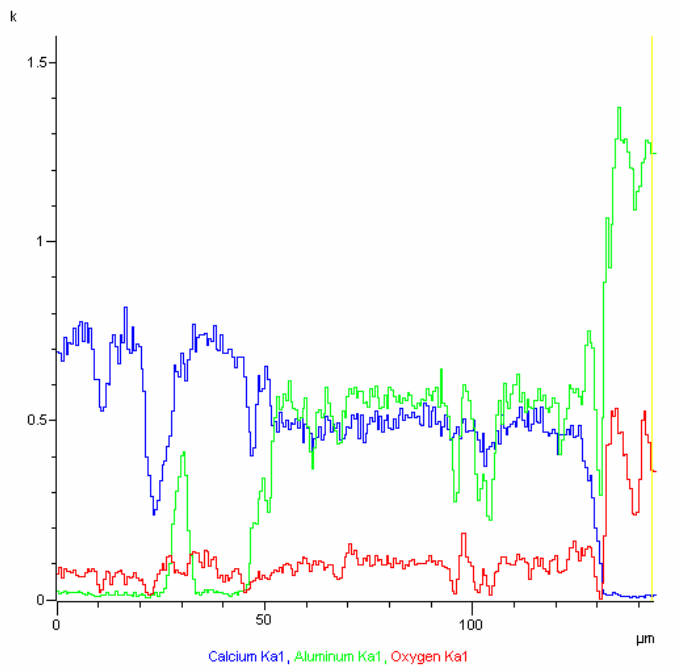

(b)

Figure 21. *Test 18, 1405°C, 12 min. Phases C_3A, $C_{12}A_7$ and CA. (Lines: blue= calcium, green=aluminium and red= oxygen). (a) BE-image from the reaction layer (b) Linescan from the 80 µm thick reaction layer.*

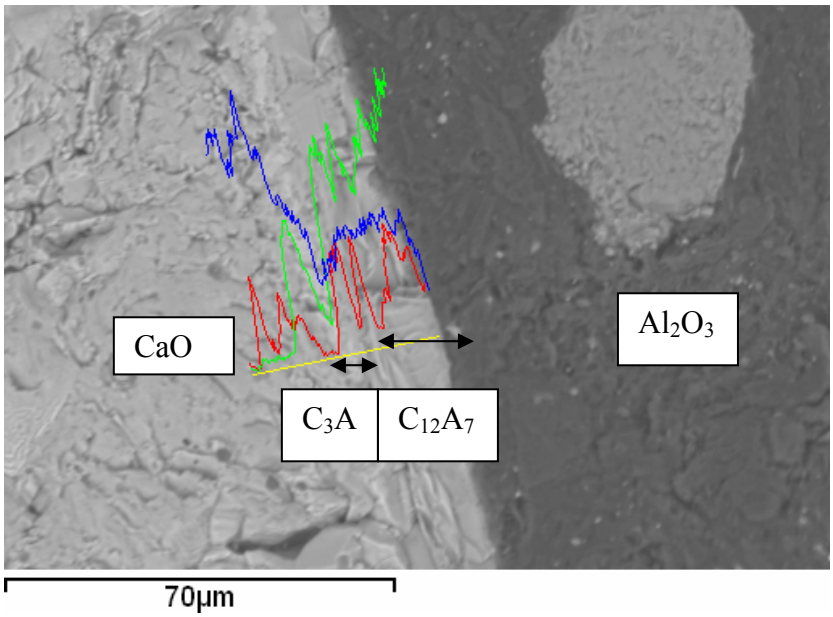

Figure 22. *Test 14, 1390°C, 42 min. Phases C_3A and $C_{12}A_7$. (Lines: blue= calcium, green=aluminium, and red= oxygen). BE image from the 40 µm thick reaction layer.*

4.1.3 Reactions between CaO and Al_2O_3 powders

Experiments using γ-alumina powder and similar CaO powder as in previous experiments were performed. A cylinder 11.5 mm in diameter was pressed from a well mixed powder combination. In experiment number 28, 0.566 g of CaO powder and 0.709 g of Al_2O_3 powder were used to make the cylinder. This cylinder was kept in a laboratory furnace for six hours at 1400°C. Figure 23 shows results from SEM/EDS taken from this sample. The dark particle in the BE-image is an alumina grain that has reacted with CaO. Linescan shows the phase CA on vector 0-8 µm, phase CA_2 on vector 8-13 µm, and 13-22 µm is pure alumina particle. Phases have been verified by point analysis. Figure 24, Table 6, and Figure 25 show results from this same experiment 28 done with x-ray diffractometer. It should be noticed that XRD was a semi-quantitative method only. Anyway, we can see that the same calcium aluminate phases can be detected with both methods (SEM/EDS and x-ray diffractometer).

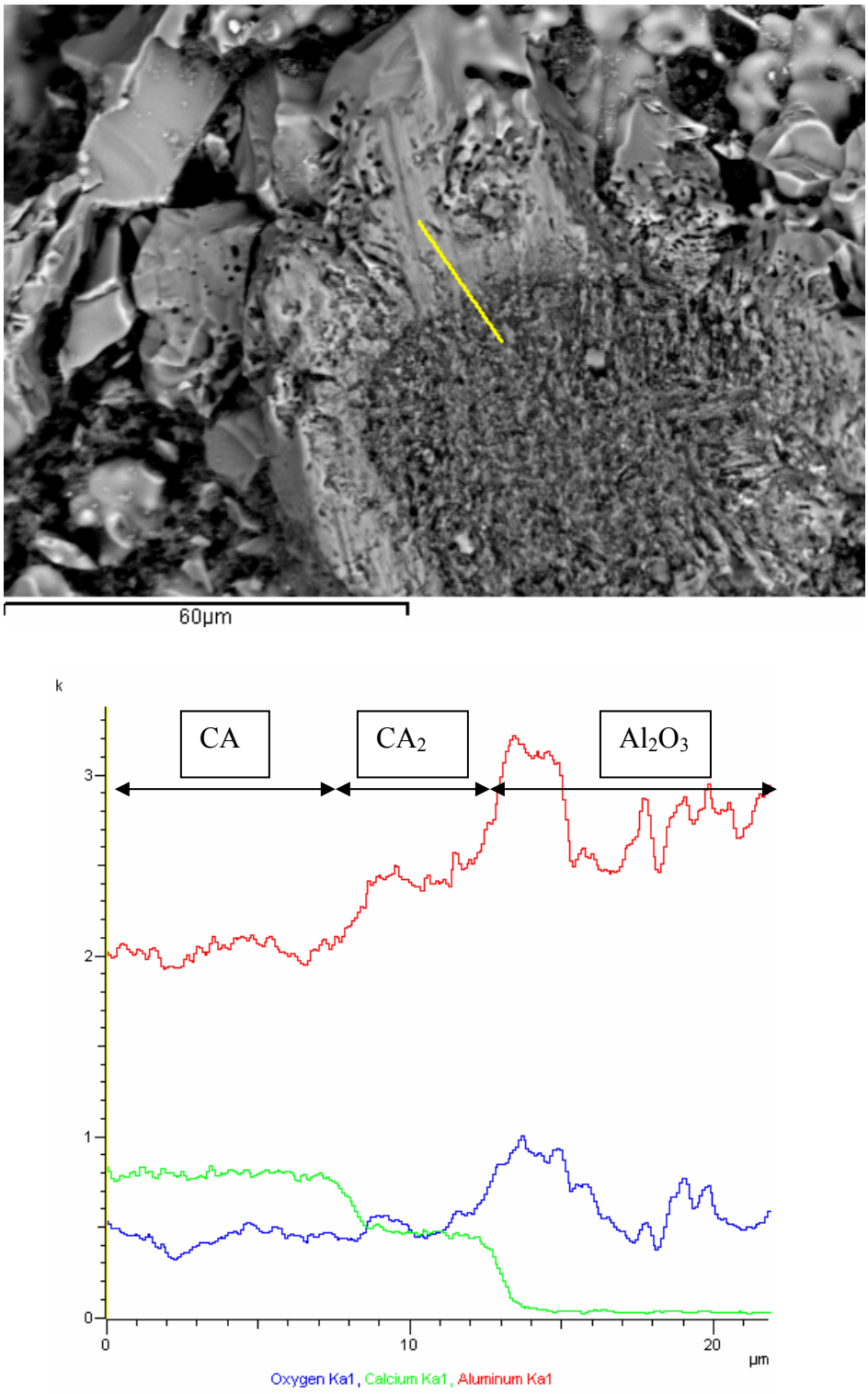

Figure 23. *Linescan analysis showing CA phase from point 0 to point 8 µm and CA_2 phase from point 8 to 13 µm around an alumina particle. Experiment no. 28: mixture of CaO and Al_2O_3 powders heated at 1400°C for 6 hours. (Lines: blue=oxygen, green=calcium and red=aluminium)*

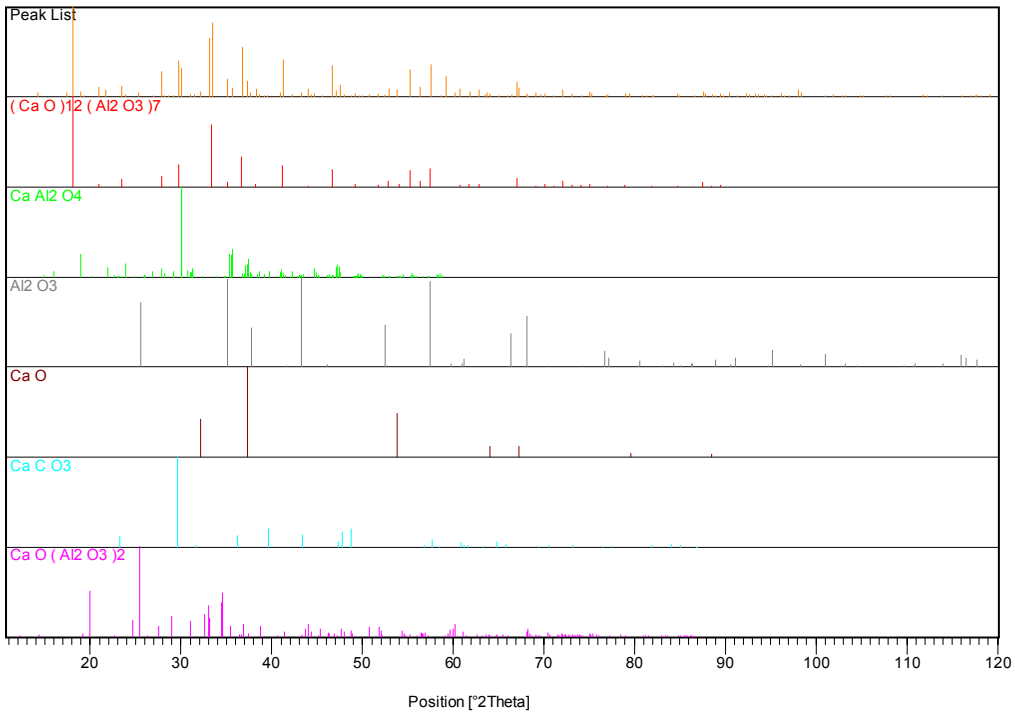

Figure 24. *Specific peaks for different phases from x-ray diffraction measurements (exp.28).*

Table 6. Detected phases and their percentages after heating mixture of CaO and Al_2O_3 powders at 1400°C for six hours. Semi-quantitative analysis was used to determine the estimated mass fractions of detected phases. The scale factor and the RIR (Reference Intensity Ratio) values (also called I/Ic values) were used to perform the calculation.

Chemical Formula	Phase	SemiQuant [%]	Scale Factor	Score	RIR	Space Group	Ref. Code	Visible
$12\ CaO{\cdot}7Al_2O_3$	$C_{12}A_7$	41	1.046	65	2.130	I-43d	01-070-2144	*
$CaO{\cdot}\ Al_2O_3$	CA	36	0.260	46	0.610	P21/n	01-070-0134	*
Al_2O_3		9	0.100	46	0.980	R-3c	00-043-1484	*
CaO		2	0.130	37	4.400	Fm-3m	01-070-4068	*
$CaCO_3$		1	0.026	17	3.120	R-3c	01-085-0849	*
$CaO{\cdot}2Al_2O_3$	CA_2	11	0.150	26	1.140	C2/c	01-089-3851	*

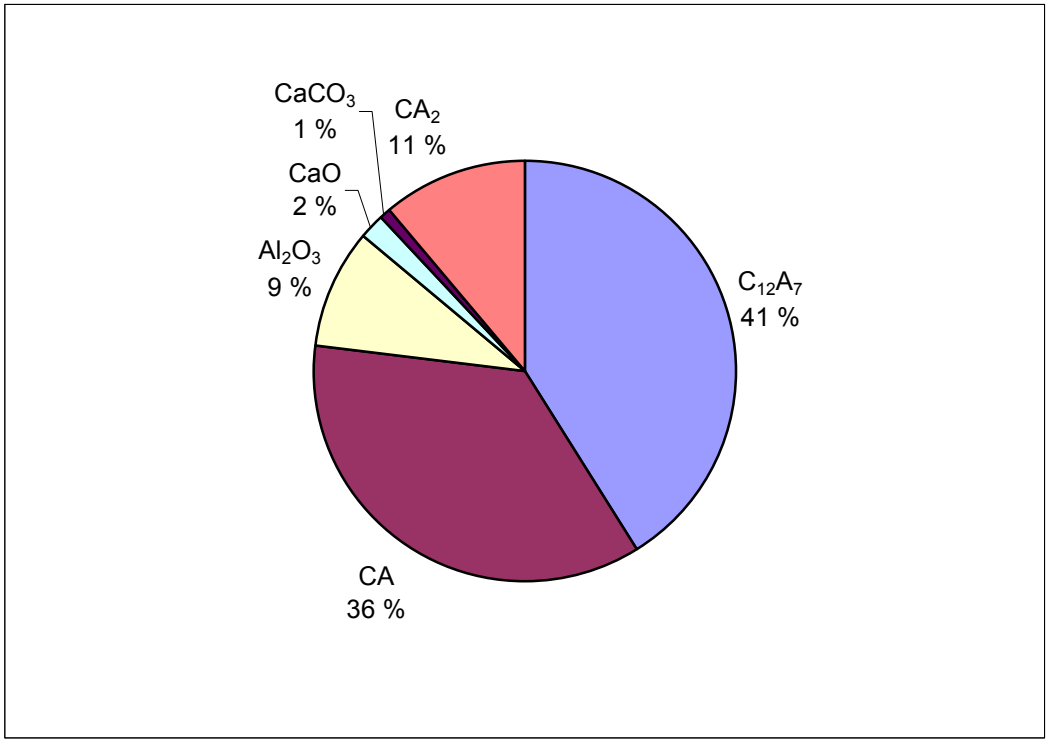

Figure 25. *Phases formed when annealing CaO and Al_2O_3 powders at 1400°C for six hours (ex.28).*

For experiment no.29, 0.492 g CaO powder and 0.657 g Al_2O_3 powder was used to make the cylinder, which was kept in a laboratory furnace for one hour at 1420°C. Table 7, Figure 26 and Figure 27 show the x-ray diffractometer results from this experiment. At a higher temperature, more of the phase CA_2 is formed, but less of the phases $C_{12}A_7$ and CA with lower melting point are formed.

Table 7. Detected phases and their percentages after heating CaO and Al_2O_3 powder at 1420°C for one hour. Semi-quantitative analysis was used to determine the estimated mass fractions of detected phases. The scale factor and the RIR (Reference Intensity Ratio) values (also called I/Ic values) were used to perform the calculation.

Chemical Formula	Phase	Semi Quant [%]	Scale Factor	Score	RIR	Space Group	Ref. Code	Visible
Al_2O_3		16	0.268	48	1.040	R-3c	01-075-0782	*
$CaO\cdot Al_2O_3$	CA	28	0.268	36	0.610	P21/n	01-070-0134	*
$CaO\cdot 2Al_2O_3$	CA_2	15	0.265	32	1.140	C2/c	01-089-3851	*
$12\ CaO\cdot 7Al_2O_3$	$C_{12}A_7$	30	0.999	59	2.130	I-43d	01-070-2144	*
CaO		10	0.658	46	4.400	Fm-3m	01-070-4068	*
$CaCO_3$		2	0.078	20	3.120	R-3c	01-085-0849	*

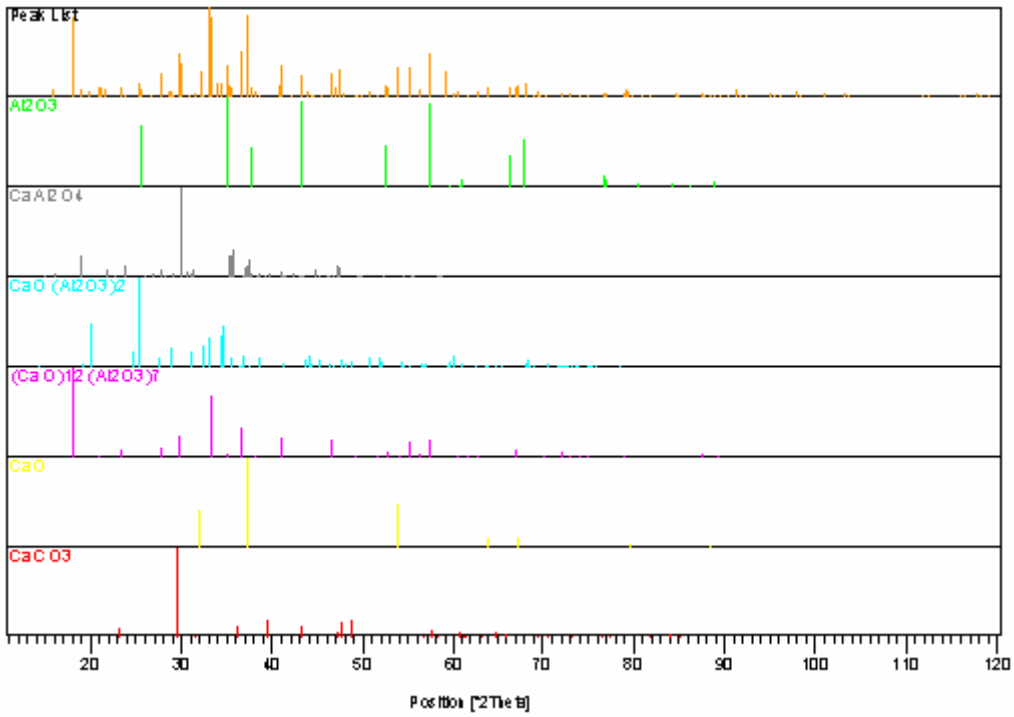

Figure 26. *Peaks from x-ray diffraction measurements (ex.29).*

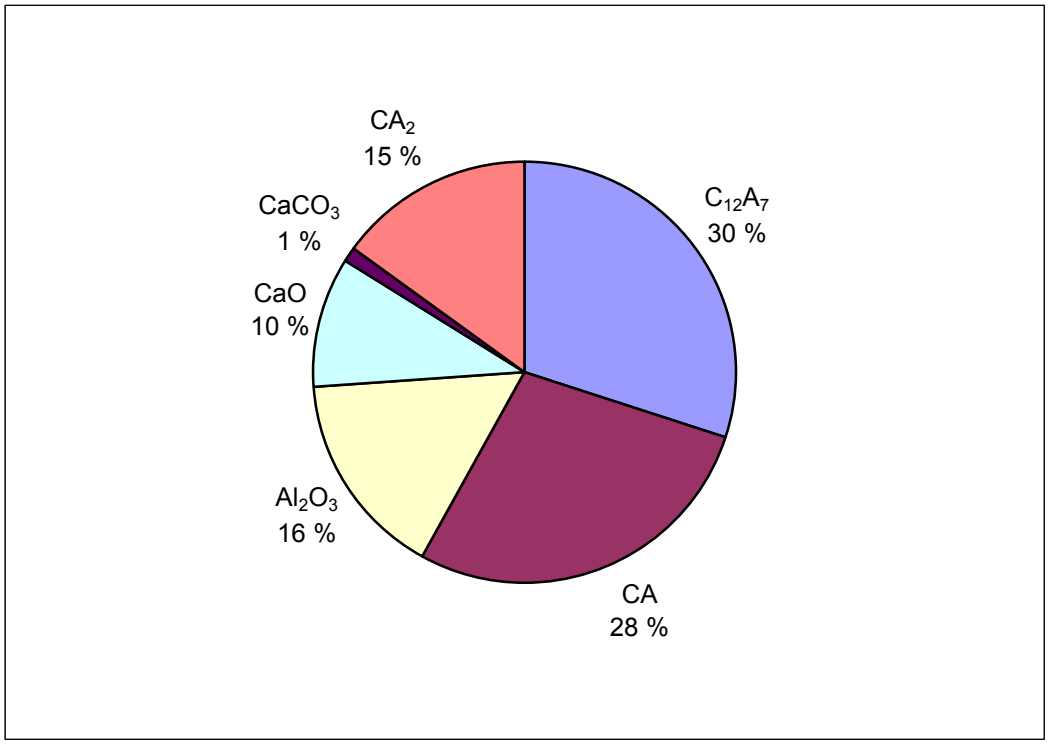

Figure 27. *Phases formed when annealing CaO and Al_2O_3 powders at 1420°C for one hour (ex.29).*

4.2 Reaction kinetics between calcium and Al_2O_3 inclusions in steel

4.2.1 Ca-treatment of Al deoxidized steel (8 kg scale)

Experiments were performed in an 8 kg induction furnace to verify the mechanism of transformation of alumina inclusions during Ca-treatment. Steel deoxidised with aluminium was melted under vacuum and then the atmosphere was turned to 0.6 bar argon. When a proper temperature (1580−1600°C) was achieved, a sample was taken from the melt and then a CaSi powder corresponding to 100 ppm [Ca] was immersed into the melt inside a steel rod. Part of the calcium dissolved into the steel, whereas a significant fraction vaporised out from the melt. Samples were then taken one per minute and analysed for Ca and Al. Inclusions were investigated by using the SEM-EDS technique. Typically, a Ca content of around 20 ppm was observed in the first samples, and the content then gradually decreased along the time.

Depending on the heat, ten to twenty minutes after the Ca-addition, the steel was cast into a steel mould and solidified to an ingot. A sample was cut about one-fourth from the ingot bottom and prepared for spectrometer analysis. In Table 8 there are analyses made with an optical emission spectrometer of the cast samples from all the heats. Also in heats 2 to 5 the total oxygen has been analysed with LECO system. The time from the Ca-addition to casting is different in different heats. In third heat, the Ca content is the highest in the cast sample, which solidified about thirteen minutes from the Ca-addition. Also in the third heat, as depicted in Figure 28, we can see that Ca is clearly a part in the oxide inclusion. In Figure 29 we can see how the Ca content changes after Ca-treatment.

Analysis of the starting steel materials were as follows:

- Heats 1-5 with analysis: 0.128 %C, 0.273 %Si, 1.12 %Mn, 0.0024 %S, and 0.032 %Al
- Heats 6-7 with analysis: 0.091 %C, 0.015 %Si, 0.68 %Mn, 0.012 %S, and 0.032 %Al
- Heat 8 with analysis: 0.1298 %C, 0.291 %Si, 1.140 %Mn, 0.009 %S, and 0.041 %Al

Table 8. Analyses from the cast heat samples after Ca- treatment in laboratory scale. Analyses were made with an OES (optical emission spectrometer), except total oxygen were made with LECO system.

	C	Si	Mn	P	S	Cr	Mo	Ti	Cu	Altot	Alsol	N	Ca	Otot
heat 1	0.12	0.29	0.92	0.014	0.006	0.06	0.00	0.00	0.04	0.002	0.002	0.007	0.00010	
heat 2	0.11	0.03	0.35	0.012	0.005	0.03	0.01	0.00	0.03	0.001	0.001	0.018	0.00050	0.0219
heat 3	0.11	0.30	0.96	0.014	0.006	0.03	0.03	0.01	0.03	0.011	0.007	0.003	0.00056	0.0068
heat 4	0.10	0.21	0.75	0.01	0.002	0.07	0.00	0.00	0.03	0.001	0.001	0.006	0.00020	0.0080
heat 5	0.11	0.28	1.01	0.01	0.005	0.03	0.00	0.00	0.03	0.019	0.018	0.005	0.00015	0.0040
heat 6	0.037	0.01	0.41	0.008	0.014	0.02	0.01	0.00	0.01	0.001	0.018	0.011	0.00010	
heat 7	0.04	0.00	0.56	0.01	0.016	0.02	0.00	0.00	0.01	0.001	0.001	0.009	0.00014	
heat 8	0.06	0.35	1.05	0.01	0.007	0.04	0.01	0.00	0.04	0.003	0.002	0.015	0.00013	

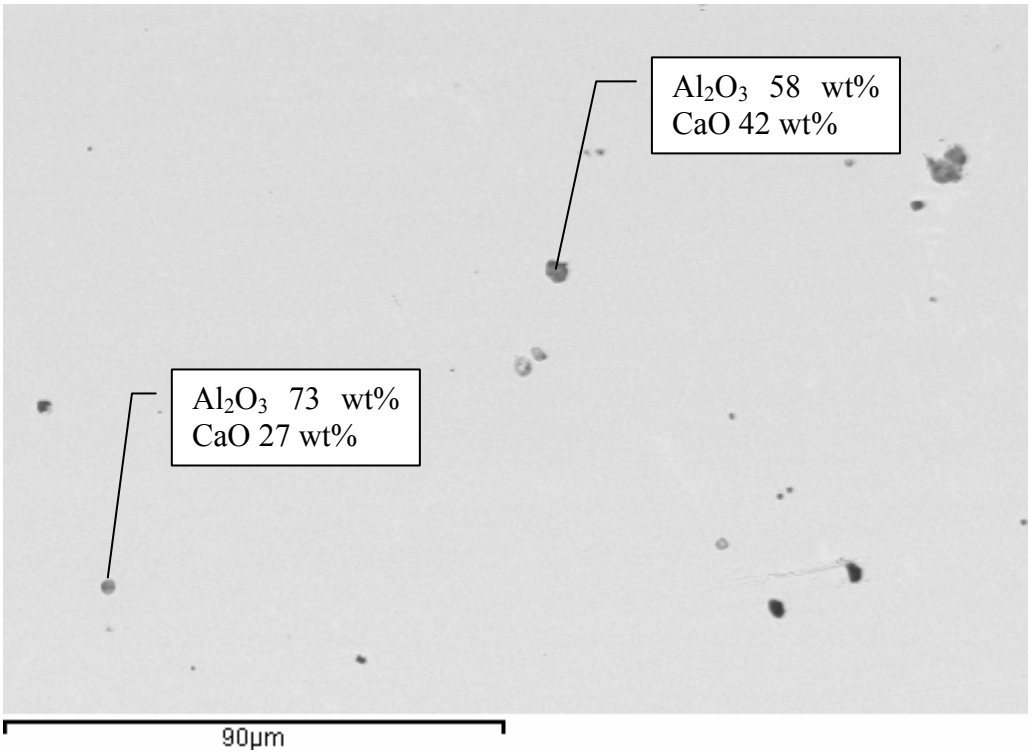

Figure 28. *Micrograph of a sample from 3rd Heat showing typical calcium aluminate inclusions. Sample was taken 230 seconds after Ca-addition.*

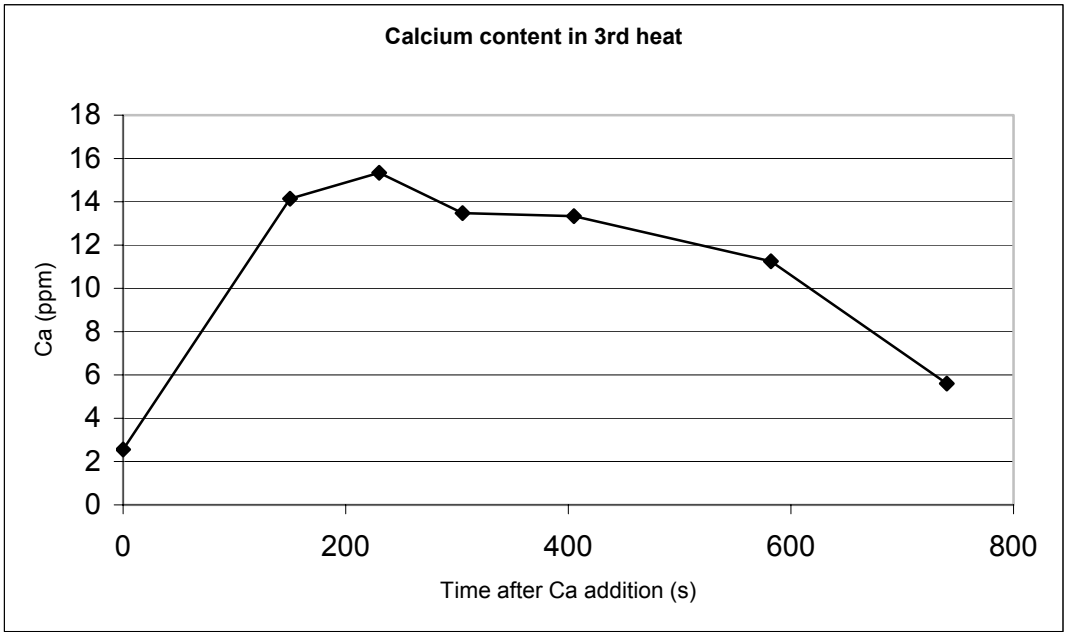

Figure 29. *Ca content at different times after Ca-treatment;, analyses made with AAS (atomic absorption spectroscopy).*

Samples taken during the experiments from the furnace were pin samples and therefore too small to be analysed with OES. So those small samples were analysed with SEM/EDS (Figure 28 and Figure 57) and with AAS (atomic absorption spectroscopy) for Ca and in some cases for Al, too. Results from the AAS analyses for Ca content in steel are shown in Figure 29 for heat 3 and in Figure 30 for heat 4. In heats 5 and 7, Al content has also been analyzed and is shown in Figure 31 and Figure 32.

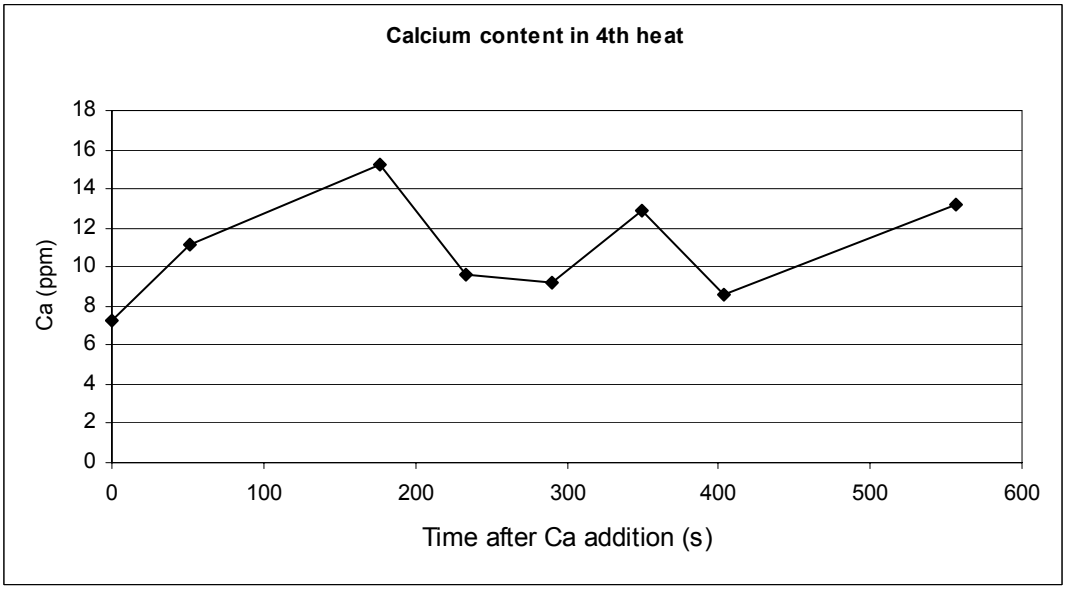

Figure 30. *Ca content at different times after Ca-treatment, analyses made with AAS (atomic absorption spectroscopy).*

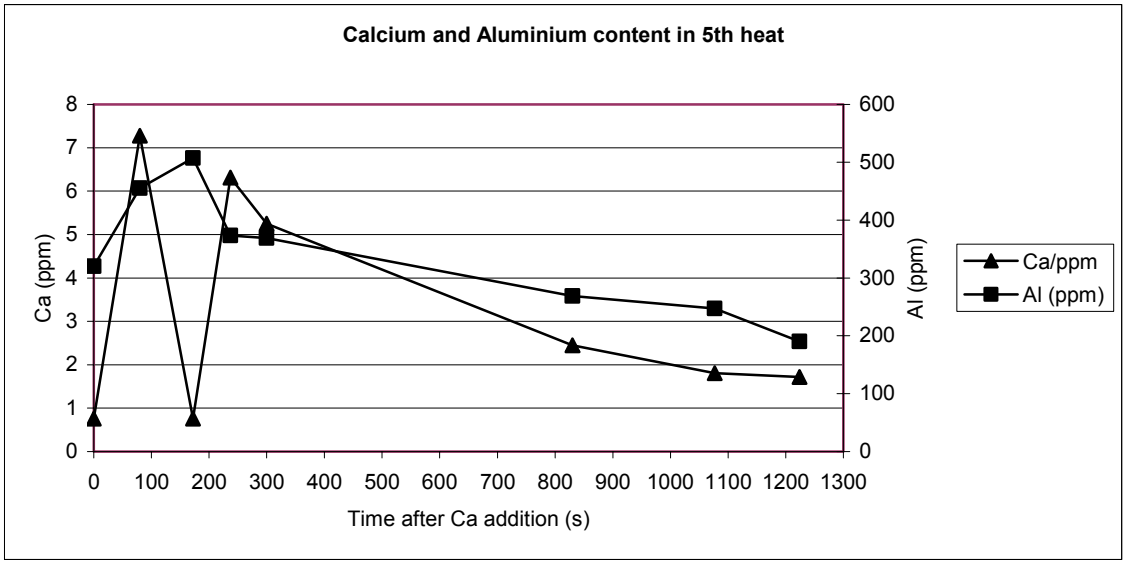

Figure 31. *Ca- and Al-contents at different times after Ca-treatment, analyses made with AAS (atomic absorption spectroscopy).*

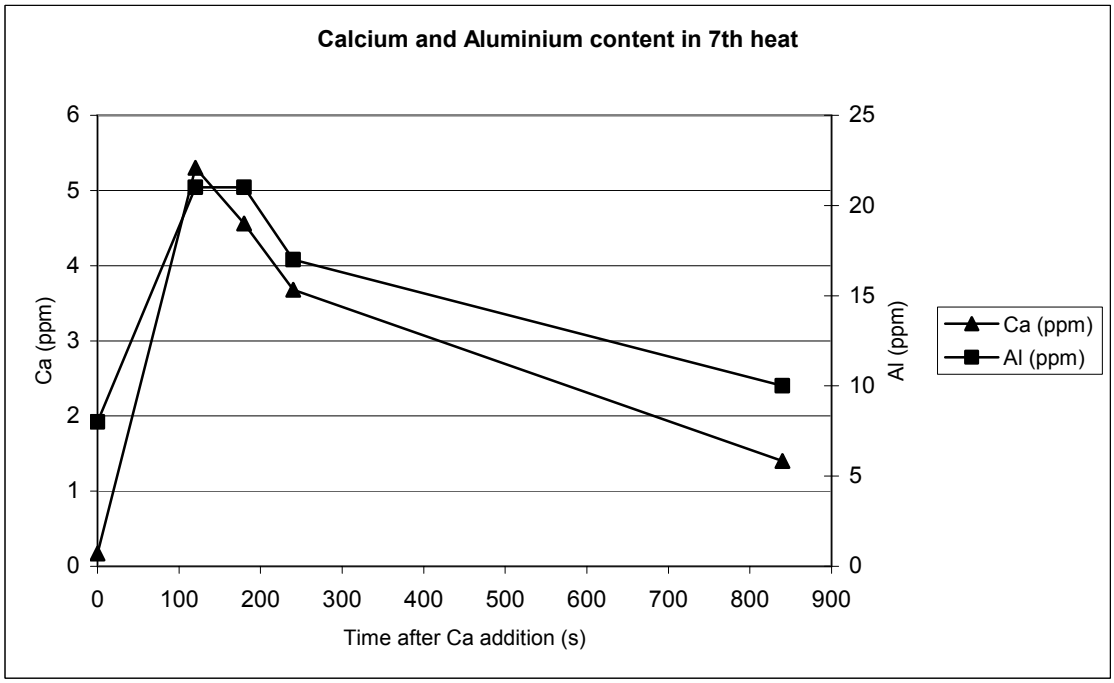

Figure 32. *Ca- and Al-contents at different times after Ca-treatment; analyses made with AAS (atomic absorption spectroscopy).*

4.2.2 Ca-treatment on industrial scale

Samples from Koverhar steelworks and Imatra steelworks have been taken before, during and after Ca-treatment. Samples have been analyzed with the SEM/EDS program INCA Feature. INCA Feature is a tool for automated collection of chemical and morphological data from inclusions in steel.

The following figures show the composition and size of the biggest inclusions from different samples. The information from each sample (analysed area 2mm x 2 mm) consists of information on over one hundred inclusions. Information on the smallest inclusions less than the value shown on the x-axis is not seen in these bar-chart figures. In the figures, inclusion analysis provides the inclusion type. The weight percentages of the inclusions are shown so that eventual matrix (Fe) has been excluded from the analysis results. The fraction of the matrix (Fe) could be quite high in small inclusions. In big inclusions (>5 μm), the matrix (Fe) had little or no influence on the EDS analysis. From each sample at least 30 inclusions which were biggest in length are presented in the figures, so that the analysis and size of each individual inclusion can be seen.

After the bar-chart figures are presented, there are three figures (Figure 38, Figure 46, and Figure 52) which show the inclusion paths. In those figures the oxide inclusions (~200 in each sample) have been calculated, so that the average amount of MnS, CaS, CaO and Al_2O_3 can be seen at different times after the Ca treatment. The calculation was done so that first from the manganese content of an inclusion the amount of manganese sulphide was determined, secondly the rest of the analyzed sulphur was used to form calcium sulphide, thirdly the rest of the analyzed calcium was used to form calcium oxide, and fourthly the amount of aluminium oxide was calculated from aluminium analysis.

Figure 33 - Figure 36 provide the results of analyzed steel samples from Koverhar works before and after the Ca-treatment. The time between taking these first two samples is four minutes. In these four figures, we can see that the average size of the biggest inclusion has changed: It is over 3 μm before Ca-treatment (Figure 33) and under 3 μm after it (Figure 34 and Figure 35). Also in Figure 34, it can be seen that in only twelve inclusions from forty three Ca has been detected. In Figure 35-Figure 36 all of the inclusions contain calcium.

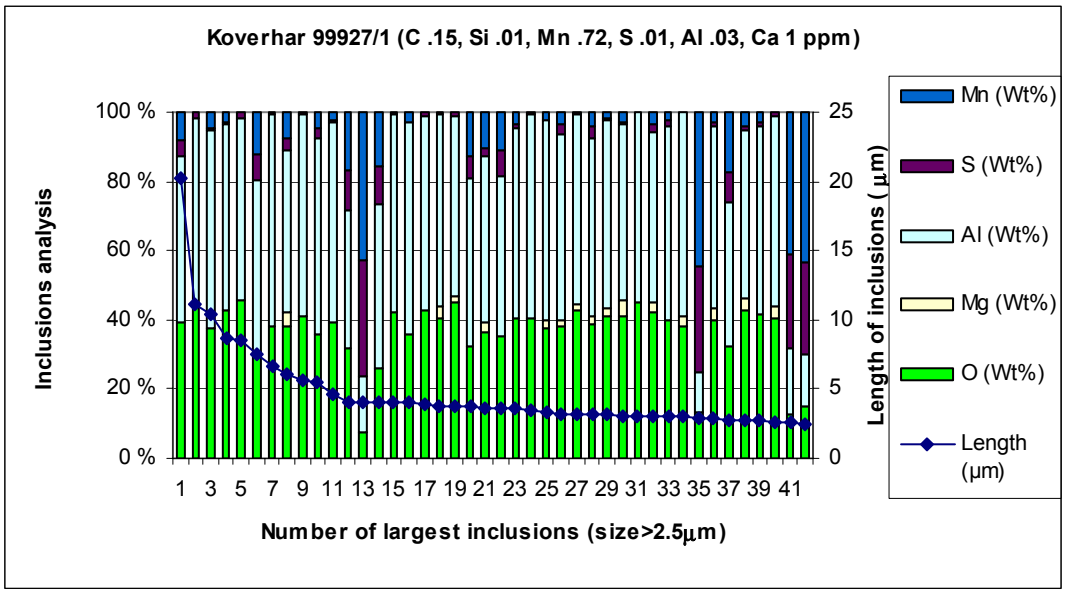

Figure 33. *Sample taken just before Ca-treatment.*

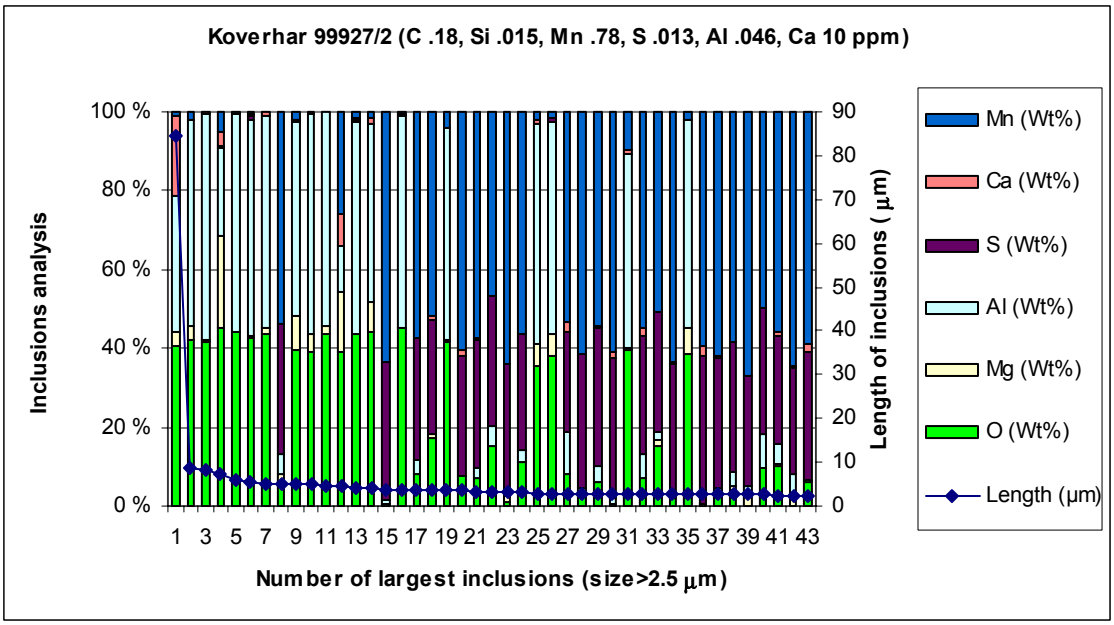

Figure 34. *Sample taken right after Ca-treatment.*

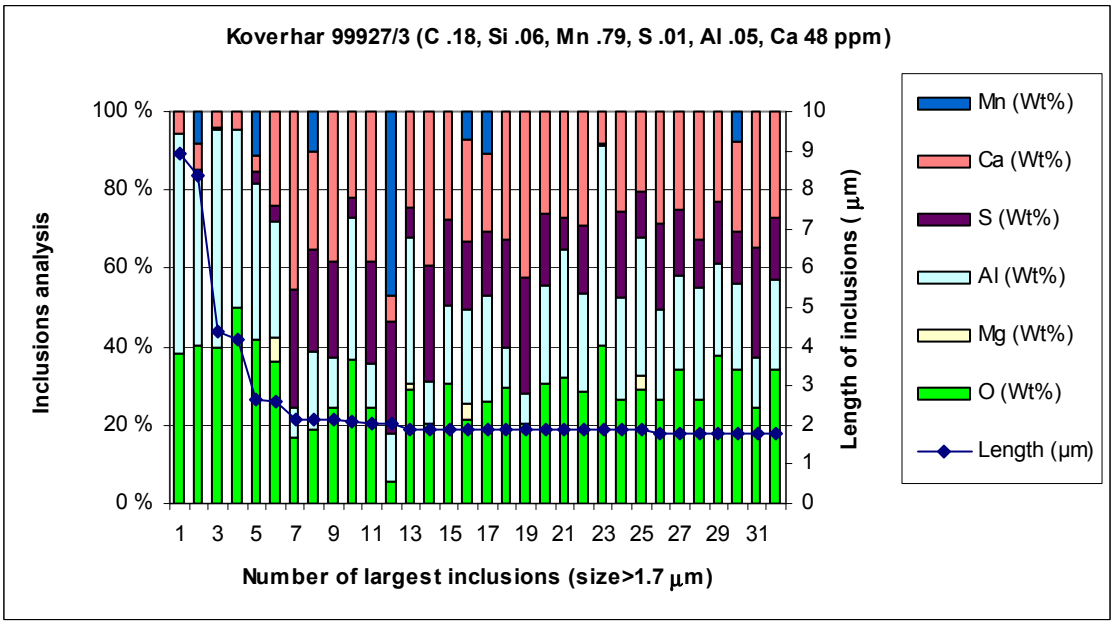

Figure 35*. Sample taken four minutes after Ca-treatment.*

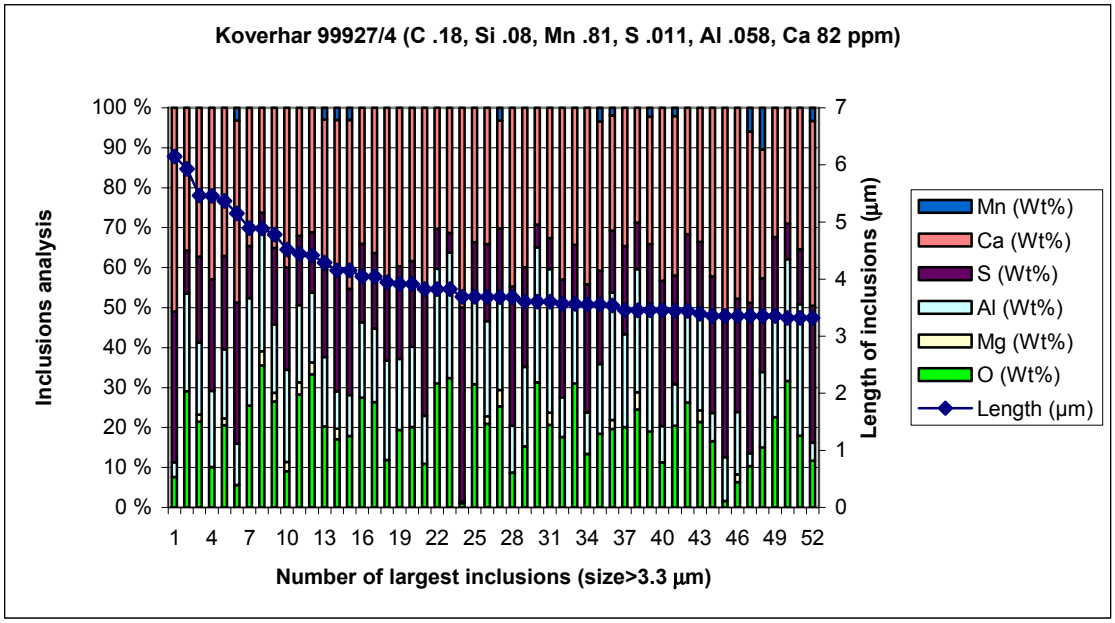

Figure 36. *Sample taken 15 minutes after the main Ca-treatment and two minutes after an extra Ca and Al addition.*

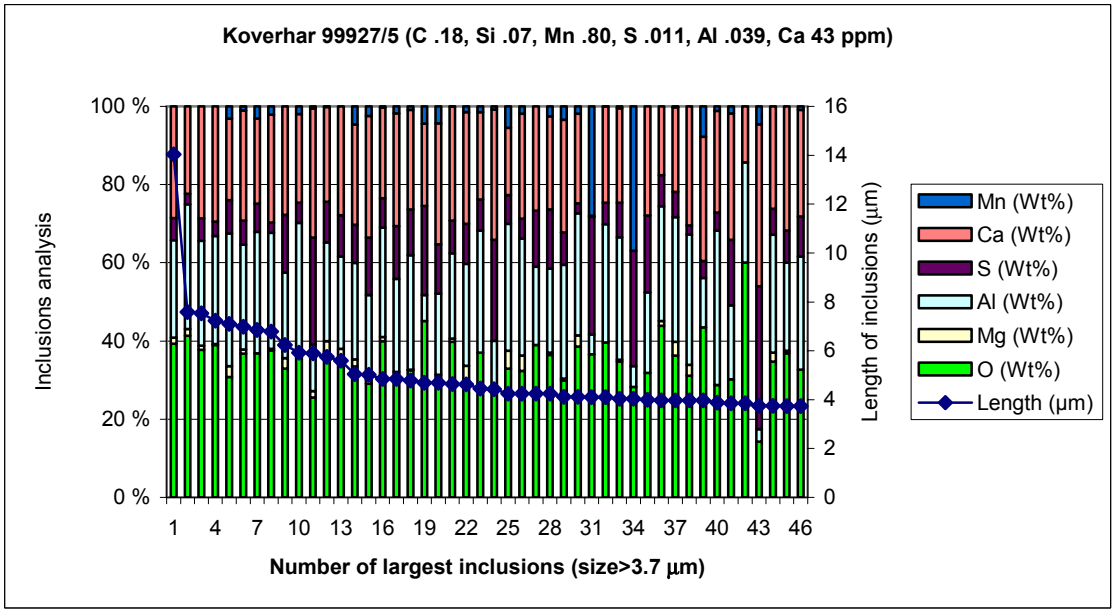

Figure 37. *Sample taken 30 minutes after the main Ca-treatment and 17 minutes after the extra Ca and Al addition.*

Before the sample 4, as shown in Figure 36, there has been an extra addition of aluminium and calcium, so that calcium content 82 ppm is higher than in any of the other examined samples. From Figure 36 we can see that calcium is the dominating component in all of the inclusions, just before the ladle goes to casting station. Figure 37 shows forty six biggest inclusions in sample which is taken from the continuous casting mould.

Figure 38 shows the average composition of inclusions at different times before and after Ca-treatment. These values have been calculated so that 200 inclusions with analysis containing most oxygen have been selected. From these analyses we get an

average analysis for each sample. This average analysis has been turned to MnS, CaS, CaO, and Al_2O_3 weight percentages. Sometimes the run made with the program INCA Feature gives less than 200 inclusions, and because of this all the inclusions in those cases are taken into account.

Figure 38 shows that the proportions of aluminium oxide and manganese sulphide in the inclusions decrease and calcium oxide and calcium sulphide increase in ladle samples (time until 900 seconds).

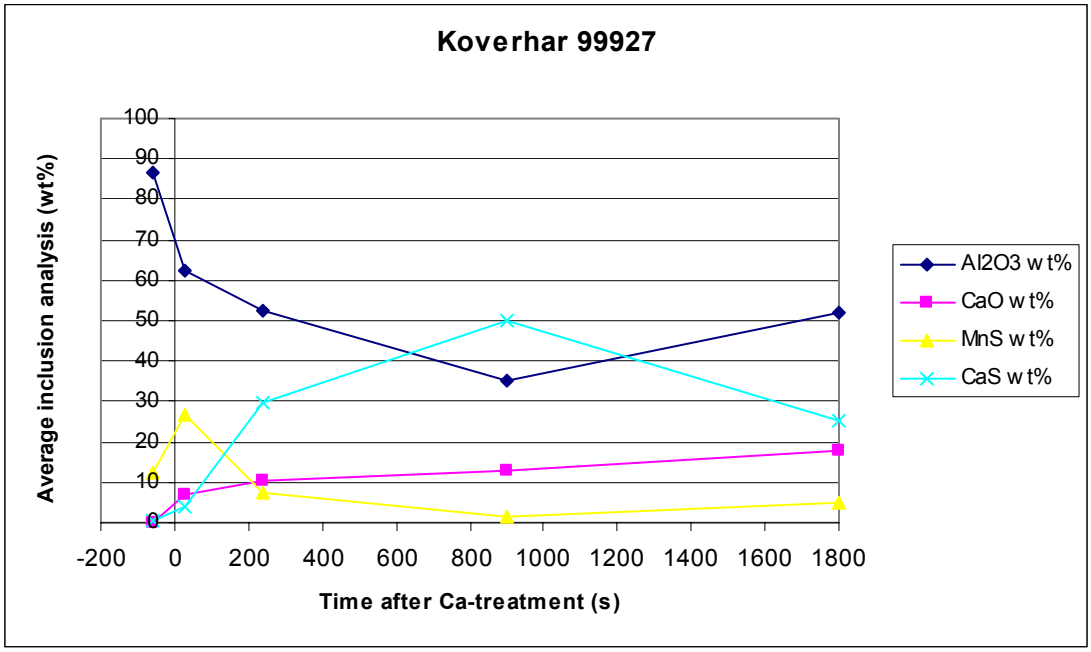

Figure 38. *Change of inclusion composition during ladle treatment in heat 99927. Each point represents composition of over hundred of oxide inclusions analysed by the SEM/EDS program INCA Feature.*

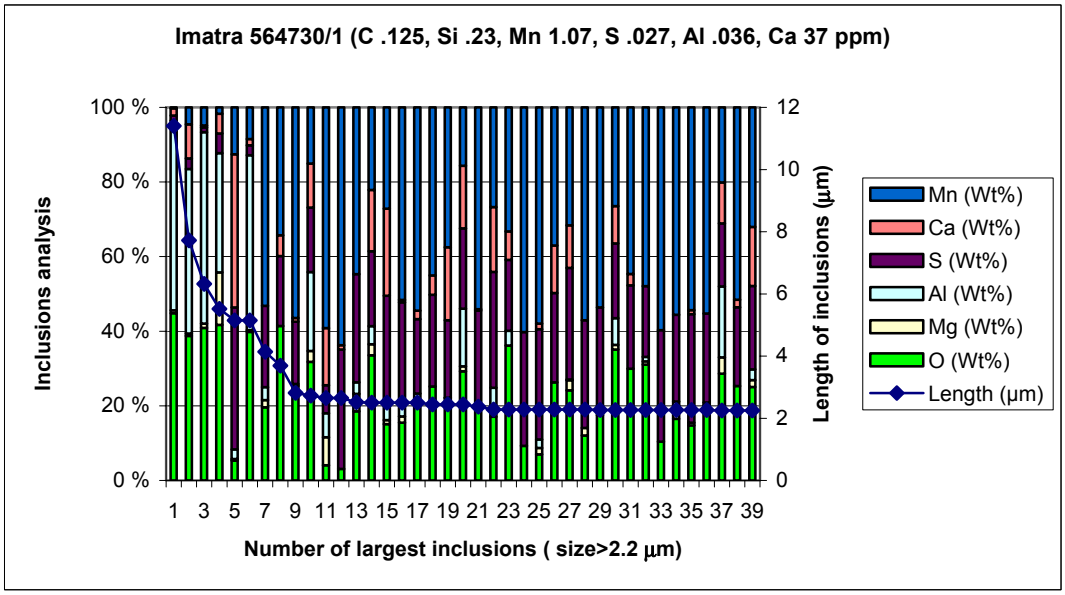

Figure 39. *Sample taken 55 seconds after Ca-injection.*

All the samples from Imatra steelworks have been taken after Ca-treatment. The size of the heat 564730 in Imatra was 77.2 t and 46 kg CaSi was injected. In Figure 39 we can see that the inclusions composition is aluminium oxide and manganese sulphide, and more than half of the thirty nine biggest inclusions, when the sample has been taken fifty five seconds after CaSi-injection, have a detection of calcium in the form of either calcium sulphide or calcium aluminate. Some of the inclusions also have a detection of magnesium, which supposes that the inclusion has been exogenously formed. In Figure 40 calcium is present in forty out of the forty four biggest inclusions, and the average size of inclusions is only a little smaller than in the previous sample, but the size of the first five biggest inclusions is much smaller. Figure 42 is very similar (inclusion size and composition) with the previous Figure 41, and that is because only less than three minutes has elapsed between sample taking and with no operations between them.

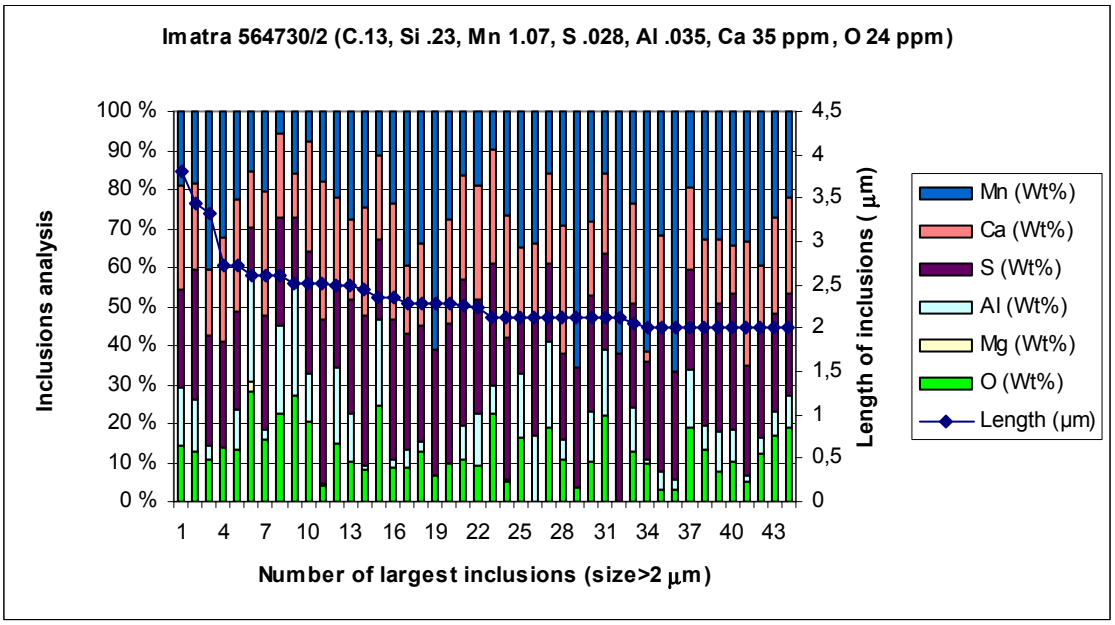

Figure 40. *Sample taken 2 minutes 50 seconds after Ca-injection*

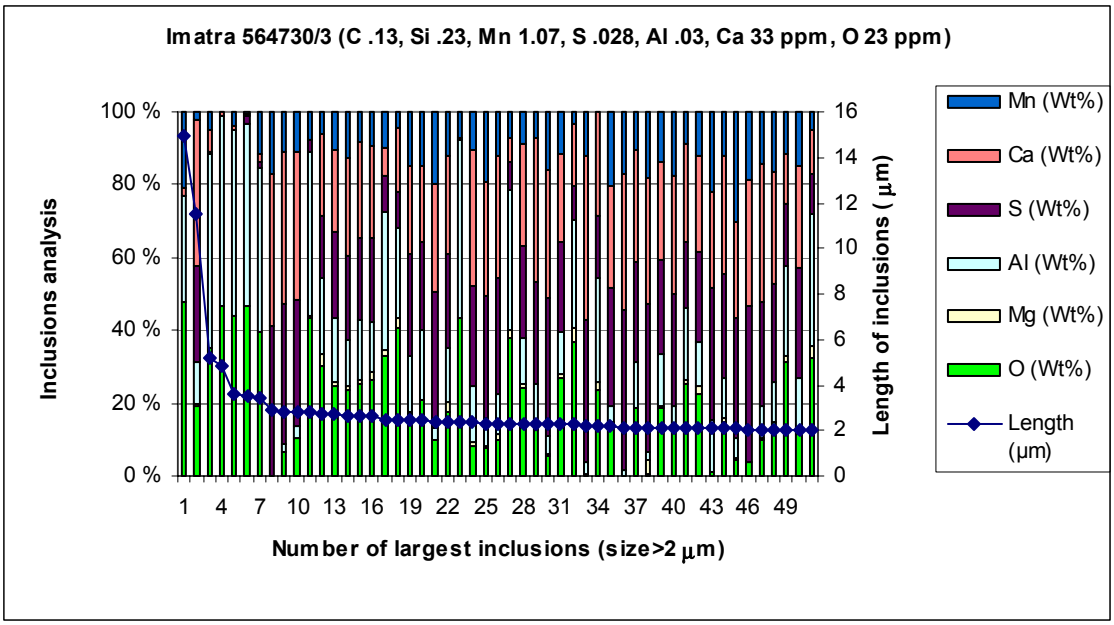

Figure 41. *Sample taken 5 minutes 5 seconds after Ca-injection.*

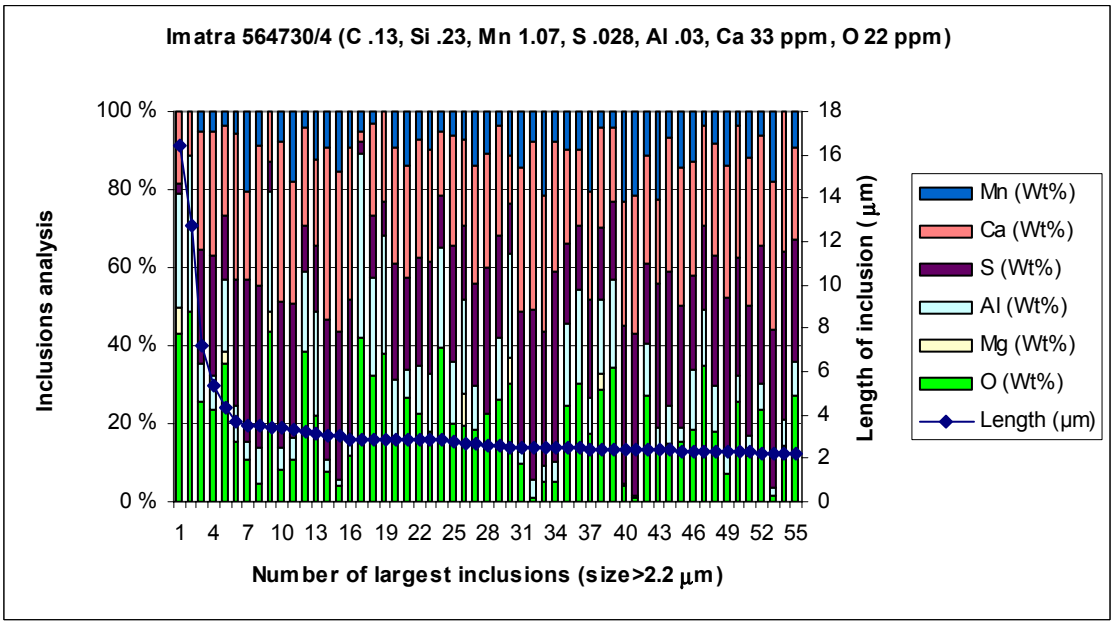

Figure 42. *Sample taken 7 minutes 20 seconds after Ca-injection.*

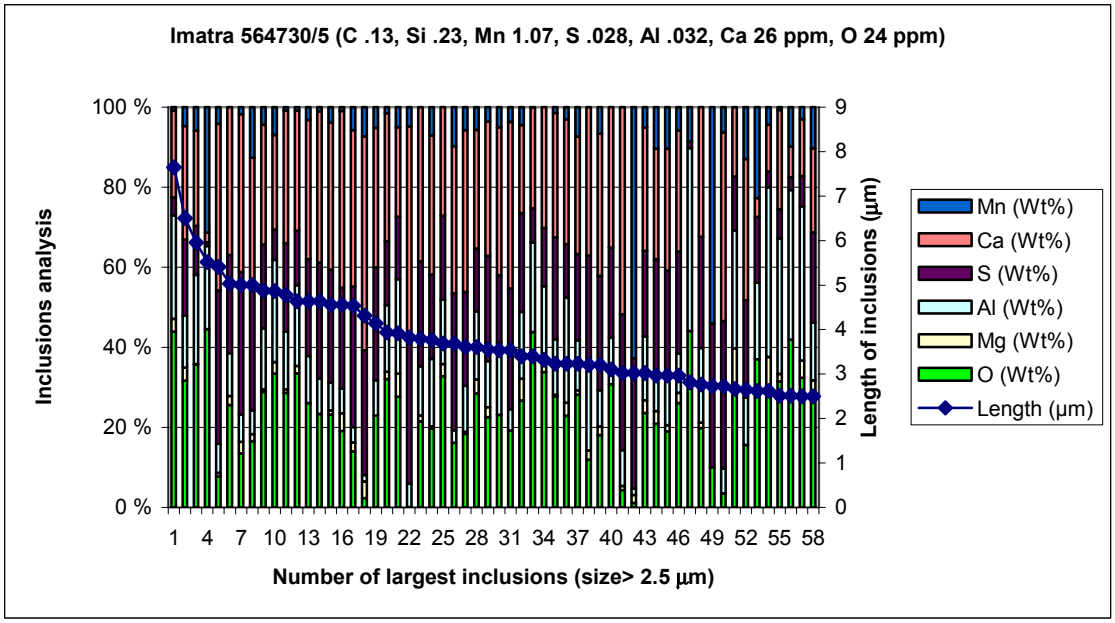

Figure 43. *Sample taken 16 minutes 35 seconds after Ca-injection.*

In Figure 43 the biggest inclusion is only 8 µm long. Between samples 5 (Figure 43) and 6 (Figure 44) 173 kg of FeMn, 177 kg of FeCr, and 35 kg of FeAl have been added. It can be seen that these additions have some effect on the steel composition and that the inclusions are richer in aluminium in the later sample. In Figure 45 the sample has been taken from the cast mould, and the calcium content has dropped to 8 ppm. Oxidic inclusions are still mainly calcium aluminates, but due to high sulphur content, pure manganese sulphides can be detected.

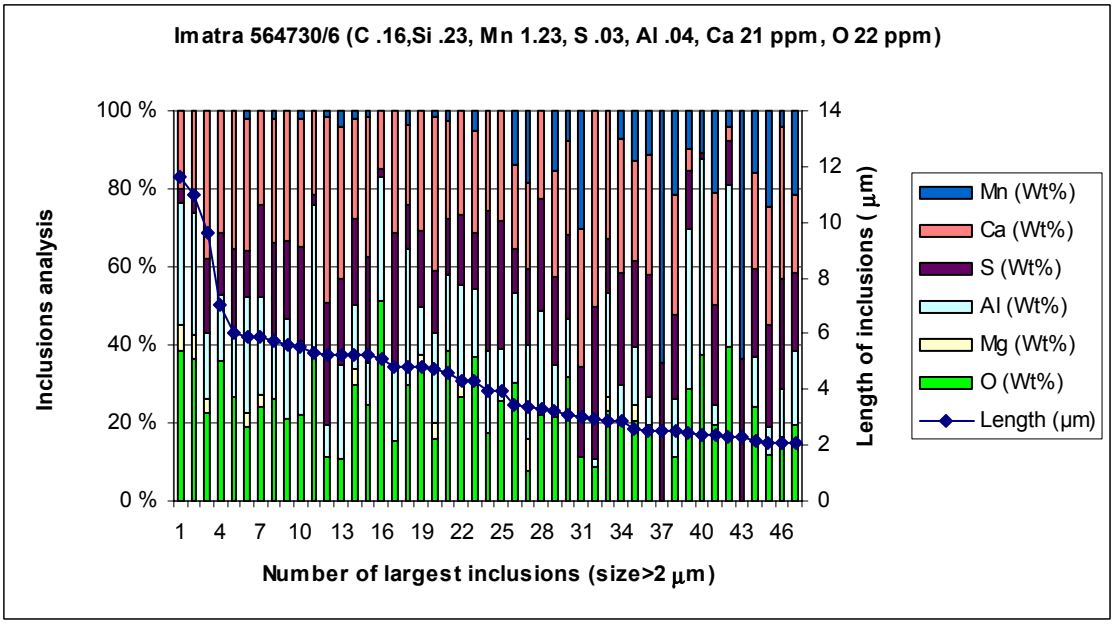

Figure 44. *Sample taken 27 minutes 30 seconds after Ca-injection.*

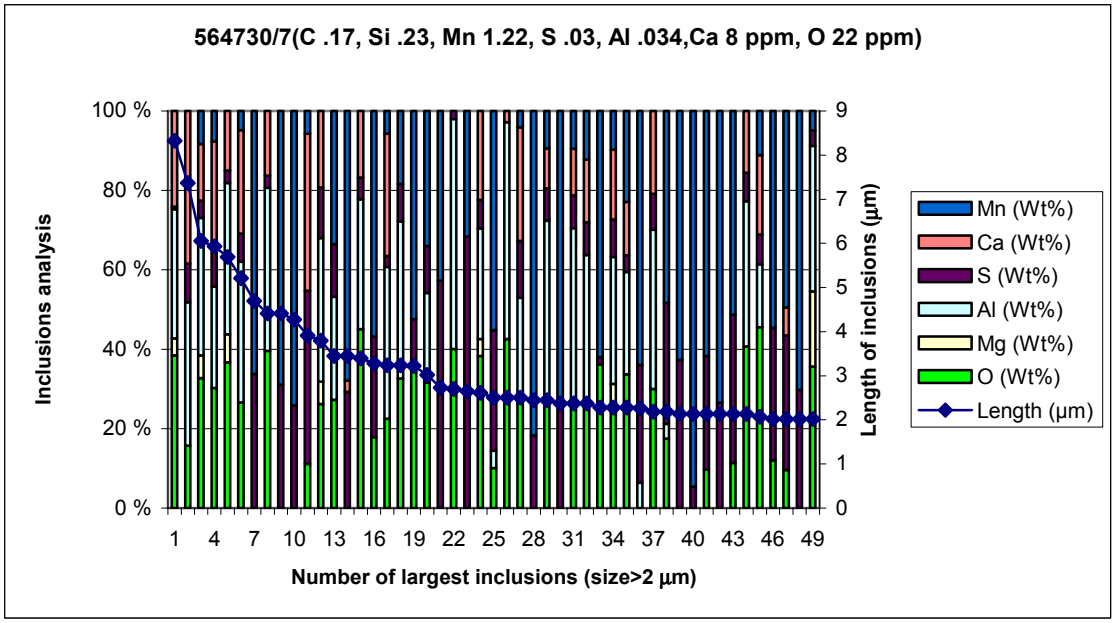

Figure 45. *Sample taken 92 minutes after Ca-injection.*

Figure 46 shows the inclusions analyses and average size presented at different times after Ca- treatment. Average size of inclusions is only given from heat 564730 (Figure 46), because there is information from 200 oxide inclusions from each sample in this heat. In the two other heats the number of oxide inclusions which were analysed in each sample was less than 200 and, therefore, was not presented. When comparing this figure with the Koverhar heats, such as in Figure 38, similar trends are evident in the time range of up to 900 seconds. After this time in Figure the CaS content drops, and MnS content rises. Due to relatively high sulphur content, manganese sulphides are formed during sample solidification.

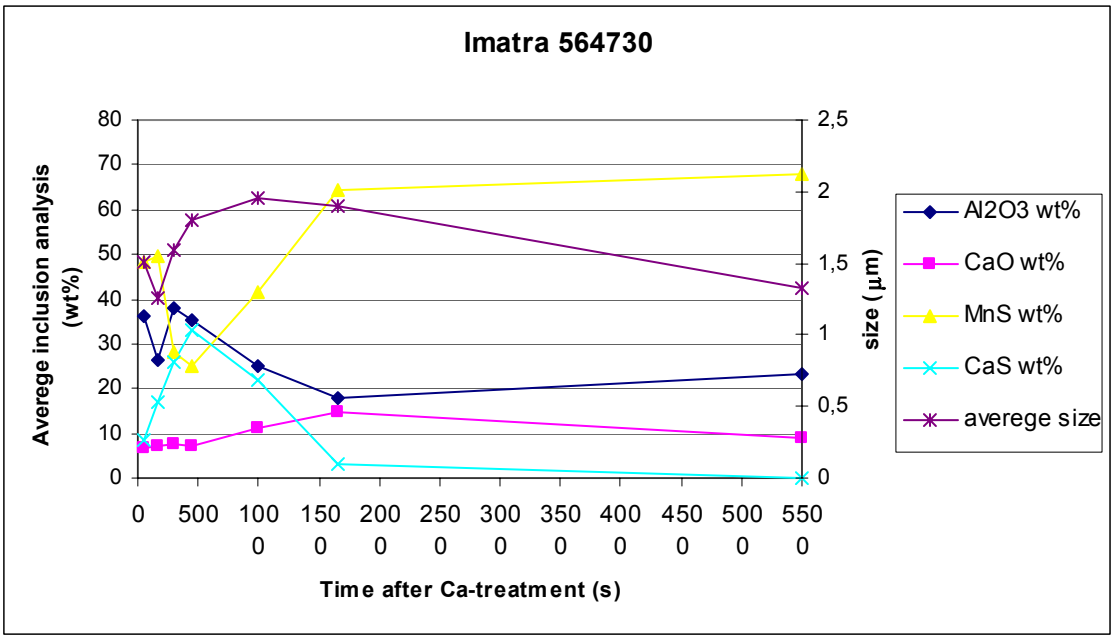

Figure 46. *Change of inclusions composition in heat 564730. Each point represents the average of 200 inclusion compositions and size.*

Heat 568480 from Imatra steelworks has higher silicon content, lower sulphur content and lower aluminium content. Figure 47 to Figure 51 show the biggest inclusions from samples taken at different times after Ca-injection.

In Figure 47, the sample was taken from the ladle one minute after calcium injection. In this sample, all of the forty three biggest inclusions had calcium, and all but one contained also calcium sulphide. In addition, the steel analysis shows high calcium content 74 ppm.

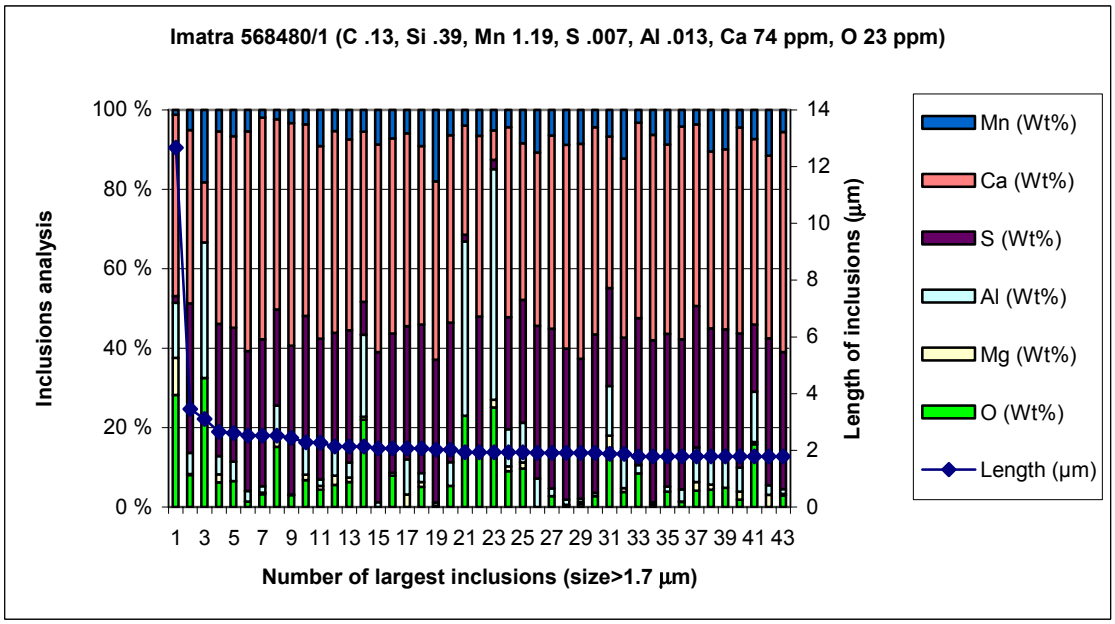

Figure 47. *Sample taken one minute after Ca-injection.*

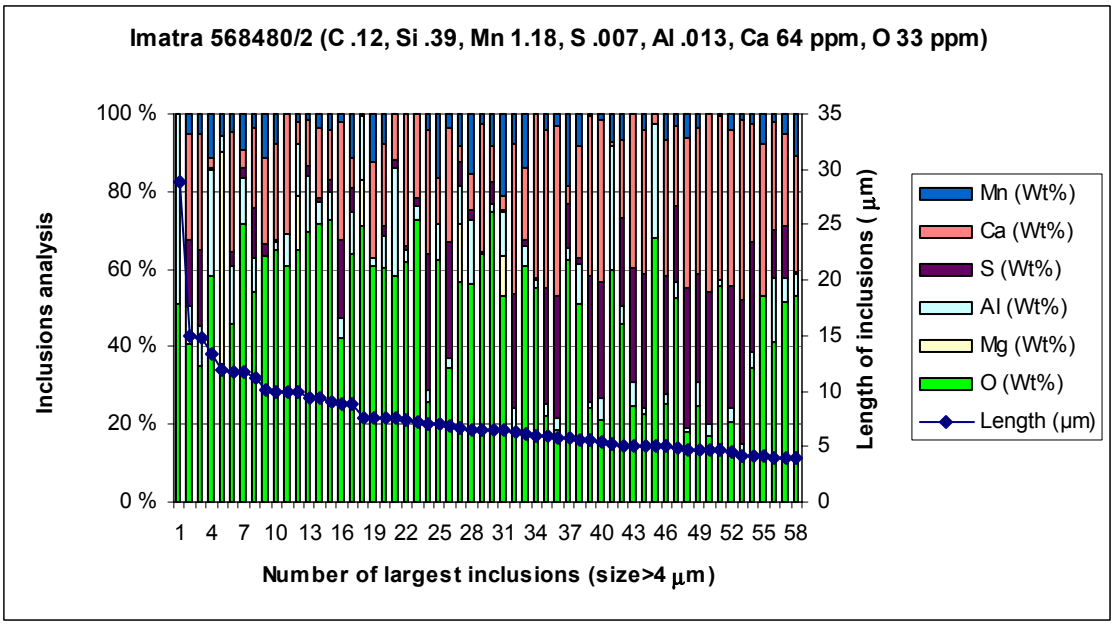

Figure 48. *Sample taken 4 minutes after Ca-injection.*

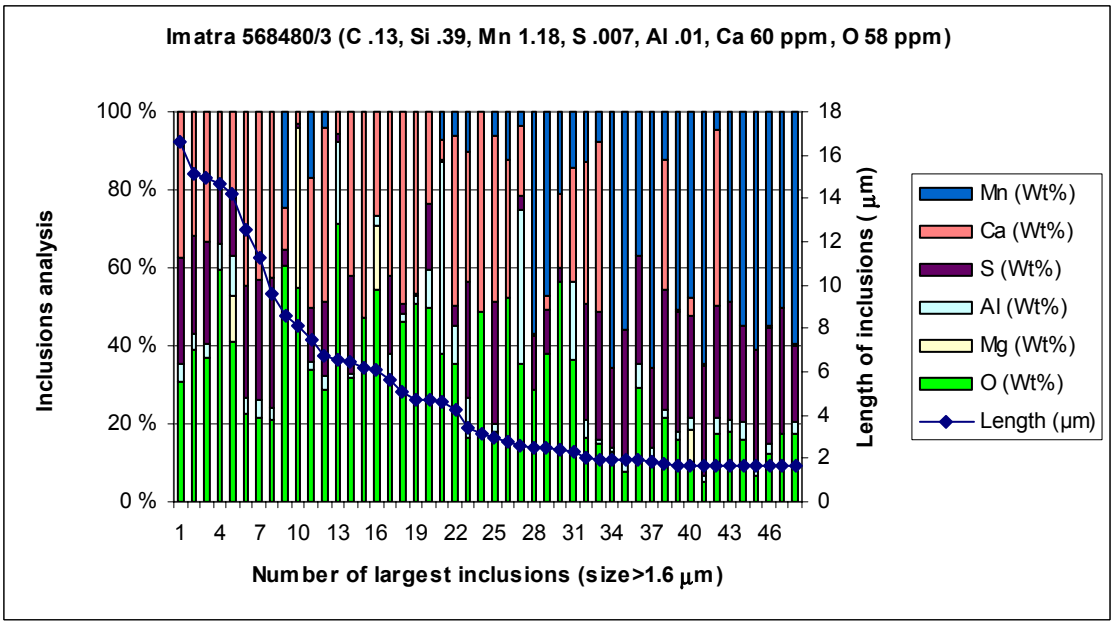

Figure 49. *Sample taken 14 minutes after Ca-injection.*

In Figure 48, the sample has been taken from the ladle at the ladle furnace station four minutes after Ca injection. It can be seen that the oxygen content is higher and the inclusions are larger than in the previous sample.

In Figure 49, the sample was taken fourteen minutes after Ca-injection and it shows that the average size of the biggest inclusions has decreased to half, because inclusions have been removed to the top slag and on the refractory lining. In Figure 50, the sample of the steel analysis shows 27 ppm of Ca, which is less than half of the previous sample 3

in which Ca content was 60 ppm. There has also been a final adjustment of the steel composition so that the Al content is higher in sample 4 than in sample 3. When looking at the inclusion analyses, these changes in the steel composition cannot be clearly seen.

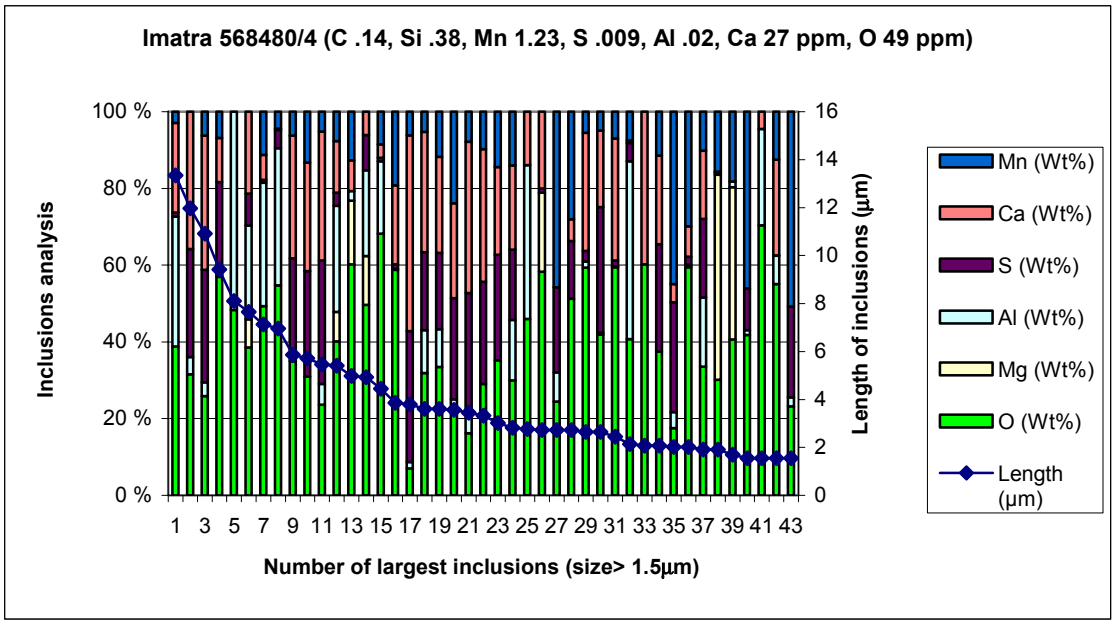

Figure 50. *Sample taken 21 minutes after Ca-injection.*

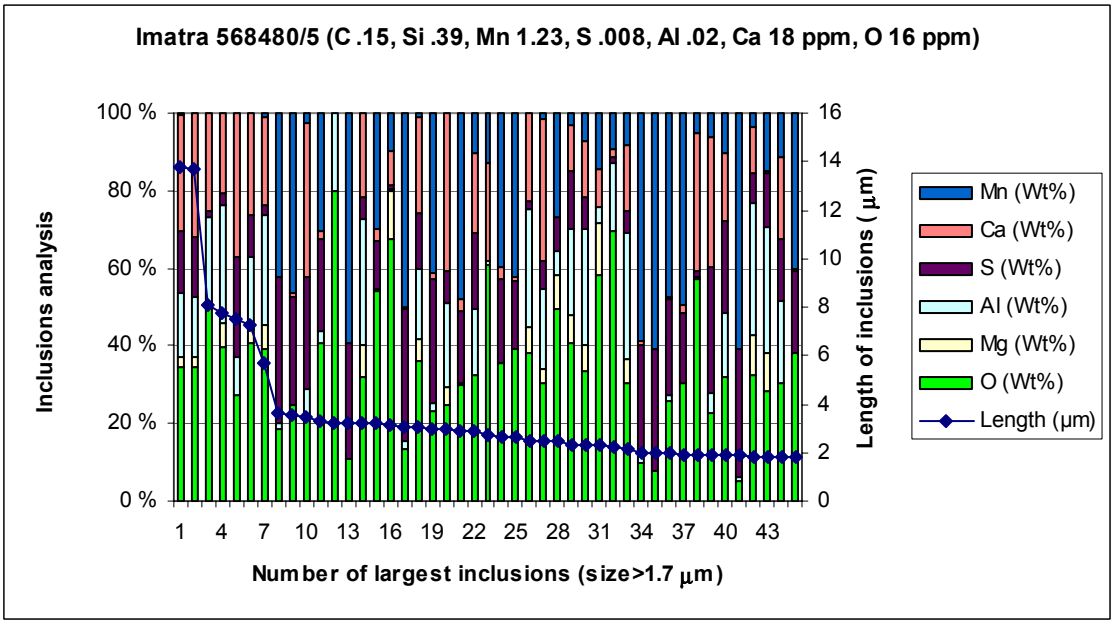

Figure 51. *Sample taken 44 minutes after Ca-injection.*

The sample in Figure 51 has been taken from the cast mould forty four minutes after Ca- injection. Oxygen and calcium in the steel analysis have the lowest levels from these heats and analysed samples.

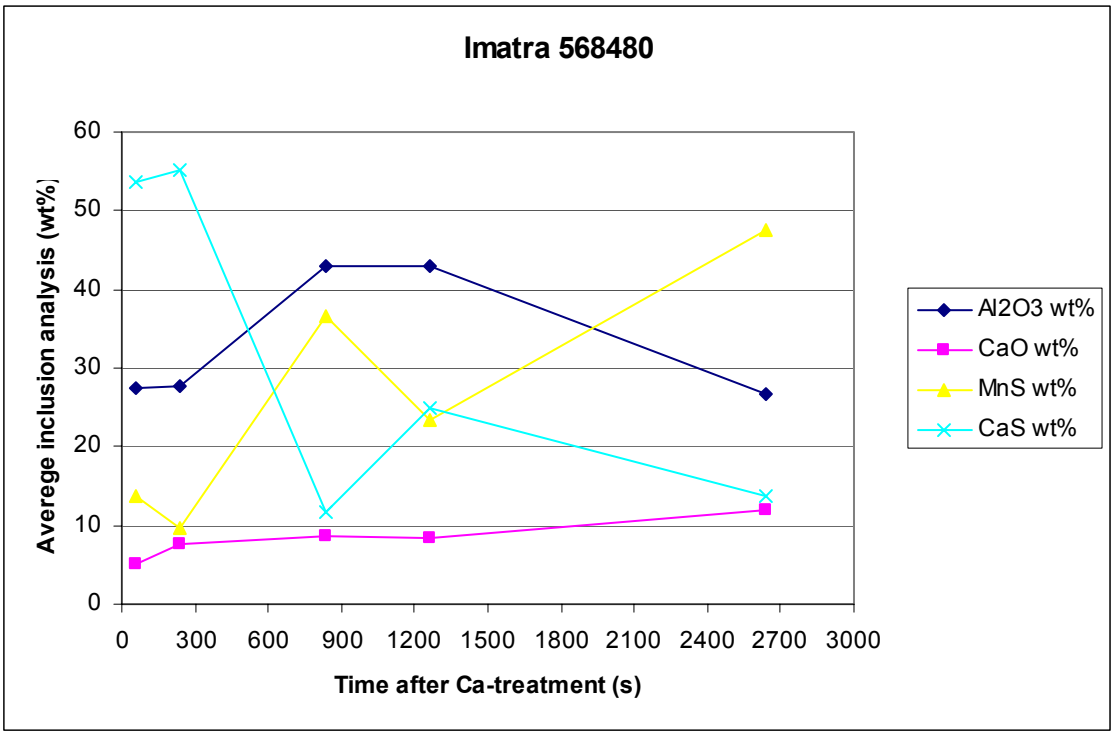

Figure 52. *Change of inclusion composition during ladle treatment, in heat 568480. Each point represents the average of over hundred inclusions composition analysed by SEM/EDS program Feature.*

Figure 52 shows the average inclusion composition at different times after Ca-injection in heat 568480. CaS and Al_2O_3 amounts in the inclusions have decreased and MnS and CaO amounts have increased at 45 minutes from Ca-injection.

5. DISCUSSION

5.1 Experiments between CaO and Al_2O_3

The reaction between CaO and Al_2O_3 were studied at temperatures between 1350 and 1600°C. The annealing times at different temperatures varied. Data from these experiments are shown in Appendix II. The amount of measurements at different temperatures varies, and the SEM/EDS analyses are also not the same with each sample. However, the dissolution of the sample in HCl acid and the reacted amount of Al_2O_3 is similarly done with every sample. These results and calculations are shown in Appendix II.

Appendix I shows the SEM/EDS analyses made from the samples in the low-temperature range. Two similar charts as in Appendix I are shown in Figure 53. In this figure the reaction layer has been analysed in test 18 where temperature was 1405°C and annealing time 12 minutes. Figure 53(a) shows 15 points analysed along a line across the whole 100 μm thick reaction layer. It can be seen that in this case the reaction layer has been mainly C_3A phase. In Figure 53(b) 5 point analyses are shown from the reaction layer, 20 μm inside from the pure alumina phase (point 5). These analyses correspond to phases $C_{12}A_7$, CA and CA_6.

Appendix II shows a table of 28 diffusion couple experiments which were performed between CaO and Al_2O_3 at temperatures from 1350°C to 1600°C and annealing times from 2 minutes to 48 hours. From each experiment we have weighed the reacted amount of Al_2O_3 marked as Δm. In lower temperature region (1350–1405°C) we have two values of Δm because the experiments were performed so that the CaO cylinder was put between two alumina cylinders and these three cylinders were pressed together in horizontal direction. So the Δm used at lower temperatures is an average of the two values which are from the two alumina cylinders at each side of the CaO cylinder. From the value of Δm the reaction rate r and reaction rate constant *k* were calculated. Reaction rate constant k has been calculated twice, first using the reaction rate r and, secondly, through calculating the reaction layer thickness h from the Δm, not from SEM results. The reaction layer thickness is the same as the diffusion distance and also the reaction time is the same as the annealing time. From these values the chemical diffusion coefficient can then be calculated.

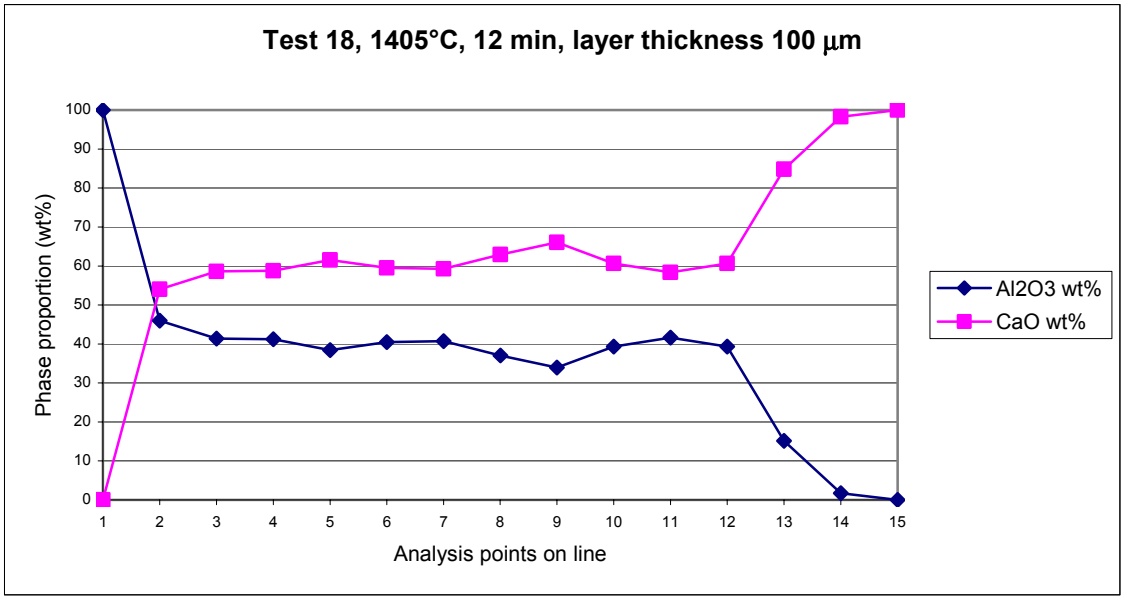

(a)

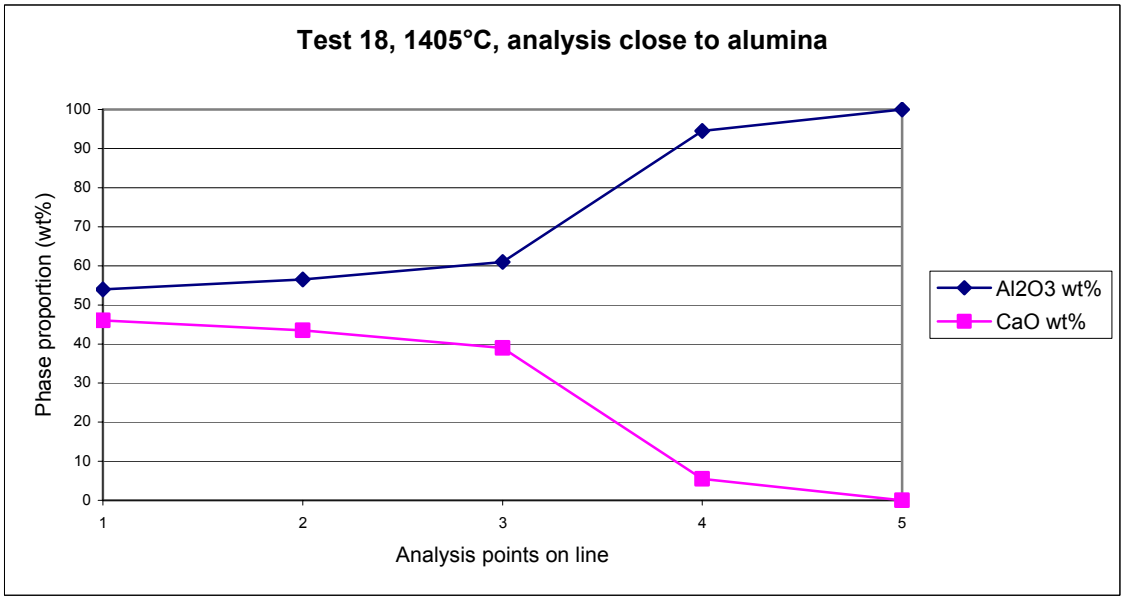

(b)

Figure 53. *Point analyses on line between Al_2O_3 and CaO (a), and from reaction layer 20 µm to alumina phase (b).*

5.2 Evaluation of reaction mechanisms

By measuring the reaction area, reaction time, mass of product, and composition of the liquid product, the $k_{overall}$ is obtained. This parameter could be used to describe the kinetics of the alumina inclusion modification. The chemical diffusion coefficient determined in this study is assumed constant and independent of composition.

Calculations were performed to get the diffusion coefficient by using the following equation:[44]

$$h = 2\sqrt{Dt} \tag{22}$$

Where h is diffusion distance (μm), D is chemical diffusion coefficient and t is time (s).

The chemical diffusion coefficient is greater at higher temperatures. Also the value of the coefficient changes at the same temperature at different annealing times. It can be seen in Appendix II that at temperatures 1450°C and 1500°C the longer the annealing time, the bigger the diffusion coefficient is. This is due to the formation of liquid at the start of the reaction which makes diffusion coefficient smaller in shorter annealing times and at longer annealing time the liquid layer has grown thicker, and the measured diffusion coefficient is bigger. Diffusion happens more easily when the liquid layer exists.

Table 9 shows the average values from many measurements at each temperature. Certain shift of magnitude can be seen in the temperature region of 1390−1420°C. In this temperature region the controlling mechanism of reaction is evidently changing. The same phenomenon can be seen in Figure 54 where a dark square (1405°C) and a rectangle (1390°C) are in this region. In this temperature region the reaction rate is very temperature sensitive, and the apparent activation energy is very high indicating a transition in the controlling mechanism.[40] The rate controlling mechanism in temperatures under this region is Ca diffusion.[35] In temperatures over the region the chemical reaction between alumina and liquid calcium aluminate is assumed to be the rate-controlling mechanism.

Table 9. Rate constants and diffusion coefficients at different temperatures

T(°C)	1350	1370	1390	1405	1420	1450	1500	1550	1600
K (m/s)	1.0×10^{-9}	1.7×10^{-9}	1.2×10^{-8}	5.8×10^{-9}	1.3×10^{-6}	2.0×10^{-6}	8.2×10^{-6}	1.4×10^{-5}	4.3×10^{-5}
D ($m^2 s^{-1}$)	7.1×10^{-15}	6.5×10^{-15}	2.7×10^{-13}	4.3×10^{-13}	1.1×10^{-10}	2.2×10^{-10}	7.0×10^{-10}	2.7×10^{-9}	1.1×10^{-8}

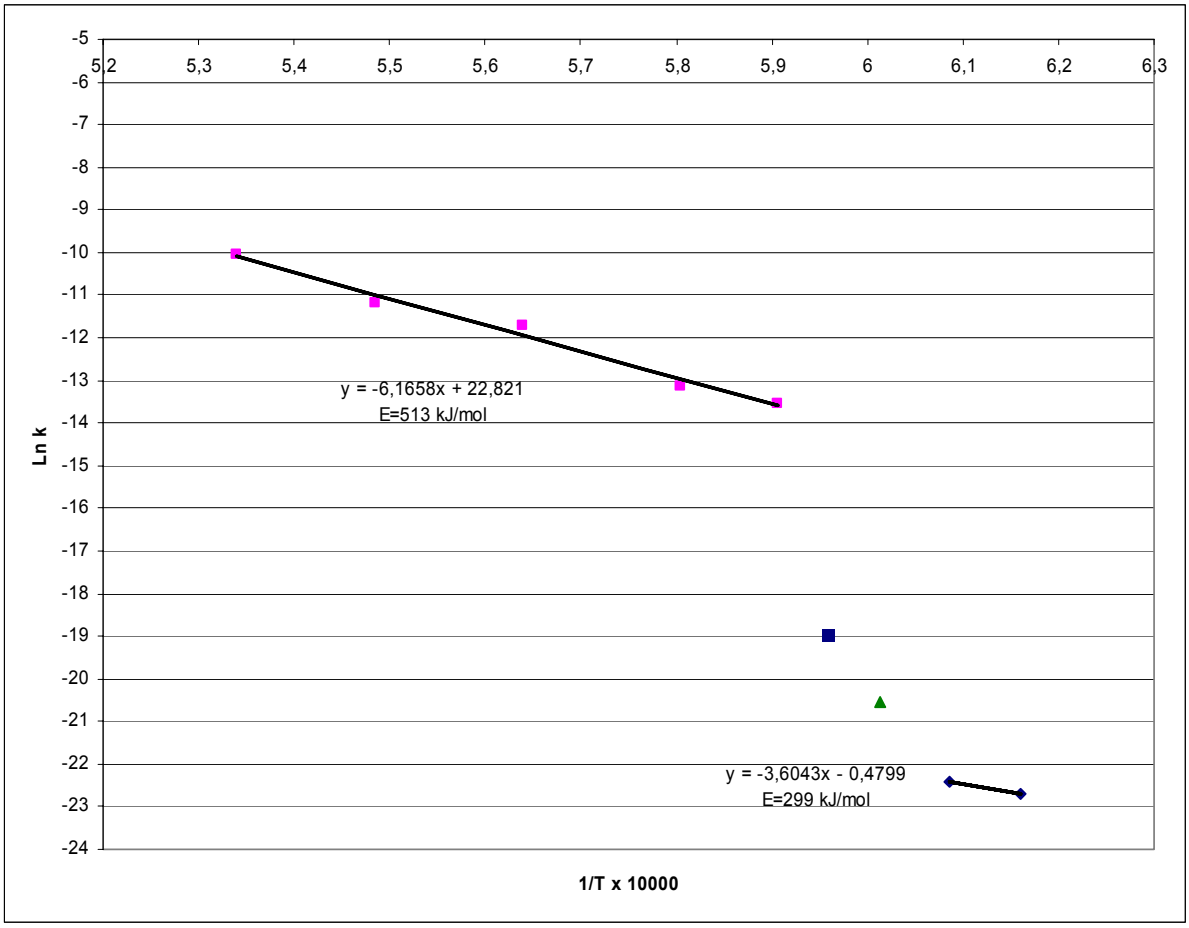

Figure 54. *Natural logarithm of rate constant versus reciprocal temperature (1/K) showing the temperature dependency of the reaction rate. Activation energy E is shown for temperature ranges 1420–1600°C and 1350 –1370°C.*

5.3 Model demonstrating reaction between alumina inclusion and calcium oxide

Based on the concept developed in this work for modification of alumina inclusions by calcium treatment, a model was created by Karri Penttilä and Pertti Koukkari at VTT Chemical Technology, Finland. This model called IncApp utilizes the CHEMSHEET program, which is an Excel application calculating the equilibrium composition.[34] It has its own simplified routines for calculating diffusion for different time steps (one-dimensional model presented in a spherical geometry). Experimental work and its results shown in this work (SEM pictures and diffusion coefficients) have given the basic data to build the model. The chemical database used comes from FactSage and the slag phase model (CaO-Al_2O_3) used is QSOL.[21] The rest of the phases are stoichiometric. Inclusion modification is assumed to be diffusion controlled.

Locally, in every calculation area the diffusion rate is calculated using formula:

$$1/D = X(p1) / D(p1) + X(p2) / D(p2) \ldots \quad (23)$$

where X is mass fraction

p1, p2,… are phase indexes

Calculations were done for an alumina inclusion with a radius of 600 μm. The temperature was 1500°C and the diffusion coefficients were:

$D_{liq}=3*10^{-9}$ m^2/s, $D_{sol}=3*10^{-11}$ m^2/s.

Figure 55 and Figure 56 show results using this IncApp application to demonstrate alumina inclusion modification by calcium. It can be seen that liquid calcium aluminate is the dominant phase when an alumina inclusion is modified at temperature 1500°C. This same result was also supported by the experimental work.

In Figure 55 there is a series of pictures demonstrating the progress of modification of a spherical alumina particle. The size of the alumina particle before calculation is marked with black line. Different colours indicate different phases: Al_2O_3 (red), CA_6 (pink), CA_2 (violet), CA-liquid (blue), C_3A (turquoise), and CaO (green).

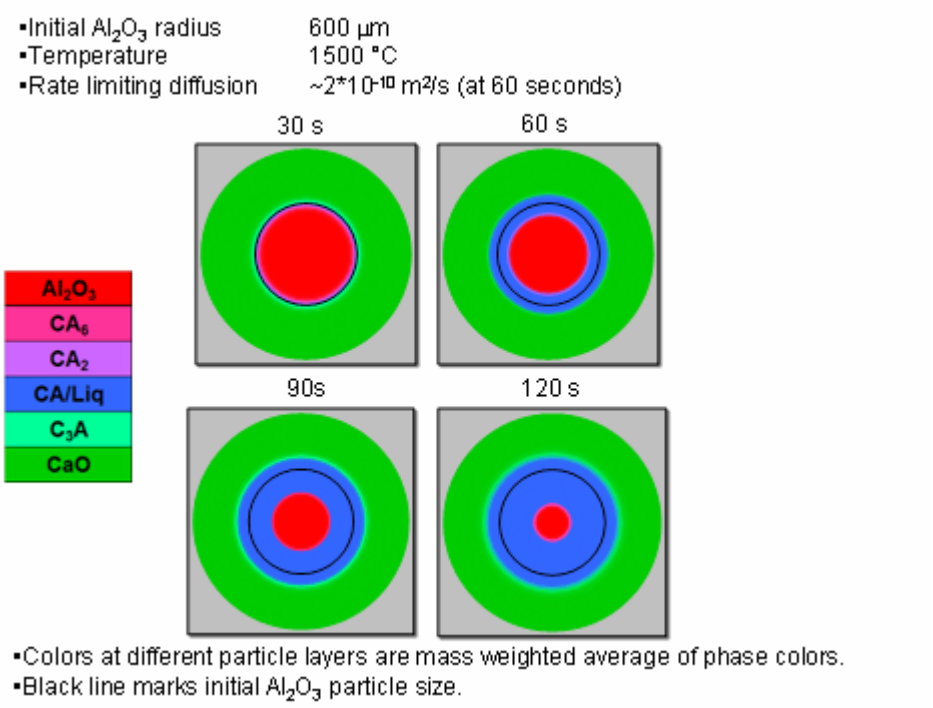

Figure 55. *Reaction of Al_2O_3 particle with CaO calculated by ChemSheet program. Picture shows different phases present at different times after the reaction starts.*

Figure 56 gives a calculated "line scan analysis" from the centre of the Al_2O_3 inclusion to the surface. Mass fractions of the phases through the inclusion are seen at 90 seconds after the reaction start. The same result is also shown in Figure 55 as a cross section of a spherical particle (left bottom).

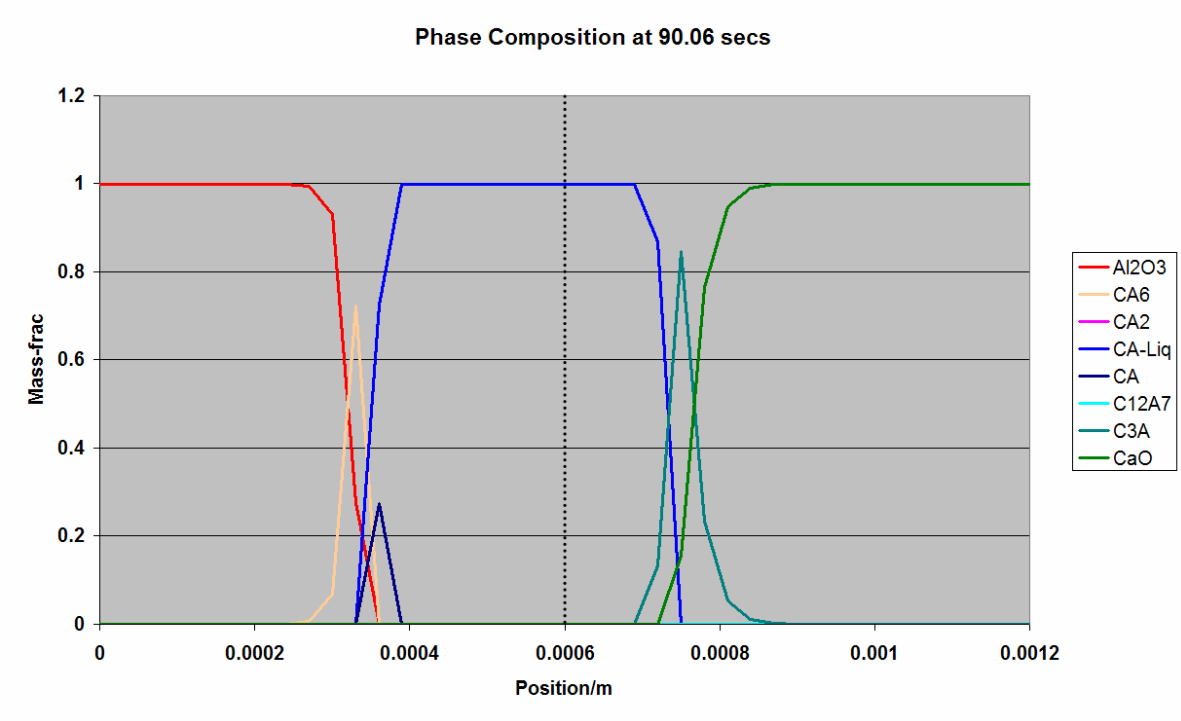

Figure 56. *Mass fraction of phases between Al_2O_3 core and surrounding CaO at 90.06 seconds after the reaction start at 1500°C.*

5.4 Inclusions found in Ca treatment experiments done with 8 kg steel melt

An example of the inclusion transformation "path" resulted from calcium addition is shown in Figure 57. Before Ca addition the inclusions were of pure alumina type. The first sample was taken one minute after the Ca addition. No pure alumina inclusions could be detected any more, and the transformation phenomenon proceeded rapidly to liquid inclusions CA_x with x=1.15 corresponding to a liquidus temperature of approximately 1600°C in the binary system. In process of time, the CaO content in inclusions tended to decrease, presumably due to reoxidation phenomenon which is evidenced by increasing contents of SiO_2 and MnO in inclusions. Anyway the results support the conception of the fast transformation process of inclusions when adding calcium into the steel melt.

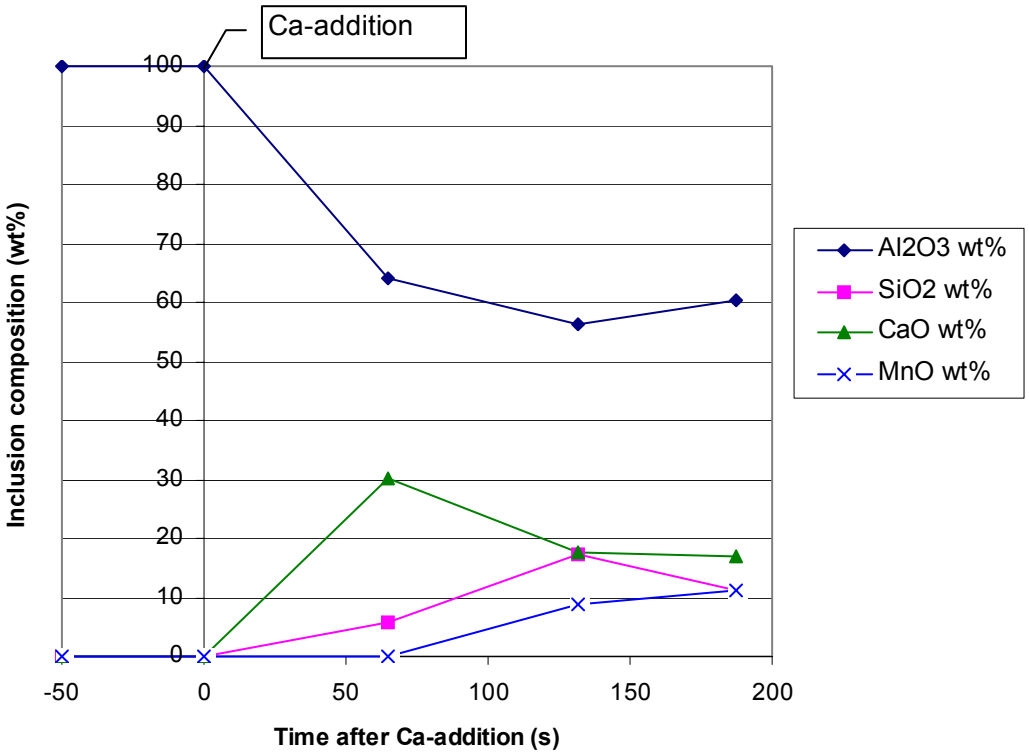

Figure 57. *Change of inclusions composition in the 4th heat, due to Ca-treatment of Al deoxidized steel.*

5.5 Inclusion analysis with INCA Feature

The analyzed area can be determined by the operator; in this case the area was 2 mm x 2 mm. When comparing the figures before (Figure 38, Figure 46, and Figure 52) from these three heats it can be seen clearly that the fractions of sulphide inclusions (MnS and CaS) change quite much from the Ca treatment to the casting. When examining the heats from Koverhar and Imatra steel plants and comparing the samples taken during the first 5 minutes after Ca treatment, certain differences can be found. In the Koverhar heat the calcium sulphide content goes gradually up and remains on relatively high level, but in the Imatra heats the calcium sulphide content goes first up and then falls down. This phenomenon is related to different sulphur contents in steels as well as other components i.e. manganese, calcium and aluminium contents which can be found in the figure headings of the corresponding heats. When further scrutinizing the figures the CaO content and CaO : Al_2O_3 ratio can be considered surprisingly low.

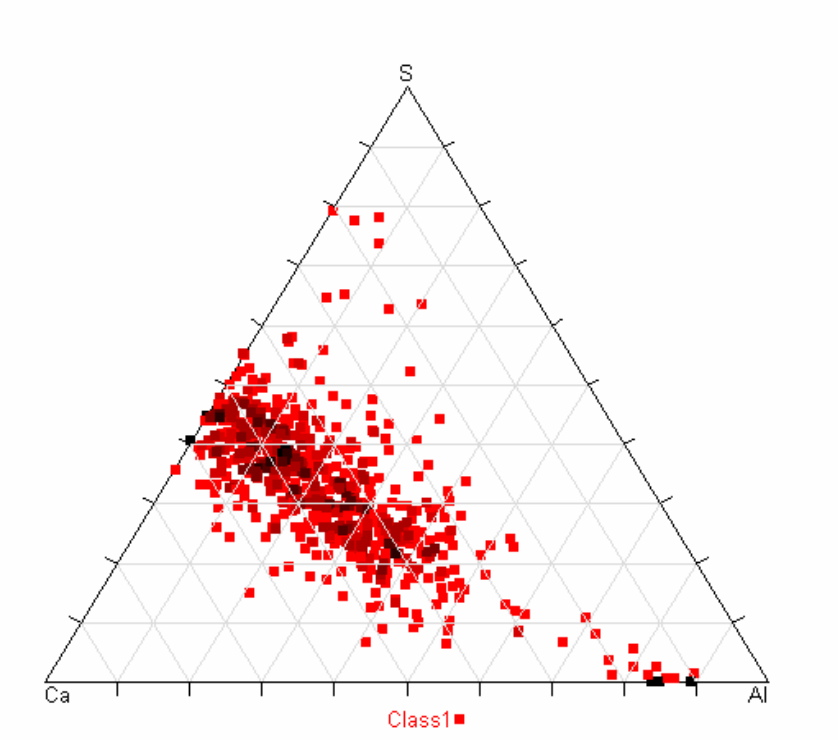

Figure 58. *Inclusions found in sample taken four minutes after Ca treatment at Koverhar steelworks. Only inclusions containing calcium and with size >0.8 µm length were taken into account (Class 1)*

The system INCA Feature provides different ways to present the inclusions that are found in the specified sample area (2mm x 2 mm in this work).Figure 58 to Figure 60 represent the calcium containing inclusions that have a length over 0.8 µm placed in a ternary diagram.

These ternary diagrams have been constructed in a similar way as Story et al. (ref. 42) have done, using the data from the Koverhar steelworks heat. Ternary diagrams (Figure 58 and Figure 59) clearly show that the inclusions after Ca-treatment in this heat contain a lot of CaS in duplex inclusions, this same result could be seen in Figure 38 where the inclusions at the end of ladle treatment mainly consist of calcium sulphide and calcium aluminates. Figure 60 shows inclusion compositions in a sample taken from the continuous casting mould. Inca Feature gives an option to form ternary phase diagrams for single elements or for oxides. In Figure 60 the same data are shown in these two modes. These diagrams show what has been the inclusion composition during casting, so they can be compared with the diagram in Figure 11. The comparison shows that inclusion composition has been in a good area to maintain stable castability, because a significant portion of the inclusions fell within the liquid or semi-liquid (50%) region.

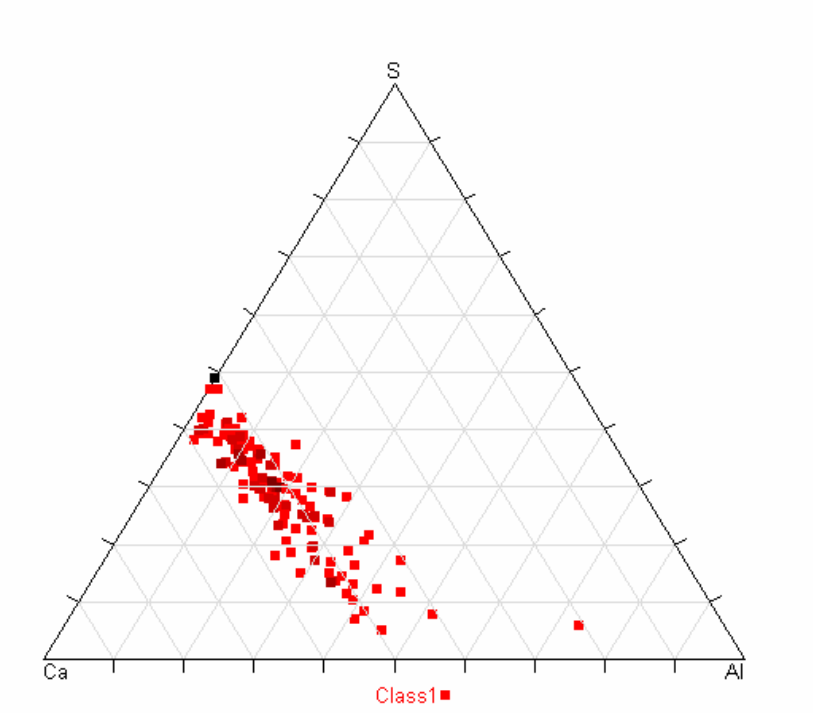

Figure 59. *Inclusions found in sample taken fifteen minutes after Ca treatment at Koverhar steelworks.*

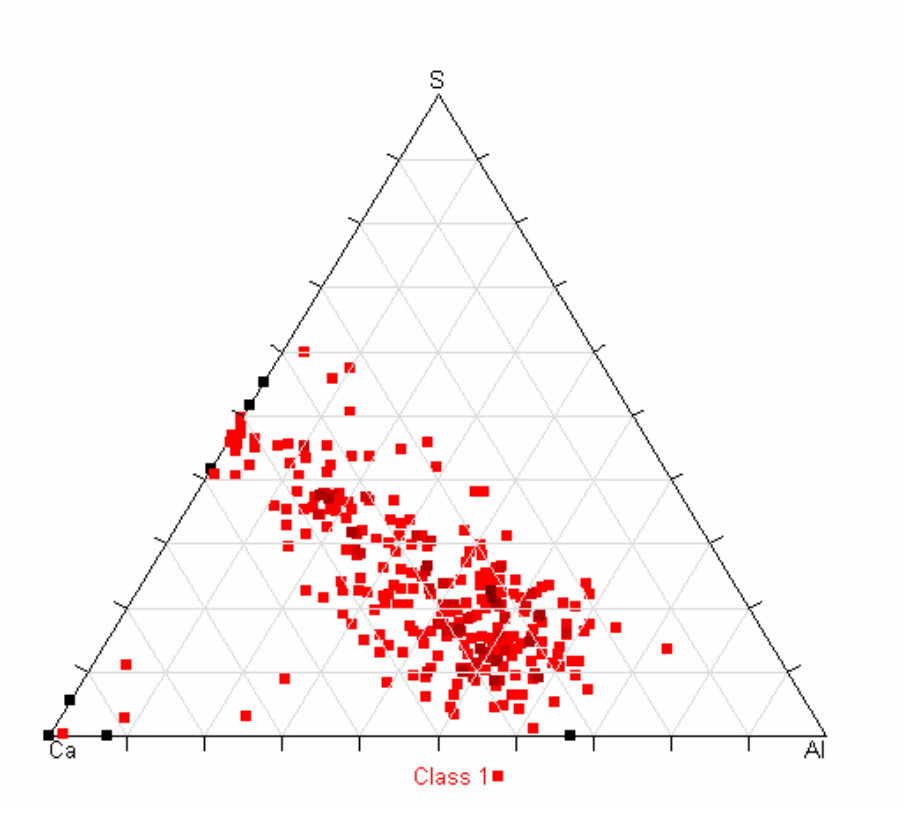

(a)

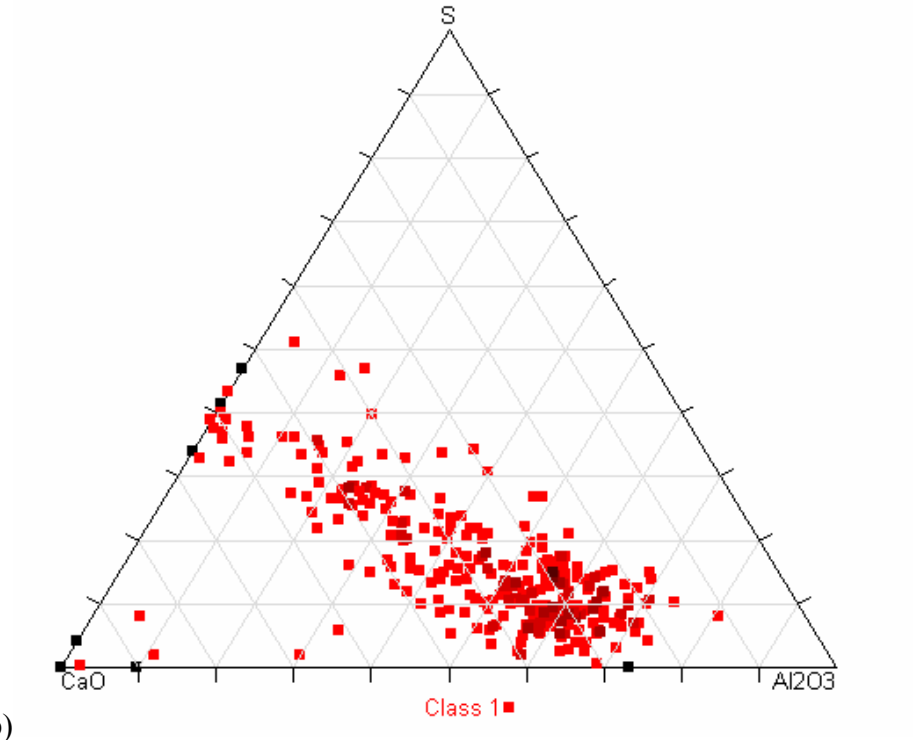

(b)

Figure 60. *Inclusions found in sample taken thirty minutes after Ca treatment at Koverhar steelworks.*

6. CONCLUSIONS

The mechanism and kinetics of alumina inclusion modification were investigated by studying the reaction between CaO and Al_2O_3 as well as between calcium and Al_2O_3 inclusions in steel melts. Experiments can be divided into three different groups which support each others: 1) Reactions between Al_2O_3 and CaO in a laboratory resistance furnace 2) Ca treatment made to Al-killed steel in an 8 kg induction furnace and 3) Ca treatment made on industrial scale with sampling from three different heats at Imatra and Koverhar steelworks.

From the first type of experiments it was possible to see how the reactions proceed between CaO and Al_2O_3. The exact amount of reacted alumina was measured and the reaction rate constant was calculated in the temperature range 1350–1600°C. Reaction rate constants were drawn as a function of temperature, so that the activation energies could be calculated from a straight line. The function shows that in the temperature range 1370–1420°C it happens a shift in the controlling mechanism of the reaction, so linear dependence cannot be applied in this region. The result is interpreted to mean that at the lower temperatures the reaction is diffusion controlled but becomes chemical reaction controlled at higher temperatures. Concerning the interaction between liquid calcium aluminate and an alumina inclusion, the chemical reaction between solid alumina and liquid calcium aluminate was assumed to be the rate-controlling step at temperatures above 1420°C.

Also experiments between mixed and pressed alumina and CaO powders were performed close to the Al_2O_3-CaO eutectic temperature. These samples were analyzed with SEM/EDS and x-ray diffractometer to identify the calcium aluminate phases formed. The phases formed at 1400°C in 6 hours were $12CaO{\cdot}7Al_2O_3$ (41%), $CaO{\cdot}Al_2O_3$ (36%), $CaO{\cdot}2Al_2O_3$ (11%) and the rest were the starting materials, CaO and Al_2O_3.

The second group of experiments was made in an induction furnace with 8 kg steel melt. These experiments showed that at 1600°C alumina inclusions are converted to calcium aluminates very quickly after the Ca addition. SEM/EDS analysis confirmed that in samples taken one minute from Ca injection, alumina inclusions had already substantially converted to calcium aluminates.

The third group of experiments were Ca treatments done in industrial scale. The samples taken from the melt at certain intervals after the Ca addition were analyzed with the new SEM/EDS software called INCA Feature, which automatically collects chemical and morphological data from inclusions in steel. Figures showing the changes in the inclusion composition and size after Ca-treatment were given. For example the data from 1400 inclusions showed consistently that the dominating inclusions in the final steel were calcium aluminates and manganese sulphides, the average size of inclusions being under 1.5 μm by length.

By combining the data and knowledge from the different experiments and literature a thermodynamic – kinetic model for the transformation of alumina inclusions to calcium aluminates was constructed. The transformation is driven by Gibbs energies of formation of calcium aluminates whereas diffusivities and the formation of liquid aluminate phase are the rate-determining factors.

REFERENCES

[1] Llewellyn, D.T., Steels: Metallurgy and Applications, Oxford 1992, Butterworth-Heinemann, pp. 302.

[2] Janke, D., Zhongting, MA. et al., Improvement of Castability and Quality of Continuously Cast Steel, ISIJ International, Vol.40, No.1, 2000, pp. 31-39.

[3] Ma, Z. and Janke, D., Characteristics of Oxide Precipitation and Growth during Solidification of Deoxidized Steel, ISIJ International, Vol. 38, No. 1, 1998, pp. 46-52.

[4] Lu, D.-Z., Irons, G.A. and Lu, W.-K., Kinetics and Mechanisms of Calcium Absorption and Inclusion Modification of Steel, Scaninject VI, Luleå, Sweden, 2-4 June, 1992, pp. 239-263.

[5] Turkdogan, E.T, Fundamentals of Steelmaking, The Institute of Materials, The University Press, Cambridge, UK, 1996, pp. 331.

[6] The Japan Society for the Promotion of Science, The 19th Committee on Steelmaking, Steelmaking data sourcebook, revised edition, Gordon and Breach Science Publishers, 1988, p. 325.

[7] Ozawa, M., Ohtsuka, Y., Hori, Y. and Mori, T., 19th Committee, Japan Society for the Promotion of Science, No. 9839, June 1976.

[8] Suzuki, K., Nakamura, H., Ejima, A. and Sanbongi, K., 19th Committee, Japan Society for the Promotion of Science, No. 10057, September 1975.

[9] Haida, O., Matsuno, J., Emi, T., Imai, T., Emoto, K. and Sekine, M., Tetsu-to-Hagane, 65, A21, 1979.

[10] Miyashita, Y. and Nishikawa, K., Tetsu-to-Hagane, 57 (1971), 1969.

[11] Kobayashi, S., Ohmori, Y. and Sanbongi, K., Trans. Iron Steel Inst. Japan, 11, 1971, p. 260.

[12] Ototani, T., Kataura, Y. and Degawa, T., Tetsu-to-Hagane, 61, 2168, 1975.

[13] Gustafsson, S., Scand. J. Met., 9, 1980, p.111.

[14] Suzuki, K., 19th Committee No 10587, Japan Society for the Promotion of Science, November 1984.

[15] Shepherd, E.S., Rankin, G.A. and Wright, F.E., Am. J. Sci. 1909, vol.28, pp.293-333.

[16] Rankin, G.A. and Wright, F.E., Am. J. Sci. 1915, vol.39, pp.1-79.

[17] Lagerqvist, K., Wallmark, S. and Westgren, A.,Z., Anorg. Allg, Chem. 1937, vol. 234, pp.1-16.

[18] Filonenko, N.E. and Lavrov, I.V., Dokl. Akad.Nauk S.S.S.R., 1949, vol.66, pp.673-76.

[19] FactSage 5.4.1, Developers: Bale, C.W., Pelton, A.D., Thompson, W.T., Erikson, G., Hack, K., Chartrand, P., Decterov, S., Melancon, J. and Petersen, S., www.Factsage.com

[20] Nurse, R.W., Welch, J.H. and Majumdar, A.J., Trans. Br. Ceram. Soc., 1965, vol. 64, pp.323-32.

[21] Nityanand, N. and Fine, H.A., Metall. Trans. B, 1983, vol. 14B, pp. 685-92.

[22] Eriksson, G. and Pelton, A.D., Critical Evaluation and Optimization of the Thermodynamic Properties and phase diagrams of the CaO-Al_2O_3, Al_2O_3-SiO_2, and CaO-Al_2O_3-SiO_2 Systems, Metallurgical Transactions B, Volume 24B, 1993, pp. 807-815.

[23] Schlackenatlas, Slag Atlas, Verlag Stahleisen, Düsseldorf, 1981, 282 pp.

[24] Kiessling, R., Non-metallic inclusions in steel., Second edition, including Part II, London 1978, The Metals Society, p. 37.

[25] Tähtinen, K., Väinölä, R. and Sandholm, R., Ladle Injection – A way to continuously cast aluminium-killed steels for billets at Ovako, Scaninject II, International conference on injection metallurgy, Luleå, Sweden, June 12-13, organized by Mefos and Jernkontoret, 1980, pp. 24:1-24:14.

[26] Holappa, L.E.K., Ladle injection metallurgy, International Metals Reviews, 1982, Vol. 27, No.2, pp. 53-76.

[27] Holappa, L. and Ylönen, H., The effect of sulfur on non-metallic inclusions in Ca-treated Al-killed steel, Fifth International Iron and Steel Congress, Steelmaking proceedings, Vol. 69, Washington, DC, Publication of ISS/AISE, 1986, pp. 277-283.

[28] Holappa, L., Hämäläinen, M., Liukkonen, M. and Lind, M., Thermodynamic examination on inclusion modification and precipitation from calcium treatment to solidified steel, Ironmaking and Steelmaking, Vol.30, No. 2, 2003, pp. 111-115.

[29] Backman, J., Ca-injection treatment of steels from users point of view, Scaninject III, Luleå, Sweden, June 15-17, 1983, Part I, pp. 2:1-2:13.

[30] Gaye, H., Gatellier, C., Nadif, M., Riboud, P.V., Saleil, J. and Faral, M., Slags and inclusions control in secondary steelmaking, Clean Steel 3, Balatonfured, Hungary, June 2-4, 1986, pp. 137-147.

[31] Eriksson, G. and Hack, K., Metall. Trans. B, 1990, 21B, pp. 1013-1023.

[32] Miettinen, J., Metall. Trans. A, 1992, 23A, pp. 1155-1170.

[33] Koukkari, P., Penttilä, K., Hack, K. and Petersen, S., Proc. Euromat 99, Vol.3, 323-330, 2000, Weinheim, Wiley-VCH.

[34] Lu, D.-Z., Irons, G.A. and Lu, W.-K., Kinetics and mechanisms of calcium dissolution and modification of oxide and sulphide inclusions in steel, Ironmaking and Steelmaking, Vol. 21, No. 5, 1994, pp. 362-371.

[35] Kohatsu, I. and Brindley, G. W. Solid State Reactions between CaO and α–Al_2O_3, Zeitschrift für Physikalische Chemie Neue Folge, Bd. 60, 1968, pp. 79-89.

[36] Weisweiler, W. and Ahmed, S.J., Kinetik der Festkörperreaktionen im System CaO-Al_2O_3, Zement-Kalk-Gips, Nr. 2, 1980, pp. 84-89.

[37] Jerebtsov, D.A. and Mikhailov, G.G., Phase diagram of CaO-Al_2O_3 system, Ceramics International, Volume 27, Issue 1, 2001, pp. 25-28

[38] Cho, W.D. and Fan, P., Diffusional Dissolution of Alumina in Various Steelmaking Slags, ISIJ International, Vol. 44, No. 2, 2004, pp. 229-234.

[39] Valdez, M., Prapakorn, K., Shidhar, S. and Cramb, A.W., Dissolution of Inclusion in Steelmaking Slags, ISSTech 2003 Conference Proceedings, 2003, pp. 789-798.

[40] Levenspiel, O., Chemical Reaction Engineering, 3rd edition, John Wiley & Sons, New York, 1999, pp. 586.

[41] Fogler, H.S., Elements of Chemical Reaction Engineering, Prentice-Hall International, Inc., USA, 1992, pp. 838.

[42] Story, S.R., Piccone, T.J. and Fruehan, R.J., Inclusion Analysis to Predict Casting Behavior, Iron and Steel Technology, ISSTech 2003, article taken from http://www.aist.org, Sept. 2004, pp. 163-169.

[43] Han, Z., Lind, M. and Holappa, L., Mechanism and Kinetics of Transformation of Alumina Inclusions by Ca Treatment, International Conference on Non-metallic Inclusions Control and Continuous Improvement of Processes based on Objective Measurement, STÅL 2004, 5-6 May 2004, Borlänge, Sweden, 2004, pp. 13.

[44] Uchida, M., Numakura, H., Yamabe-Mitarai, Y. and Bannai, E., Chemical diffusion in Ir_3Nb, Scripta Materialia, Volume 52, Issue 1, January 2005, pp. 11-15.

APPENDIX I

Point analyses along a line from the reaction layer between Al_2O_3 and CaO temperature range 1350-1405°C

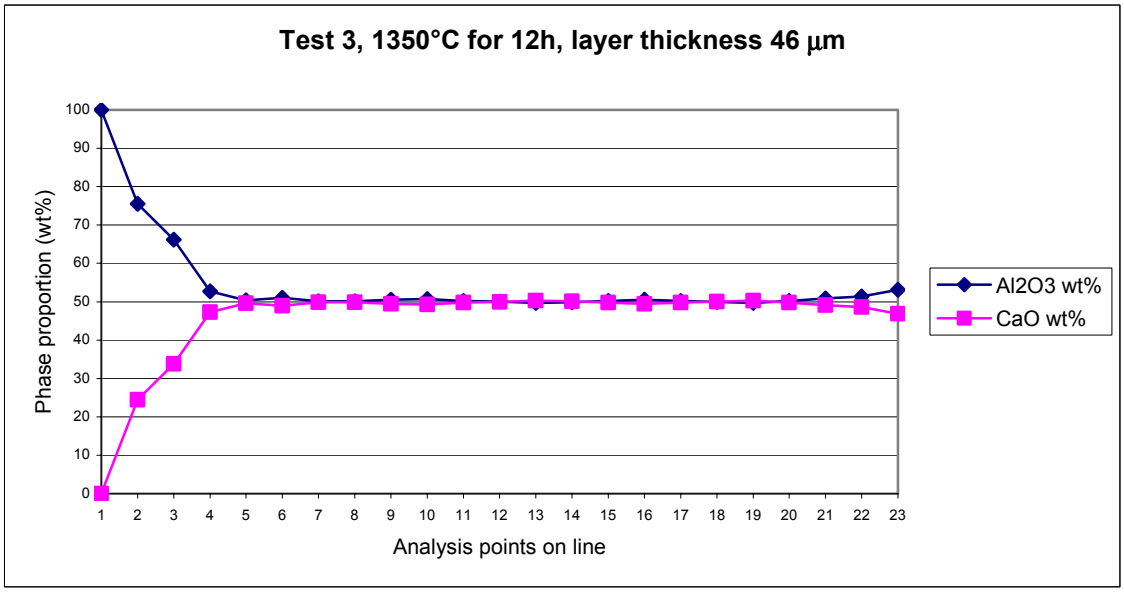

Figure a1. *Point analyses along a line showing the phases CA_2, CA and $C_{12}A_7$.*

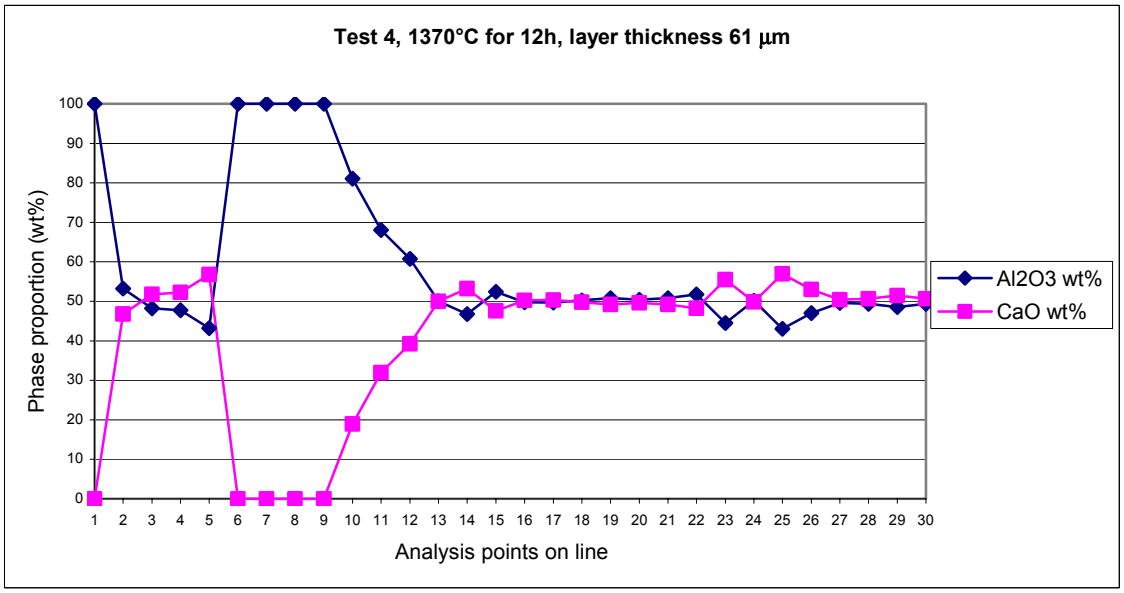

Figure a2. *Point analyses along a line showing the phase $C_{12}A_7$.*

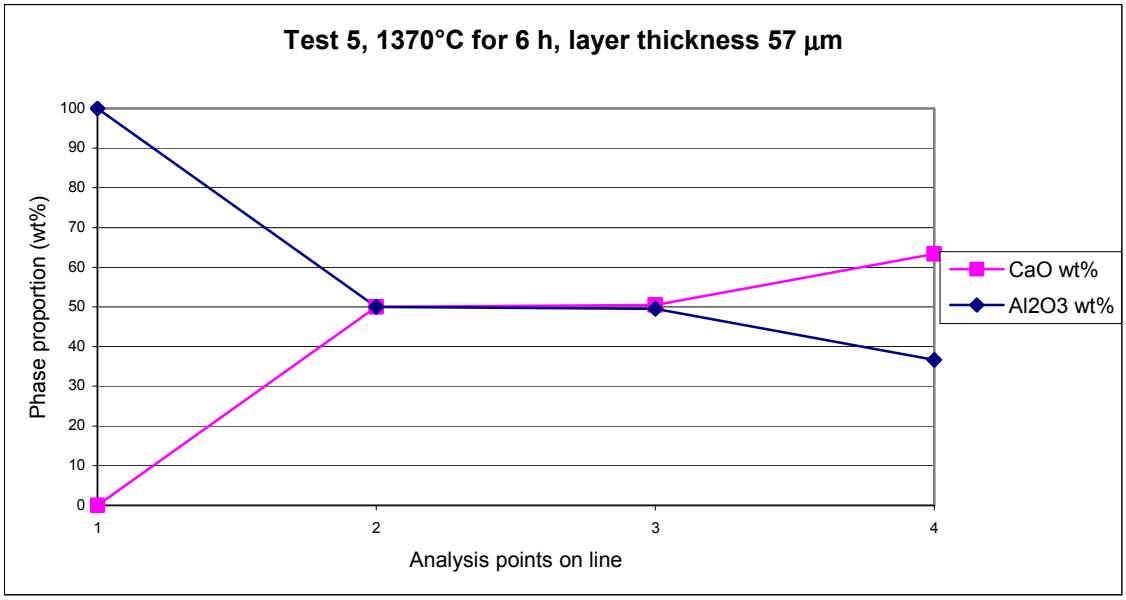

Figure a3. *Point analyses along a line showing the phases $C_{12}A_7$ and C_3A.*

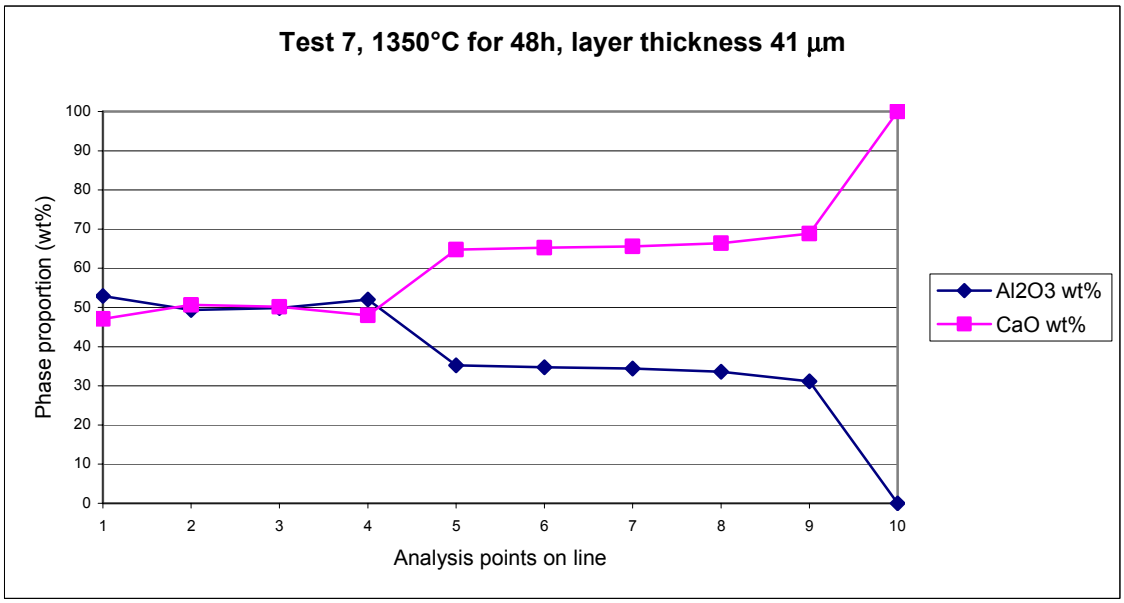

Figure a4. *Point analyses along a line showing the phases $C_{12}A_7$ and C_3A.*

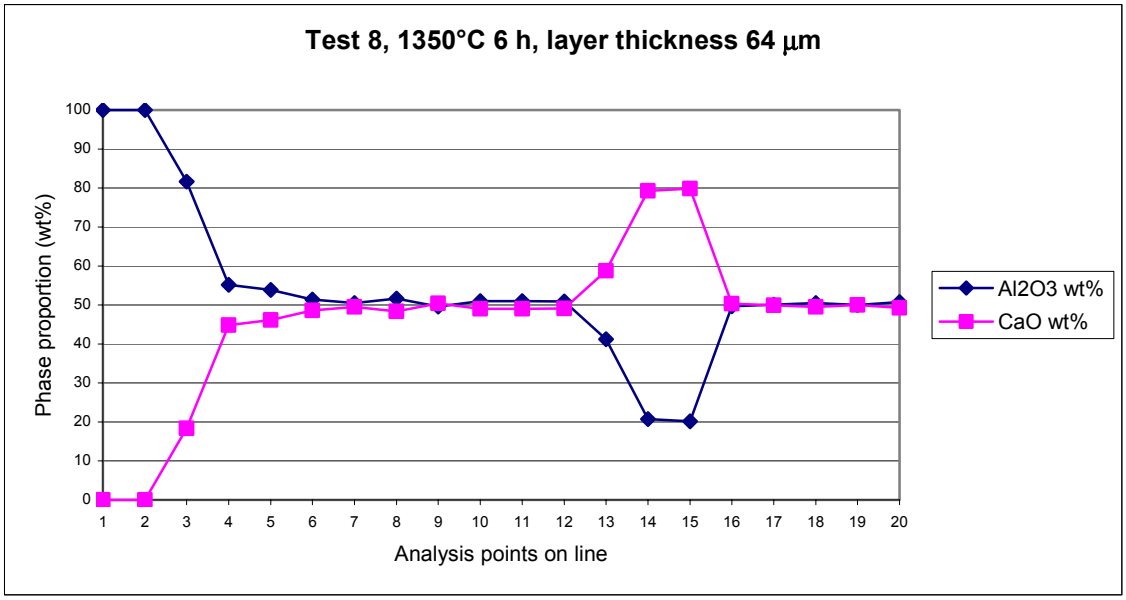

Figure a5. *Point analyses along a line showing the phases CA_2, $C_{12}A_7$, and C_3A.*

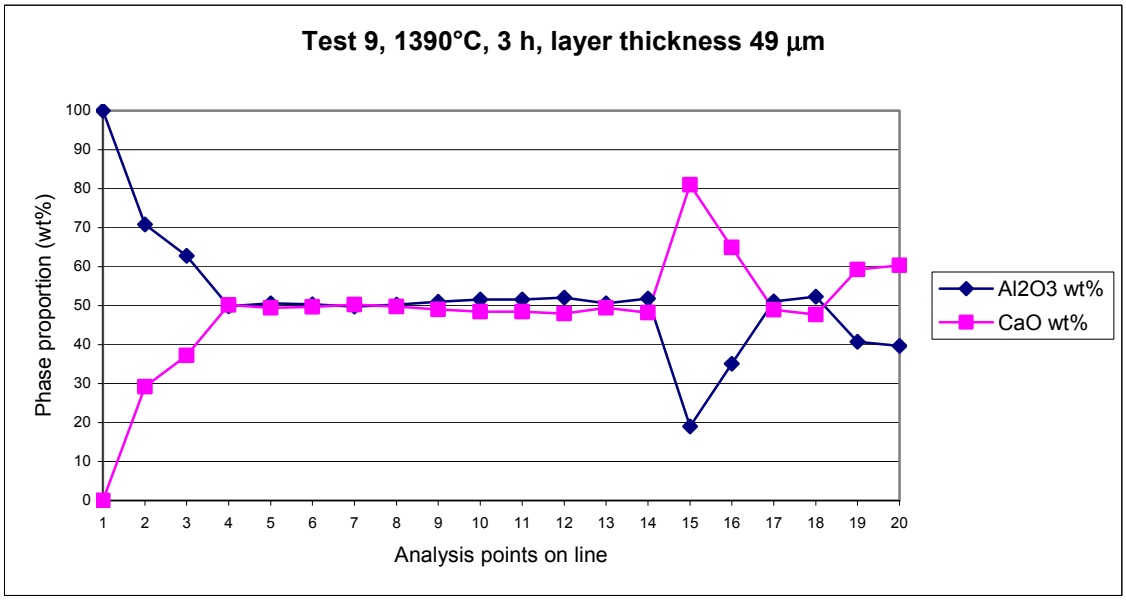

Figure a6. *Point analyses along a line showing the phases CA, $C_{12}A_7$, and C_3A.*

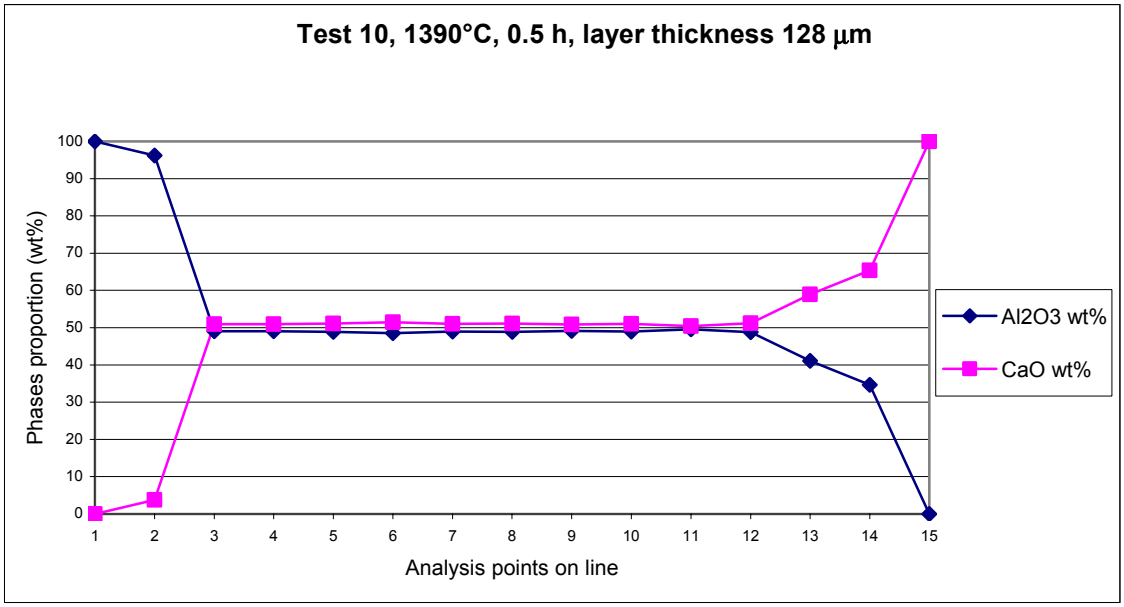

Figure a7. *Point analyses along a line showing the phases $C_{12}A_7$ and C_3A.*

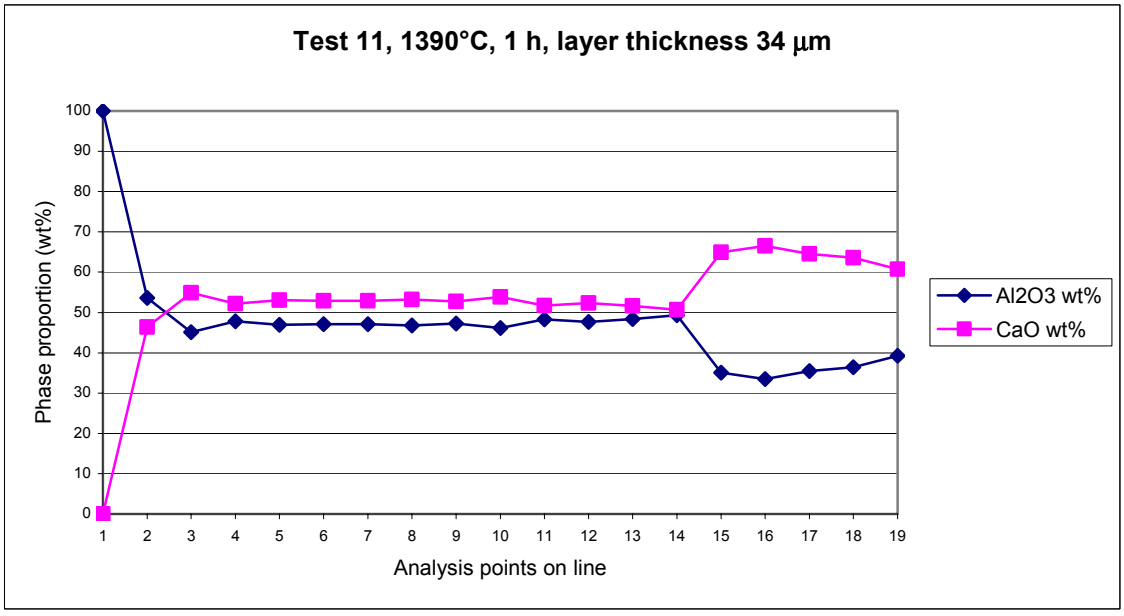

Figure a8. *Point analyses along a line showing the phases $C_{12}A_7$ and C_3A.*

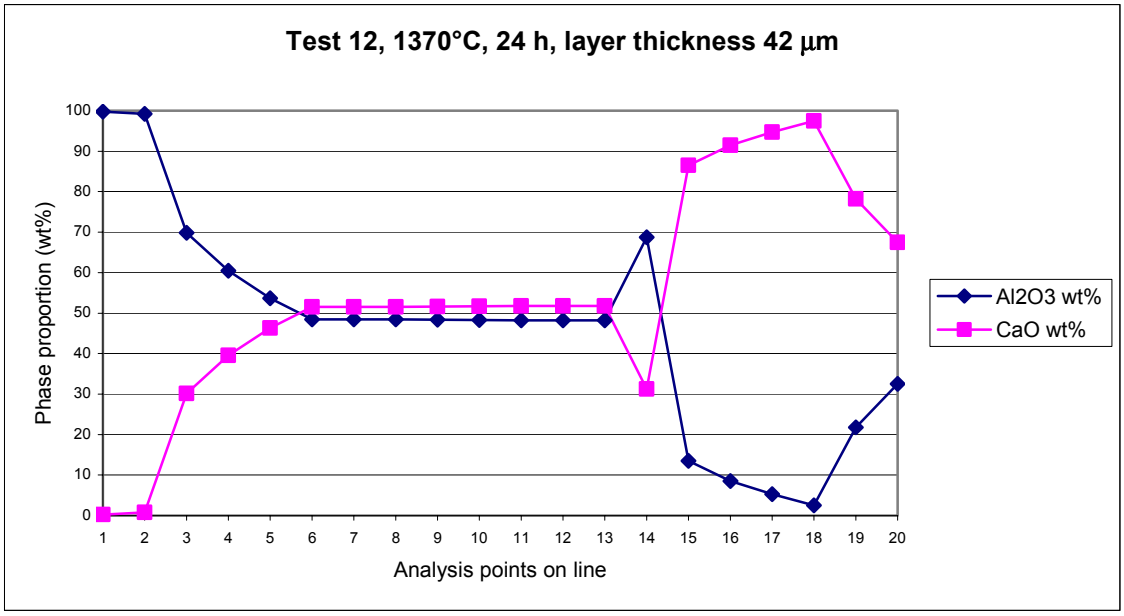

Figure a9. *Point analyses along a line showing the phases CA, $C_{12}A_7$, and calcium oxide rich phase.*

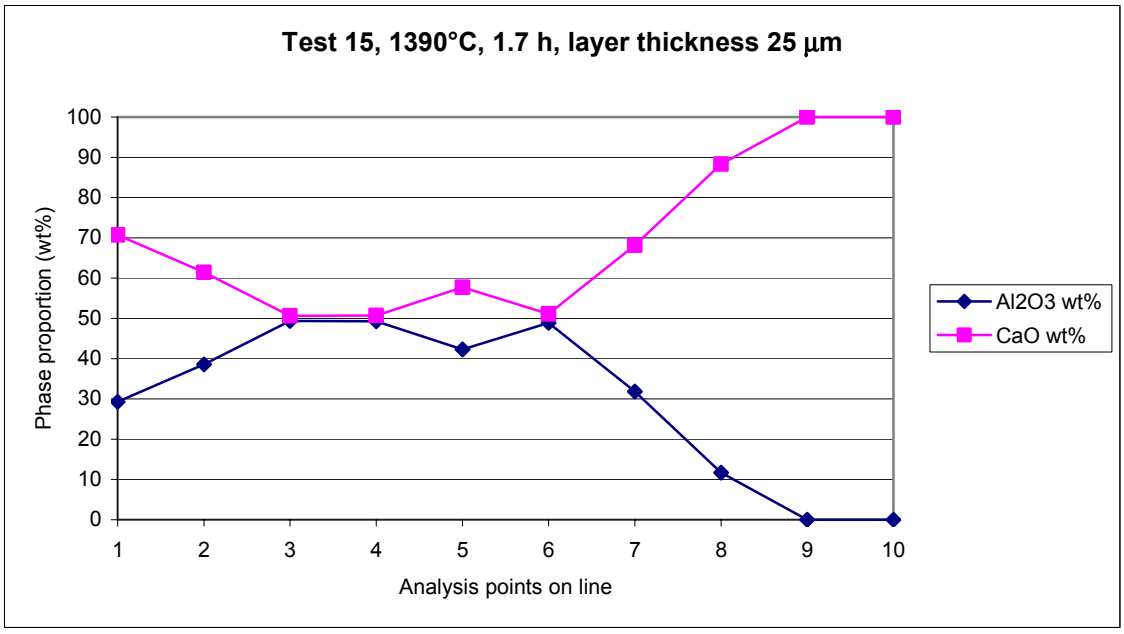

Figure a10. *Point analyses along a line showing the phases C_3A and $C_{12}A_7$.*

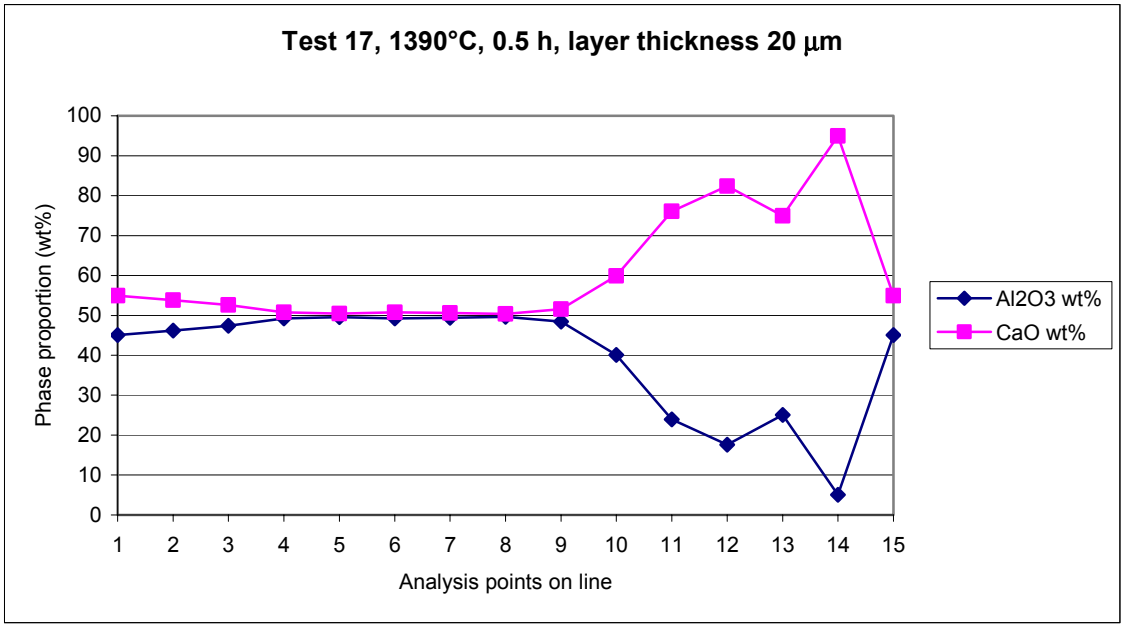

Figure a11. *Point analyses along a line showing the phases $C_{12}A_7$ and C_3A.*

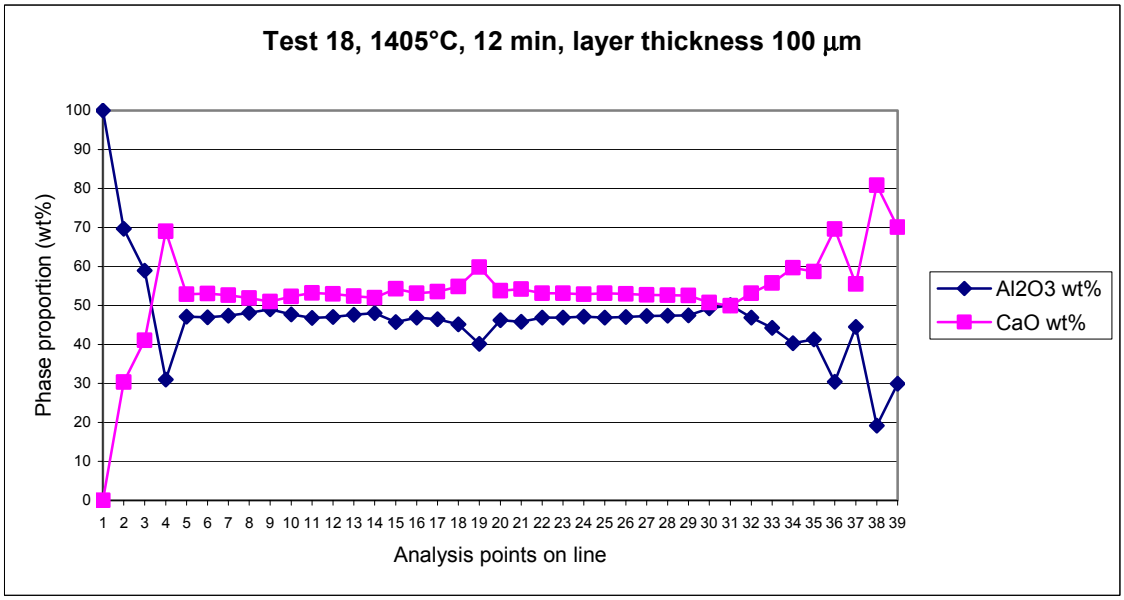

Figure a12. *Point analyses along a line showing the phases CA, $C_{12}A_7$, and C_3A.*

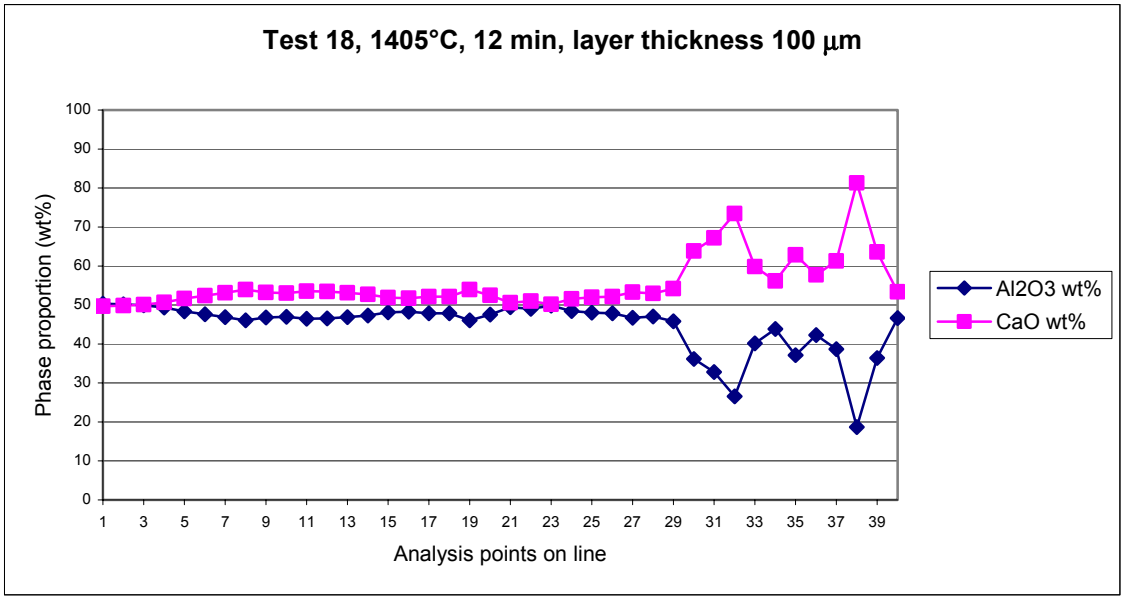

Figure a13. *Point analyses along a line showing the phases $C_{12}A_7$ and C_3A.*

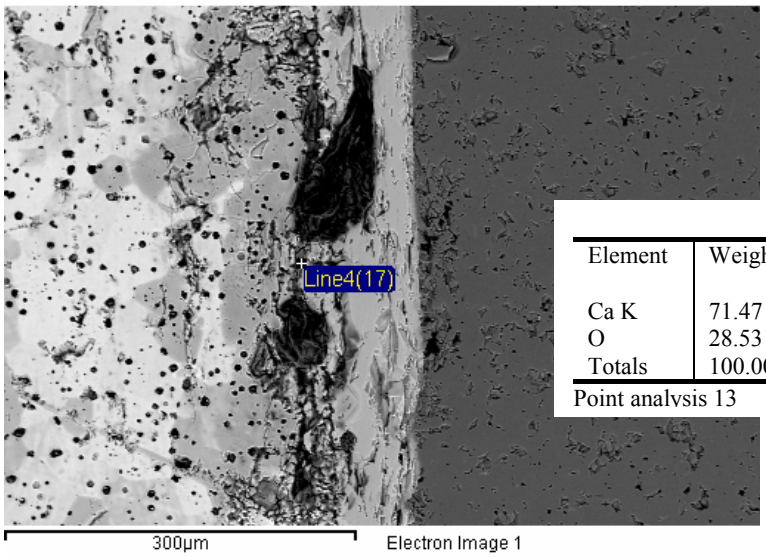

Element	Weight%	Atomic%	Compd%	Formula
Ca K	71.47	50.00	100.00	CaO
O	28.53	50.00		
Totals	100.00			

Point analysis 13

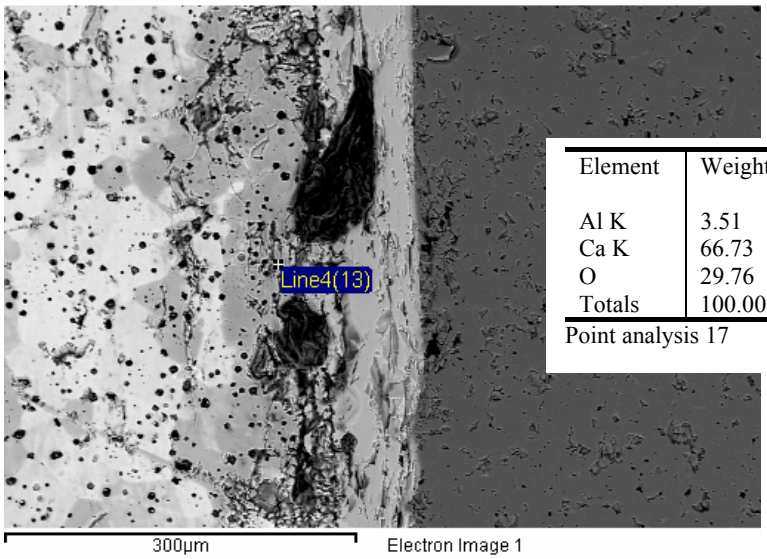

Element	Weight%	Atomic%	Compd%	Formula
Al K	3.51	3.56	6.63	Al2O3
Ca K	66.73	45.55	93.37	CaO
O	29.76	50.89		
Totals	100.00			

Point analysis 17

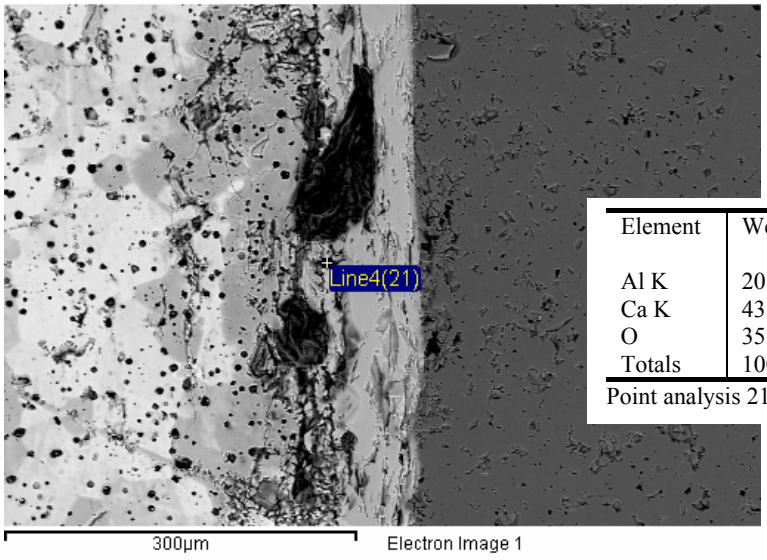

Element	Weight%	Atomic%	Compd%	Formula
Al K	20.80	18.84	39.29	Al2O3
Ca K	43.39	26.46	60.71	CaO
O	35.82	54.71		
Totals	100.00			

Point analysis 21

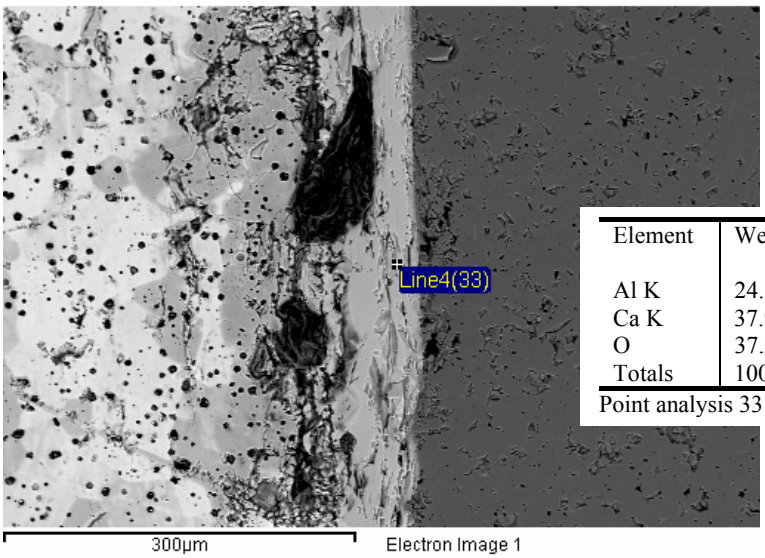

Element	Weight%	Atomic%	Compd%	Formula
Al K	24.85	21.96	46.95	Al2O3
Ca K	37.91	22.55	53.05	CaO
O	37.24	55.49		
Totals	100.00			

Point analysis 33

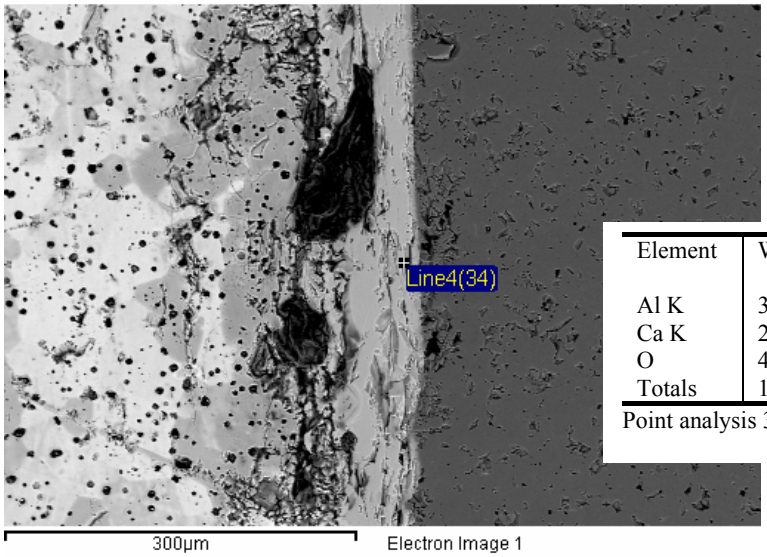

Element	Weight%	Atomic%	Compd%	Formula
Al K	35.48	29.46	67.03	Al2O3
Ca K	23.56	13.17	32.97	CaO
O	40.96	57.37		
Totals	100.00			

Point analysis 34

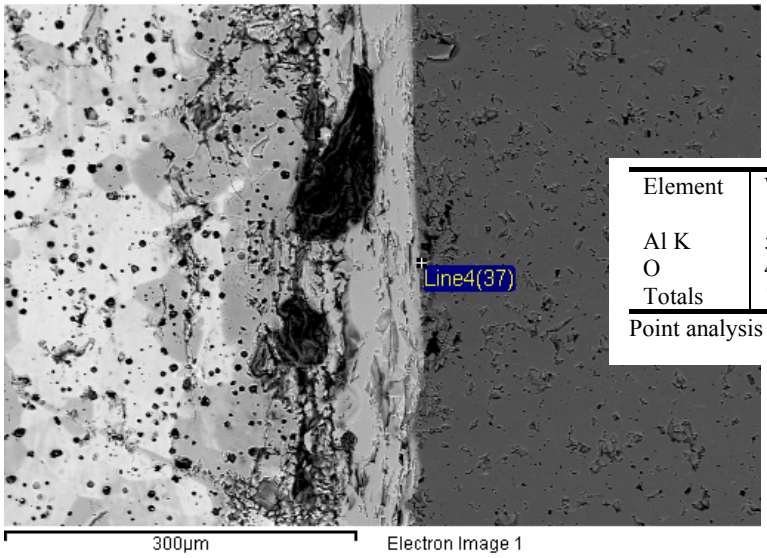

Element	Weight%	Atomic%	Compd%	Formula
Al K	52.93	40.00	100.00	Al2O3
O	47.07	60.00		
Totals	100.00			

Point analysis 37

Figure a14. *SEM pictures (BEI) and EDS point analyses over the reaction layer in test 18 (1405°C, 12min). Selected points showing analyses for phases CaO (p.13), calcium rich phase "$C_{14}A$" (p.17), C_3A (p.21), $C_{12}A_7$ (p.33), CA (p.34), and Al_2O_3 (p.37)*

Table of the experimental data, calculated reaction rate constant (k), and diffusion coefficient (D) from reaction between Al_2O_3 and CaO in the temperatures 1350-1600°C

Temperature (°C)	1350°C	1350°C	1350°C	1370°C	1370°C	1370°C	1390°C	1390°C	1390°C	1390°C	1390°C	1390°C	1390°C	1405°C
Reaction time (h)	6	12	48	3	6	12	0,5	0,5	0,7	1	1,7	2,3	3	0,2
Number of test	Test 8	Test 3	Test 7	Test 13	Test 5	Test 4	Test 10	Test 17	Test 14	Test 11	Test 15	Test 16	Test 9	Test 18
Al_2O_3 (mass)	1) 0,3800 g 2) 0,3633 g	1) 0,3087 g 2) 0,3264 g	1) 0,3488 g 2) 0,3693 g	1) 0,3654 g 2) 0,3598 g	1) 0,3766 g 2) 0,3660 g	1) 0,2797 g 2) 0,2724 g	1) 0,3910 g 2) 0,3698 g	1) 0,4050 g 2) 0,4218g	1) 0,3580 g 2) 0,3393g	1) 0,3910 g 2) 0,3698 g	1) 0,3093g 2) 0,3087 g	1) 0,2867 g 2) 0,2645 g	1) 0,4236 g 2) 0,4224 g	1) 0,5716 g 2) 0,5539 g
CaO (mass)	0,1718 g	0,1463 g	0,1991 g	0,1519 g	0,1435 g	0,1428 g	0,1747 g	0,1819 g	0,1425g	0,1330 g	0,1300 g	0,1518 g	0,1699 g	0,1740 g
CaO dimension	h = 2,696 mm d = 5,151 mm	h = 2,246 mm d = 5,162 mm	h = 3,059 mm d = 5,203 mm	h = 2,437 mm d = 5,096 mm	h = 2,246 mm d = 5,170 mm	h = 2,337 mm d = 5,179 mm	h = 2,853 mm d = 5,184 mm	h = 2,744mm d = 5,211 mm	h = 2,267mm d = 5,172 mm	h = 2,109 mm d = 5,168 mm	h = 2,0 mm d = 5,285 mm	h = 2,480 mm d = 5,123 mm	h = 2,671 mm d = 5,145 mm	h = 2,720 mm d = 5,249 mm
Al_2O_3 (mass) after annealing	1) 0,3792 g 2) 0,3618 g	1) 0,3064 g 2) 0,3256 g	1) 0,3446 g 2) 0,3660 g	1) 0,3650 g 2) 0,3594 g	1) 0,3757 g 2) 0,3641 g	1) 0,2774 g 2) 0,2702 g	1) 0,3903 g 2) 0,3685 g	1)0,4026g 2)0,4201g	1) 0,3578g 2) 0,3392g	1) 0,3698 g 2) 0,3917 g	1) 0,3087 g 2) 0,3080 g	1) 0,2855 g 2) 0,2639 g	1) 0,4126 g 2) 0,4118 g	1) 0,5707 g 2) 0,5517 g
Al_2O_3 (mass) dissolved in acid	1) Δm = 0,8 mg 2) Δm = 1,5 mg	1) Δm = 2,3 mg 2) Δm = 0,8 mg	1) Δm = 4,2 mg 2) Δm = 3,3 mg	1) Δm = 0,4 mg 2) Δm = 0,4 mg	1) Δm = 0,9 mg 2) Δm = 1,9 mg	1) Δm = 2,3 mg 2) Δm = 2,2 mg	1) Δm = 0,7 mg 2) Δm = 1,3 mg	Δm = 1,7 mg Δm = 2,4 mg	1) Δm = 0,2mg 2) Δm = 0,1 mg	1) Δm = 7,6 mg 2) Δm = 6,7 mg	1) Δm = 0,6 mg 2) Δm = 0,7 mg	1) Δm = 1,2 mg 2) Δm = 0,6 mg	1) Δm = 11 mg 2) Δm = 10,6 mg	1) Δm = 0,9 mg 2) Δm = 2,2 mg
dN=Δm/102 (mol)	1,17647E-05	1,47059E-05	3,72549E-05	3,92157E-06	1,86275E-05	2,2549E-05	1,27451E-05	1,66667E-05	1,96078E-06	7,45098E-05	6,86275E-06	1,17647E-05	0,000107843	2,15686E-05
r=(1/S)(dN/dt)	2,56469E-05	1,60293E-05	1,01519E-05	1,70979E-05	4,06075E-05	2,45782E-05	0,000333409	0,000435997	3,66384E-05	0,000974581	5,28024E-05	6,69048E-05	0,000470192	0,000940385
$k=r/C_{CaO}^{l}$	1,07293E-09	6,7058E-10	4,24701E-10	7,15286E-10	1,6988E-09	1,02822E-09	1,39481E-08	1,82398E-08	1,53276E-09	4,07713E-08	2,20897E-09	2,79894E-09	1,96704E-08	3,93407E-08
ρ*A	0,062321158	0,062321158	0,062321158	0,062321158	0,062321158	0,062321158	0,062321158	0,062321158	0,062321158	0,062321158	0,062321158	0,062321158	0,062321158	0,062321158
h=Δm/(ρ*A)	2,40689E-05	3,69056E-05	6,73928E-05	6,41837E-06	3,04872E-05	3,69056E-05	2,08597E-05	2,72781E-05	3,20918E-06	0,000121949	1,12321E-05	1,92551E-05	0,000176505	3,5301E-05
h(μm)	24,069	36,906	67,393	6,42	30,49	36,91	20,8597	27,27	3,209	121,95	11,23	19,255	176,51	35,3
$k=(h)^2/2t$	1,34101E-10	1,57645E-10	1,31418E-10	1,90817E-11	2,15194E-10	1,57679E-10	1,20869E-09	2,0657E-09	2,04319E-11	2,06549E-08	1,03033E-10	2,23886E-10	1,4424E-08	5,76926E-09
k, cm2s-1*10-12	134,1011021	157,6450042	131,4183	19,08166667	215,1944676	157,6791782	1208,686345	2065,7025	20,43190675	20654,9425	103,033415	223,8858847	14423,97227	5769,262042
lg k	-9,872567653	-9,802319788	-9,881344155	-10,7193837	-9,667168898	-9,802225652	-8,917686384	-8,684932225	-10,6896911	-7,68497601	-9,987021905	-9,649973287	-7,840915121	-8,238879735
1/T (1/K)	6,160860056	6,160860056	6,160860056	6,085871649	6,085871649	6,085871649	6,012686769	6,085871649	6,012686769	6,012686769	6,012686769	6,012686769	6,012686769	5,958942884
ln k	-22,73242711	-22,57067542	-22,75263575	-24,6822931	-22,259479	-22,57045866	-20,53373173	-19,99779547	-24,61392338	-17,6953112	-22,99596776	-22,21988464	-18,05437427	-18,97072166
Annealing time (s)	21600	43200	172800	10800	21600	43200	1800	1800	2520	3600	6120	8280	10800	720
Diffusion distance $2(Dt)^{-1/2}$ (μm)	24,069	36,906	67,393	6,42	30,49	36,91	20,8597	27,27	3,209	121,95	11,23	19,255	176,51	35,3
Chemical diffusion coefficient, D ($m^2 s^{-1}$)	6,70498E-15	7,88208E-15	6,57088E-15	9,53598E-16	1,07578E-14	7,88208E-15	6,04343E-14	1,03346E-13	1,02171E-15	1,03275E-12	5,15363E-15	1,11944E-14	7,21158E-13	4,32695E-13

Temperature (°C)	1420°C					1450°C				1500°C			1550°C	1600°C
Reaction time t (min)	5	10	15	30	60	5	10	15	30	3	5	10	5	2
Al_2O_3 (mass) (g) dissolved in acid	Δm=0.025	Δm=0.012	Δm=0.043	Δm=0.042	Δm=0.111	Δm=0.017	Δm=0.028	Δm=0.055	Δm=0.122	Δm=0.037	Δm=0.044	Δm=0.105	Δm=0.113	Δm=0.142
dN=Δm/102 (mol)	0,000245098	0,000117647	0,000421569	0,000411765	0,001088235	0,000166667	0,00027451	0,000539216	0,001196078	0,000362745	0,000431373	0,001029412	0,001107843	0,001392157
r=(1/S)(dN/dt)	0,038470286	0,009232869	0,022056297	0,01077168	0,014234006	0,026159794	0,02154336	0,028211543	0,031289166	0,094893372	0,067707703	0,0807876	0,173885692	0,54627806
k=r/C_{CaO}^{l}	1,60939E-06	3,86254E-07	9,22719E-07	4,5063E-07	5,95475E-07	1,09439E-06	9,0126E-07	1,18022E-06	1,30897E-06	3,96984E-06	2,83253E-06	3,37973E-06	7,27446E-06	2,28534E-05
ρ*A	0,062321158	0,062321158	0,062321158	0,062321158	0,062321158	0,062321158	0,062321158	0,062321158	0,062321158	0,062321158	0,062321158	0,062321158	0,062321158	0,062321158
h=Δm/(ρ*A)	0,000401148	0,000192551	0,000689974	0,000673928	0,001781097	0,000272781	0,000449286	0,000882525	0,001957602	0,000593699	0,00070602	0,001684821	0,001813188	0,00227852
h(μm)	401,1478733	192,5509792	689,974342	673,9284271	1781,096557	272,7805538	449,2856181	882,5253212	1957,601622	593,6988524	706,0202569	1684,821068	1813,188387	2278,51992
$k=(h)^2/2t$	2,68199E-06	3,08966E-07	2,6448E-06	1,26161E-06	4,40598E-06	1,24015E-06	1,68215E-06	4,32695E-06	1,0645E-05	9,79106E-06	8,30774E-06	2,36552E-05	5,47942E-05	0,000216319
k, cm2s-1*10-12	2681993,604	308965,6631	2644803,292	1261609,791	4405979,092	1240153,842	1682146,388	4326949,681	10645011,41	9791064,649	8307743,387	23655183,58	54794202,12	216318876,1
lg k	-5,571542262	-6,510089783	-5,577606623	-5,899074949	-5,355957568	-5,906524437	-5,774136213	-5,363818155	-4,972853869	-5,009170082	-5,080516927	-4,626073677	-4,261265393	-3,664905582
1/T (1/K)	5,906151257	5,906151257	5,906151257	5,906151257	5,906151257	5,803325305	5,803325305	5,803325305	5,803325305	5,639680794	5,639680794	5,639680794	5,485012204	5,338600753
ln k	-12,82895016	-14,99003569	-12,84291387	-13,58312204	-12,33254805	-13,60027512	-13,29543997	-12,35064773	-11,45041919	-11,53404036	-11,69832254	-10,65192829	-9,81192617	-8,438756961
Annealing time (s)	300	600	900	1800	3600	300	600	900	1800	180	300	600	300	120
Diffusion distance $2(Dt)^{-1/2}$ (μm)	401,1478733	192,5509792	689,974342	673,9284271	1781,096557	272,7805538	449,2856181	882,5253212	1957,601622	593,6988524	706,0202569	1684,821068	1813,188387	2278,51992
Chemical diffusion coefficient, D ($m^2 s^{-1}$)	1,341E-10	1,54483E-11	1,3224E-10	6,30805E-11	2,20299E-10	6,20077E-11	8,41073E-11	2,16347E-10	5,32251E-10	4,89553E-10	4,15387E-10	1,18276E-09	2,73971E-09	1,08159E-08

HELSINKI UNIVERSITY OF TECHNOLOGY PUBLICATIONS IN MATERIALS SCIENCE AND ENGINEERING

TKK-MT-166 Sedláková, Z., Jalkanen, H.,
Study on Steelmaking Wastes and Zinc Removal from Them. 2005

TKK-MT-167 Heiskanen, K.,
Virtaustekniikka materiaalitekniikan opiskelijoille. Kurssi MT-0.2211. 2005

TKK-MT-168 Aromaa, J.,
Korroosion estotekniikkan perusteet. 2005

TKK-MT-169 Kaskiala, M., Kaskiala, T.,
Virtaustekniikka prosessiteollisuudessa – kurssimateriaali vuosina 1990-2005. 2005

TKK-MT-170 Koponen, J., Holappa, L.,
Nanocopper. Synthesis, properties and applications.Literature survey. 2005

TKK-MT-171 Salo, T., Pehkonen, A.,
Materiaalien zeta-potentiaalin ja nollavarauspotentiaalin vaikutus adsorptioon ja saostumiseen. 2005

TKK-MT-172 Kekkonen, M.,
Materials production and synthesis / 2005. MT-0.3201. 2005

TKK-MT-173 Wang, S., Holappa, L.,
Evaluation and Prospect for Novel Casting Technologies. 2005

TKK-MT-174 Liukkonen, M., Friman, M., Koponen, J., Hämäläinen, M., Holappa, L.,
Kirjallisuustutkimus kiinteiden aineiden pintaenergian mittausmenetelmistä. 2006

TKK-MT-175 Heikinheimo, E., Selin, L., (eds)
WDS School. Graduate School Seminar. Helsinki University of Technology, Department of Materials Science and Engineering, Espoo, Finland. 2006

TKK-MT-176 Oja, M.,
Mekaanista prosessitekniikkaa materiaalitekniikan opiskelijoille. Kurssin MT-0.2216 luentomoniste. 2006

TKK-MT-177 Pystynen, K.,
Forging of Gears. 2006

TKK-MT-178 Forsén, O., Aromaa, A., Selin, L., (eds)
European Federation of Corrosion, Task Force II, Corrosion and Protection of Steel Structures, WORKSHOP IV. Properties of Steel Construction Surfaces Affecting Corrosion Resistance. 2006

TKK-MT-179 Xia, J., Nurminen, E.,
Granulation and Granulation Processes. 2006

ISBN 951-22-8251-8
ISBN 951-22-8252-6 (electronic)
ISSN 1455-2329